Title
Zirconium Complexes Supported by a Ferrocene-Based Ligand as Redox Switches for Hydroamination Reactions

Author
Shen, Yi

Publication Date
2018

Peer reviewed|Thesis/dissertation

UNIVERSITY OF CALIFORNIA

Los Angeles

Zirconium Complexes Supported by a Ferrocene-Based Ligand as Redox Switches for Hydroamination Reactions

A thesis submitted in partial satisfaction of the requirements for the degree Master of Science in Chemistry

by

Yi Shen

2018

ABSTRACT OF THE THESIS

Zirconium Complexes Supported by a Ferrocene-Based

Ligand as Redox Switches for Hydroamination Reactions

by

Yi Shen

Master of Science in Chemistry

University of California, Los Angeles, 2018

Professor Paula Loredana Diaconescu, Chair

The synthesis of (thiolfan*) $Zr(NEt_2)_2$ and (thiolfan*) $Zr(NMe_2)_2$ (thiolfan*= 1, 1'-bis (2,4-di-*tert*-butyl-6-thiophenoxy) ferrocene), and its selectivity towards catalyzing hydroamination reactions are reported. Switching the metal complex *in situ* between its oxidized and reduced states with redox reagents resulted in selectivity. We found that the reduced form of (thiolfan*)$Zr(NEt_2)_2$ can catalyze hydroamination reactions of primary aminoalkenes, whereas the oxidized form, [(thiolfan*)$Zr(NEt_2)_2$][BAr^F] can catalyze hydroamination reactions of secondary aminoalkenes.

The thesis of Yi Shen is approved.

Alexander Michael Spokoyny

Ohyun Kwon

Paula Loredana Diaconescu, Committee Chair

University of California, Los Angeles

2018

TABLE OF CONTENTS

ABSTRACT OF THE THESIS ..... **ii**

TABLE OF CONTENTS ..... **iv**

TABLE OF FIGURES ..... **vi**

LIST OF ABBREVIATIONS AND SYMBOLS ..... **viii**

ACKNOWLEDGMENT ..... **x**

Chapter 1: Synthesis, Characterization, and Electrochemical Properties of Zirconium Bis-Dimethyl/diethyl Amido Complexes Supported by a Ferrocene Backbone **1**

1.1 Introduction 1

1.1.1Ferrocene 1

1.1.1.1Ferrocene ligands 1

1.1.2 Switchable catalysis 5

1.1.2.1 Redox switchable catalysis 6

1.1.2.2 Redox switchable hydroelementation 7

1.2 Results and discussion 8

1.2.1 H_2(thiolfan)* synthesis and characterization 8

1.2.2 (thiolfan*)Zr(NEt_2)$_2$ and (thiolfan*)Zr(NMe_2)$_2$ synthesis and characterization 11

1.2.3 Electrochemical and chemical oxidation of (thiolfan*)Zr(NEt_2)$_2$ and (thiolfan*)Zr(NMe_2)$_2$ 14

1.3 Experimental 16

1.3.1 Synthetic procedure for H_2(thiolfan)* 17

1.3.2 Synthetic procedure for (thiolfan*)Zr(NEt_2)$_2$ and (thiolfan*)Zr(NMe_2)$_2$ 21

1.3.3 Synthetic procedure for $AcFcBAr^F$ 24

1.4 References 27

Chapter 2: Hydroamination reactions catalyzed by (thiolfan*)Zr(NEt_2)$_2$ and (thiolfan*)Zr(NMe_2)$_2$ 29

2.1 Introduction 29

2.1.1 Hydroamination reactions 29

2.1.2 Mechanisms 33

2.1.3 Redox-active catalysts for monocyclization and bicyclization of aminodialkenes 35

2.1.4 Bronsted acid catalysts for hydroamination reactions 36

2.2 Results and discussion 37

2.2.1 Hydroamination reactions catalyzed by (thiolfan*)Zr(NEt_2)$_2$ 37

2.2.2 Intermolecular hydroamination reactions 41

2.2.3 Control experiments 42

2.3 Experimental 44

2.3.1 Synthesis and characterization of amine substrates.....44

2.3.2 Hydroamination reactions catalyzed by the reduced state of (thiolfan*)Zr(NEt_2)$_2$ and (thiolfan*)Zr(NMe_2)$_2$ 48

2.3.3 Hydroamination reactions catalyzed by the oxidized state of (thiolfan*)Zr(NEt_2)$_2$ 49

2.3.4 Control experiments 49

2.4 References 51

Chapter 3: Conclusions 53

APPENDIX: NMR SPECTRA 54

TABLE OF FIGURES

Figure 1.1: The eclipsed and staggered configurations of ferrocene. 1

Figure 1.2: Ferrocene-based ligands and their applications..... 3

Figure 1.3: Ferrocene pro-ligands used by the Diaconescu group 4

Figure 1.4: On/off switching of a yttrium complex supported by a ferrocene backbone ... 5

Figure 1.5: On/off switch of a cobalt complex towards hydroalkoxylation 8

Figure 1.6: Synthetic route to H_2(thiolfan*) 9

Figure 1.7: HSQC spectrum of (thiolfan*)Zr(NEt_2)$_2$..... 12

Figure 1.8: HSQC spectrum of (thiolfan*)Zr(NMe_2)$_2$ 14

Figure 1.9: Cyclic voltammetry diagram of (thiolfan*)Zr(NEt_2)$_2$ 15

Figure 1.10: Cyclic voltammetry diagram of (thiolfan*)Zr(NMe_2)$_2$ 16

Figure 2.1: Scope of intramolecular hydroamination/cyclization 29

Figure 2.2: a) Indolizidine, pyrrolizidinene, pyrrolizidine and dipyroolopyrazine

b) synthesis of pyrrolizidine alkaloids c) pyrrolizidine formed by bicyclization 31

Figure 2.3: Examples of two-step hydroaminations 32

Figure 2.4: Insertion mechanism for hydroamination reactions 33

Figure 2.5: Imido mechanism for hydroamination reactions..... 34

Figure 2.6: Proposed two-step bicyclization..... 35

Figure 2.7: Proposed two-step-cyclization catalyzed by neutral (Red) and oxidized (Ox)

(thiolfan*)Zr(NEt_2)$_2$..... 36

Table 2.1: Intramolecular hydroamination catalyzed by (thiolfan*)Zr(NEt_2)$_2$ 39

Figure 2.8: Bicyclization catalyzed by neutral (“Red cat.”) and oxidized (“Ox cat.”)

(thiolfan*)Zr(NEt_2)$_2$..... 41

Figure 2.9: Intermolecular hydroamination catalyzed by (thiolfan*)Zr(NEt_2)$_2$ 42

Figure 2.10: Bronsted acid catalyzed hydroamination..... 43

List of Abbreviations and Symbols

δ	delta
Fc	ferrocenium
fc	1,1'-ferrocenediyl
Ph	phenyl
Bn	benzyl
Tol	toly
Pet	petroleum
Hex	hexanes
Cp	cyclopentadienyl
TMEDA	N,N,N′,N′-tetramethylethane-1,2-diamine
Ac	acetyl
Et	ethyl
Ts	tosyl
Me	methyl
^{t}Bu	*tert*-butyl
THF	tetrahydrofuran
HMDSO	hexamethyldisiloxane
^{i}Pr	*iso*-propyl
NMR	nuclear magnetic resonance
BAr^{F} or BArF4	tetrakis[3,5-bis(trifluoromethyl)phenyl]borate
LAH	lithium aluminum hydride
^{n}BuLi	*n*-butyllithium

DCM	dichloromethane
Et_3N	triethylamine
AcFc	acetylferrocene
ppm	parts per million
EA	elemental analysis
CV	cyclic voltammetry
HMB	hexamethylbenzene
Dppf	diphenylphosphinoferrocene
Eq	equivalent
CHO	cyclohexene oxide
$CoCp_2$	cobaltocene

ACKNOWLEDGMENT

I would like to thank all my colleagues and past members in our group, especially Scott M Shepard who started this project. I would like to thank my family who always support me in my life. Finally, but most importantly, I would like to thank Professor Paula Diaconescu for her endless help on my research.

Chapter 1: Synthesis, Characterization and Electronic Properties of Zirconium Bis-Dimethyl/Diethyl Amido Complexes Supported by Ferrocene Backbone

1.1 Introduction

1.1.1 Ferrocene

Ferrocene, discovered by Woodward and Wilkinson in 1951,[1] is an organometallic compound consisting of two cyclopentadieyl rings bound on opposite sides of an iron center. The two cyclopentadieyl rings can rotate freely resulting in the eclipsed and staggered configurations shown in Figure 1.1. Ferrocene is the first reported sandwich compound and initiated the field of metallocenes.[1-5] It has remarkable properties and applications in structure and bonding,[1] electrochemistry,[2] materials,[3] and catalysis.[4,5] Also important, ferrocene has been used as an ancillary ligand platform in organometallic chemistry.[4]

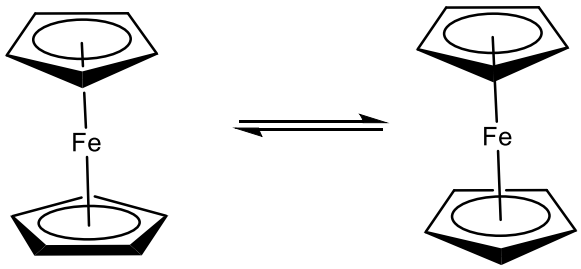

Figure 1.1: The eclipsed and staggered configurations of ferrocene

1.1.1.1 Ferrocene ligands

Ferrocene-based ligands have been extensively studied. Ligand platforms range from simple monodentate, 1,1'-bidentate, and 1,2-asymmetric bidentate to complicated polydentate or

polyferrocenes.[4] The selective functionalization of ferrocene derivatives with donor atom (P, S, N, O etc.) created different classes of chiral and achiral ferrocene ligands that have been widely applied in synthetic chemistry (Figure 1.2).[5] Symmetric ferrocene ligands, for example, 1,1'-ferrocenyldiphosphines, are used in Suzuki-Miyaura and Heck reaction, amination, and/or hydrofunctionalizations. Asymmetric ferrocene ligands have advantageous applications in asymmetric synthesis.[5] The ligand substituents are designed to be electronically and sterically different so the environment around the catalytic metal center can be altered.[6] Chiral unsymmetrical ligands may lead to the formation of an enantiopure product.[6]

Ligands	Applications
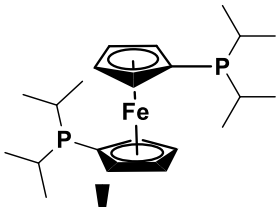	**Suzuki-Miyaura and Heck reactions; amidation; indolization; ethylene carbonylation, ketones hydrogenation; hydroamination**
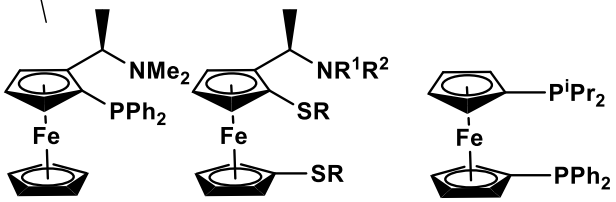	**Organometallic cross-coupling**
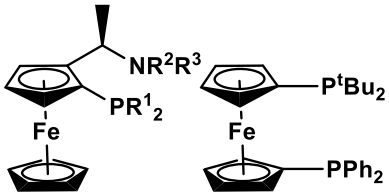	**Hydrogenation**
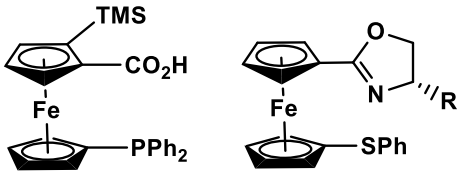	**Allylic substitution**
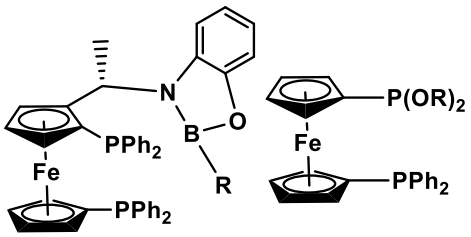	**Hydroformylation**
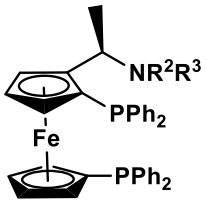	**Au, Ag catalyzed aldol reaction**

Figure 1.2: Ferrocene-based ligands and their applications [5,6]

The Diaconescu group, in the past decade, has developed numerous ferrocene-based ligands that can be classified into two categories: bidentate ferrocenediamides (NN^{fc}, where fc = 1,1'-ferrocenediyl) and tetradentate diaryloxides ($OEEO^{fc}$, where E = N or S) (Figure 1.3).[7] These ligands show special characteristics such as electronic metal-metal communication between iron

and the metal centers, redox events, and steric flexibility, which can affect the catalysis at the metal center of interest.[7]

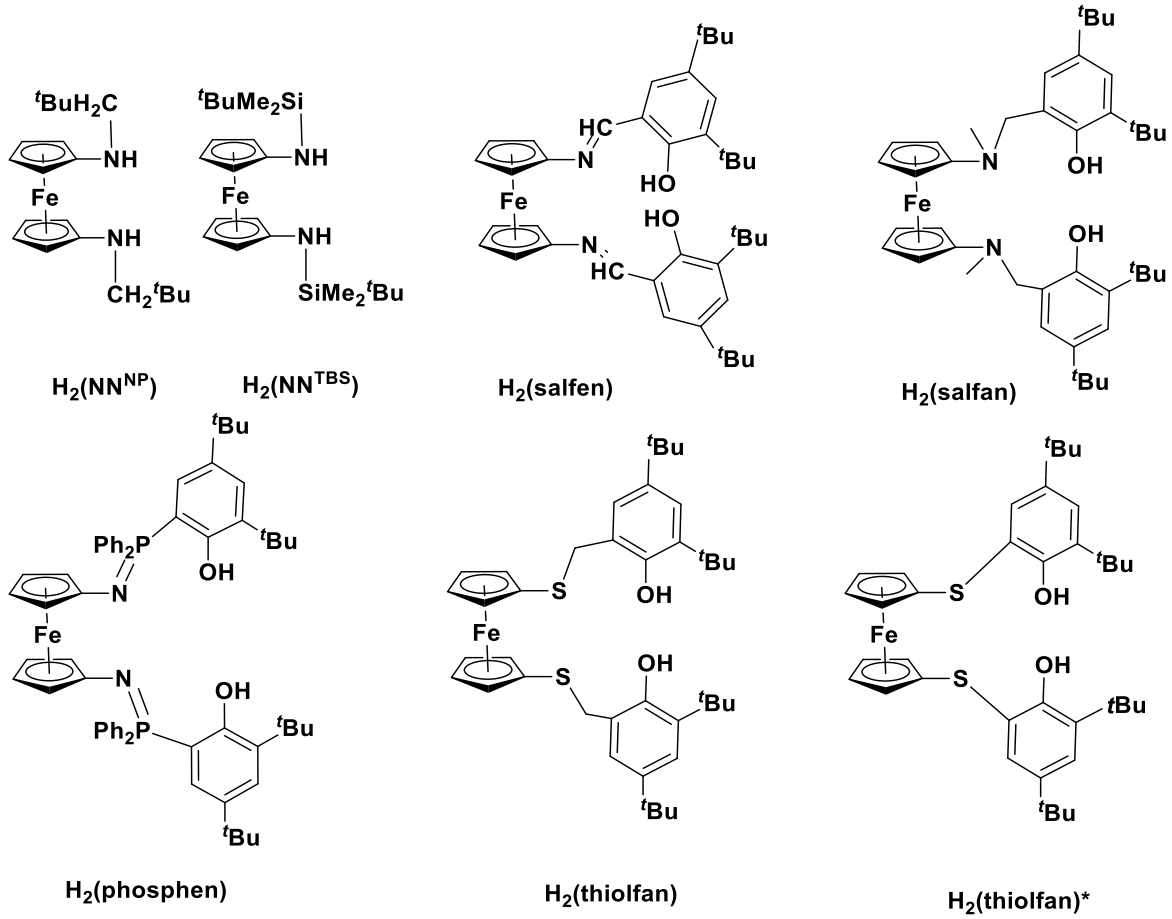

Figure 1.3. Ferrocene pro-ligands used by the Diaconescu group.[7]

Chemical and/or electrochemical oxidation/reduction were observed in metal complexes supported by these ferrocene pro-ligands. For example, the yttrium compound in Figure 1.4 was proven to be redox-switchable chemically using a simple oxidant and reductant, which could turn on and off the polymerization of L-lactide.[8,9] For example, when cobaltocene, as the reductant, was added after the yttrium compound was fully oxidized by $FcBAr^F$, the same ^1H NMR spectrum

was observed as that for the neutral compound that was employed initially. Therefore, the redox event at ferrocene affected the catalysis performed by the yttrium center. The neutral/reduced state of the yttrium catalyst was active in polymerizing L-lactide. By adding an oxidant, the oxidation state of iron center was changed from +2 to +3 and the reaction was turned off.[9]

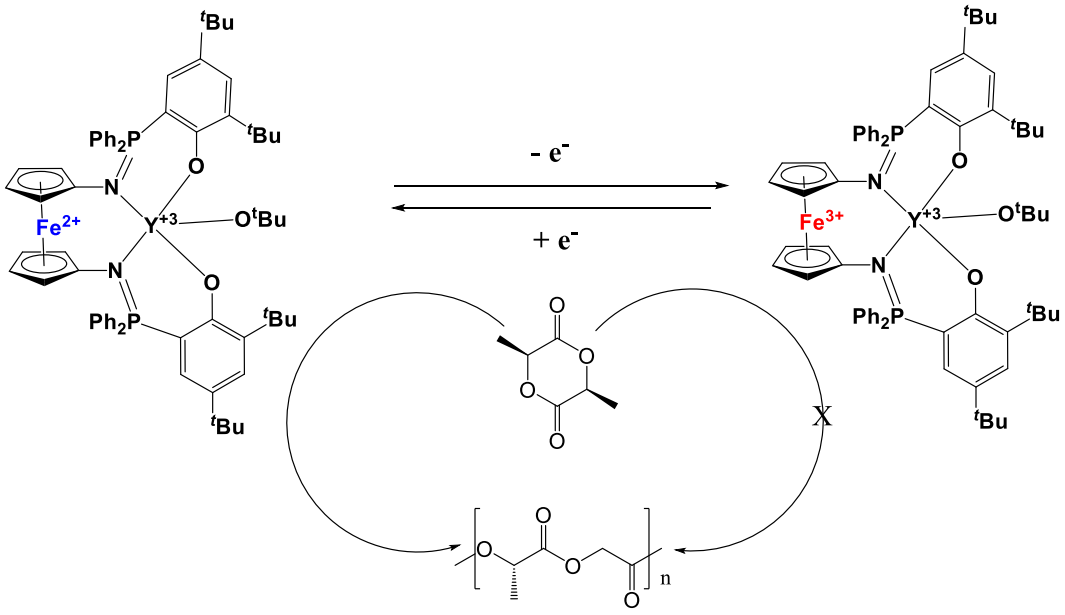

Figure 1.4: On/off switching of a yttrium complex supported by a ferrocene backbone.[9]

1.1.2 Switchable catalysis

Catalysis is key to the transformation of simple building blocks to complicated molecules and materials.[8] Inspired by Nature, recently, chemists have started to develop catalysts whose activity can be switched by an external stimulus. Using a switchable catalyst, sequences of transformations, the type of products, and their stereochemistry can be controlled.[8] Various types of stimuli can be used such as light, metal/ligand coordination, pH changes, electron transfer, mechanical forces, and changes in reaction conditions.[8]

1.1.2.1 Redox switchable catalysis

Redox-switchable catalysis is a field of growing importance, in which the redox-active functionality is usually incorporated within a ligand framework.[10,11] The activity of a metal catalyst supported by a redox-active ligand can be influenced *in situ* by the redox event occurring at the ligand. Oxidation and reduction change the electronic properties of the ligand and can result in selectivity of the catalyst of interest.[10] In 1995, Wrighton and co-workers developed a Rh(I) complex supported by dppc (1,1'-bis(diphenylphosphino)-cobaltocene), in which changing the oxidation state of cobaltocene resulted in a change of the rate of reactions such as hydrogenation and hydrosilylation.[12] Following Wrighton's work, redox-switchable catalysis has been widely applied in homogeneous catalysis. Redox-switchable polymerization is one of the most popular applications in the field. Even more than cobaltocene, ferrocene ligands are commonly used in redox-switchable catalysis. For example, in 2006, A. J. P. White and coworkers incorporated two ferrocene moieties in their ligand and achieved an on/off switch in the ring-opening polymerization of *rac*-lactide that can be turned off by adding an oxidant (AgOTf) and turned back on by adding a reductant (decamethylferrocene).[13]

The metal that undergoes catalysis can also be used as the redox switch. For example, the Byers group reported that a bis(imino)pyridine iron complex can polymerize lactide in the iron(II) oxidation state but not in the iron(III) oxidation state. On the contrary, epoxides can be polymerized by the iron(III) complex but cannot be polymerized by the iron(II) complex.[13]

The Diaconescu group, as discussed in Section 1.1.1.1, has developed several types of ferrocene-based redox-active ligands. The yttrium(III) complex shown in Figure 1.4 displayed redox-controllable activity in the polymerization of L-lactide that could be switched off by

oxidizing the iron center from Fe(II) to Fe(III).[9] In 2006, (salfan)Zr(O^tBu)$_2$ (salfan = 1,1'-di(2-*tert*-butyl-6-N-methylmethylenephenoxy)ferrocene) was synthesized and employed in the redox-switchable copolymerization of lactide and cyclohexene oxide (CHO). In the neutral state, (salfan)Zr(O^tBu)$_2$ was active toward lactide, whereas in the oxidized state it was active toward CHO. By adding an oxidant ($AcFcBAr^F$) or a reductant ($CoCp_2$), blocks of polylactide (PLA) and poly-cyclohexene oxide (PCHO) can be formed; triblock copolymers such as PLA-PCHO-PLA and PCHO-PLA-PCHO.[14]

1.1.2.2. Redox switchable hydroelementation

Besides ring-opening polymerization, redox-switchable catalysis was also tested for reactions other than ring-opening polymerization. Hydroelementation, the addition of a hydrogen and a functional group across an unsaturated bond, has broad applicability for generating molecular complexity.[15,16] The potential 100% atom economy makes hydroelementation reactions attractive. Unfortunately, little research has been reported on switchable hydroelementation catalysts. A photoredox catalyst was employed by Knowles and coworkers in the intramolecular hydroamination of secondary amines. However, their study did not investigate on whether the process is switchable.[15,17] Inspired by Hiroya and coworkers on hydrofluorination and hydroamination reactions with a Co(II) Schiff base salen complex, the Diaconescu group developed a salfen cobalt complex to promote hydroalkoxylation reactions.[18, 19] Salfen, as the Schiff base ferrocene analogue of salen has been used in the redox-switchable ring-opening polymerization reactions.[20, 21] Shown in Figure 1.5, the salfen cobalt compound was active towards the hydroalkoxylation of styrenes with methanol in the reduced state and became inactive upon the addition of the oxidant $AcFcBAr^F$.[15]

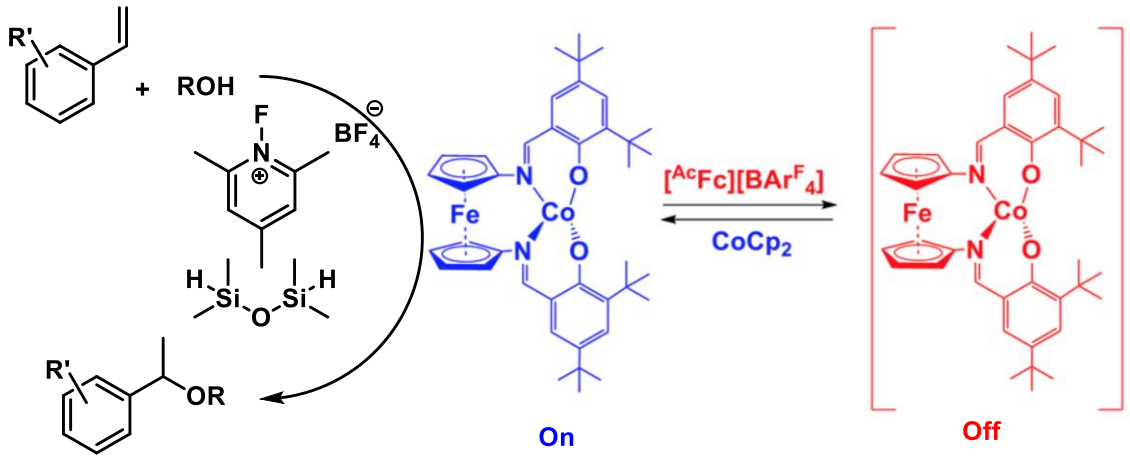

Figure 1.5: On/off switch of a cobalt salfen complex towards hydroalkoxylation

1.2 Results and discussion

1.2.1 H_2(thiolfan)* synthesis and characterization

Among all tetradentate diaryloxides (OEEO^{fc}, where E = N or S)[7] developed in our group, thiolfan* was chosen to support zirconium. This choice was made based on DFT calculation results performed by Scott Shepard that indicated that the HOMO of the corresponding zirconium complex is ferrocene based. As such, it was reasoned that the oxidation of (thiolfan*)Zr(NEt_2)$_2$ will result in a ferrocenium species as opposed to oxidizing another site of the ligand.[15] A published procedure was followed to synthesize H_2(thiolfan*) starting with ferrocene (Figure 1.6).[22] All steps were performed inside a glovebox except the synthesis of 2-iodo-4,6-di–*tert*-butylphenol and its protection. The steps requiring heating were done in sealed Schlenk flasks that were brought outside the glovebox.

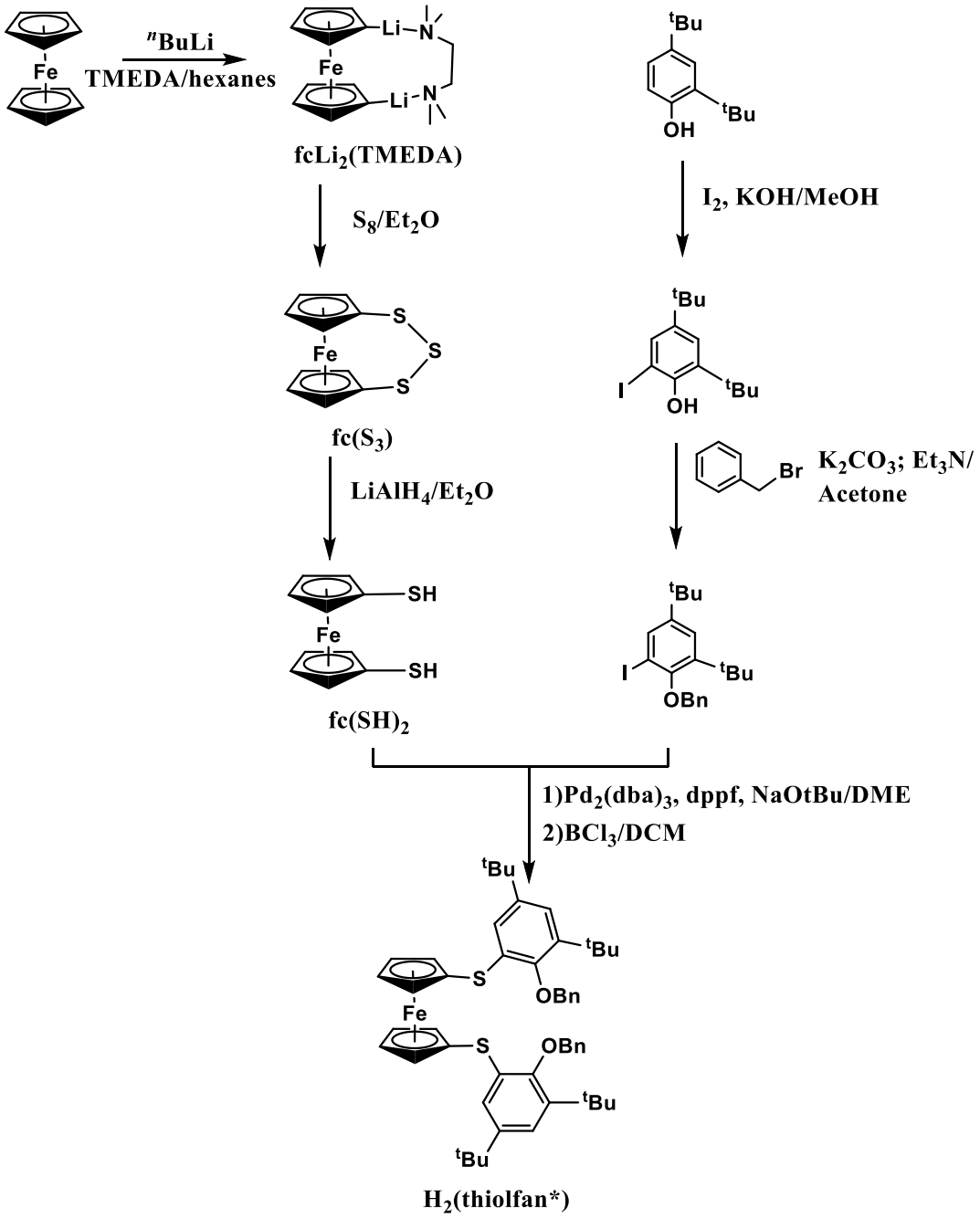

Figure 1.6: Synthetic route to H_2(thiolfan*)[5,12]

The first step is converting ferrocene to dilithioferrocene•TMEDA. ^{n}BuLi was added slowly to a hexanes solution of ferrocene and TMEDA in the first step for lithiation. After 16 hours,

the resulting orange precipitate was filtered, and the solid collected was washed with hexanes and dried under a reduced pressure. The product was air and moisture sensitive and usually kept in a vial inside the freezer in the glovebox. The average yield for this step is usually 75% because of the loss during filtering and washing; sometimes, the speed of ^{n}BuLi addition could affect the yield. To convert the ferrocene dilithium salt to the ferrocene trithiol, S_8 was added slowly to the solution of dilithium salt in diethyl ether. The reaction was stirred for 16 hours at room temperature and worked up outside the glovebox by quenching with base and extraction into diethyl ether. The resulting red powder was usually pure to use in the next step, but, to improve the yield of the next step, fcS_3 can be recrystallized from benzene or toluene resulting dark red crystals in a ca. 50% yield. fcS_3 can then be reduced by adding it slowly to a slurry of LAH in diethyl ether inside the box, then brought outside to heat at 50 °C. The addition sequence is crucial to ensure a fully reduction and increase the yield. LAH can be purified by stirring in diethyl ether or THF, filtering through Celite and drying down the solution. This can help clean up LAH and improve the yield of the reduction step. $fc(SH)_2$ was moderately air and moisture sensitive so the work-up process was usually kept within an hour and the final orange powder had to be stored inside the glovebox at -30 °C.

2-iodo-4,6-di-*tert*-butylphenol was prepared by adding an I_2 in solution of MeOH to 4,6-di-*tert*-butylphenol and KOH over an hour. The mixture was then stirred for an additional hour or two. Quenching during this step sometimes happened and resulted in a lower yield and a mixture of side products. The iodophenol was then protected by refluxing it with benzylbromide in the presence of K_2CO_3 in acetone. The reported reaction time is 24 hours; however, the reaction time may be extended as necessary (determined by monitoring the conversion to the product). The reaction was cooled down and 1.1equivalents of Et_3N was added and the mixture was refluxed

again for an additional 2 hours to consume the excess benzylbromide. The product can be purified by passing through a silica plug and washed with hexanes.

$fc(SH)_2$ and the protected phenol were added to a Schlenk flask inside the box containing dppf, $Pd_2(dba)_3$, and NaO^tBu. The order of adding the reagents had no effect on the resulting yield. This cross-coupling reaction required 3 days of heating at 100 °C and worked up by quenching with water and extraction into diethyl ether. The crude product can be purified by a silica column using DCM: Hex in a 1:10 ratio as an eluent. Fractions were collected according to the TLC result, and the volatiles were removed under a reduced pressure. The deprotection step was performed inside the box by cooling Bn_2thiolfan* to -78 °C in DCM and adding BCl_3 slowly. The reaction was stirred overnight at room temperature followed by quenching with water and extraction into diethyl ether. Pure hexanes was used to flash the column instead of DCM and hexanes, and recrystallization from hot hexanes was necessary to get pure H_2(thiolfan*).

1.2.2 (thiolfan*)$Zr(NEt_2)_2$ and (thiolfan*)$Zr(NMe_2)_2$ synthesis and characterization

$Zr(NEt_2)_4$ was prepared by adding 1 equivalent of $ZrCl_4$ to the solution of 4 equivalents of $LiNEt_2$ in THF inside the box.[23] The order of addition was crucial to get a pure product. The reaction was stirred overnight and dried under a reduced pressure, then extracted into hexanes. Side products were filtered out through a pipetted frit with Celite and the filtrate was dried under a reduced pressure yielding a yellow gel as pure $Zr(NEt_2)_4$ that is air and moisture sensitive and stored inside the freezer in the glovebox. H_2(thiolfan*) in Hex was added to a $Zr(NEt_2)_4$ hexanes solution at -78 °C. The reaction was then warmed up to room temperature and stirred for an additional hour. The volatiles were removed under a reduced pressure and the crude solid was washed with HMDSO to get rid of some impurities and then dried. (thiolfan*)$Zr(NEt_2)_2$ was

recrystallized from pentanes at -33 °C. Other solvents like diethyl ether or THF were also employed in this reaction, but hexanes gave the cleanest compound at a low temperature (-78 °C). At a higher temperature (0°C) the conversion was too fast and side products started to form.

^{1}H NMR, ^{13}C NMR, and HSQC spectroscopies were used to characterize (thiolfan*)Zr(NEt$_2$)$_2$. In the ^{1}H NMR spectrum, the protons of the aromatic ring and the protons belonging to the ^{t}Bu groups can be clearly identified. However, the protons of diethyl amide (N(C*H*$_2$CH$_3$)$_2$)$_2$ and those of the Cp rings were not differentiated and appear around 4ppm. A one scan ^{1}H NMR spectrum did not help obtain accurate integrals and only one carbon peak was observed for Cp in the ^{13}C NMR spectrum. HSQC (Figure 1.7), however, indicated that the sharp peak at 3.68 ppm and the broad peak around 3.86 ppm in the ^{1}H NMR spectrum correspond to the overlap of diethyl amide and Cp ring protons. Elemental analysis also agreed with the structure.

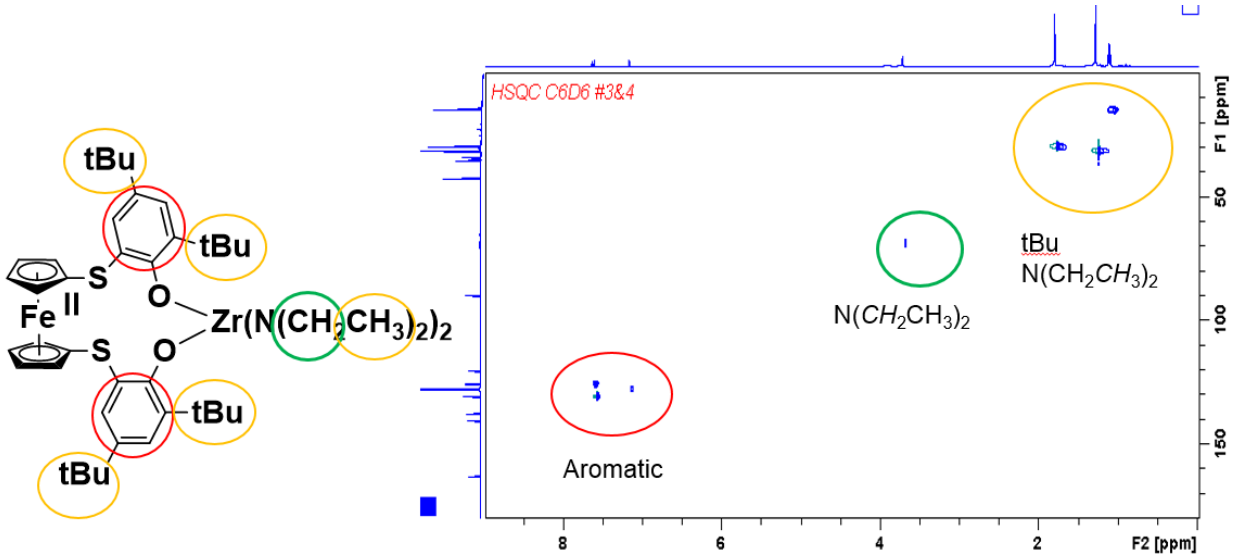

Figure 1.7: HSQC spectrum of (thiolfan*)Zr(NEt$_2$)$_2$

Zr(NMe$_2$)$_4$ was prepared by adding 1 equivalent of ZrCl$_4$ to a solution of 4 equivalents of LiNMe$_2$ in THF inside the box.[24] The order of addition was crucial to get a pure product. The

reaction was stirred overnight, and the precipitate was filtered out through a pipette. The volatiles were removed under a reduced pressure. After extraction into hexanes and removal of the solvent, the resulting crude yellow solid was sublimated under a reduced pressure yielding white crystalline $Zr(NMe_2)_4$. It is necessary to use pure crystalline $Zr(NMe_2)_4$ for the next step to reduce the formation of side products. H_2(thiolfan*) was dissolved in benzene and added to the benzene solution of $Zr(NMe_2)_4$ at room temperature. The reaction mixture was stirred for 5 min then the volatiles were removed under a reduced pressure. Lower temperatures (-78 °C and 0 °C) did not help improve the yield. The reaction performed in benzene gave the cleanest product compared to the reactions performed in hexanes, toluene, or diethyl ether. The volatiles were removed under a reduced pressure, and the crude (thiolfan*)$Zr(NMe_2)_2$ was recrystallized from pentanes after washing it with cold pentanes three times.

^{1}H NMR, ^{13}C NMR and HSQC spectroscopies were used to characterize (thiolfan*)$Zr(NMe_2)_2$. In the ^{1}H NMR spectrum, the protons of the aromatic ring and the protons belonging to the ^{t}Bu groups can be clearly identified. The singlets at 3.69 ppm and 4.30 ppm in the ^{1}H NMR spectrum indicate the protons of the Cp rings. The sharp singlet at 3.28 ppm indicates the protons of the NMe_2 group.

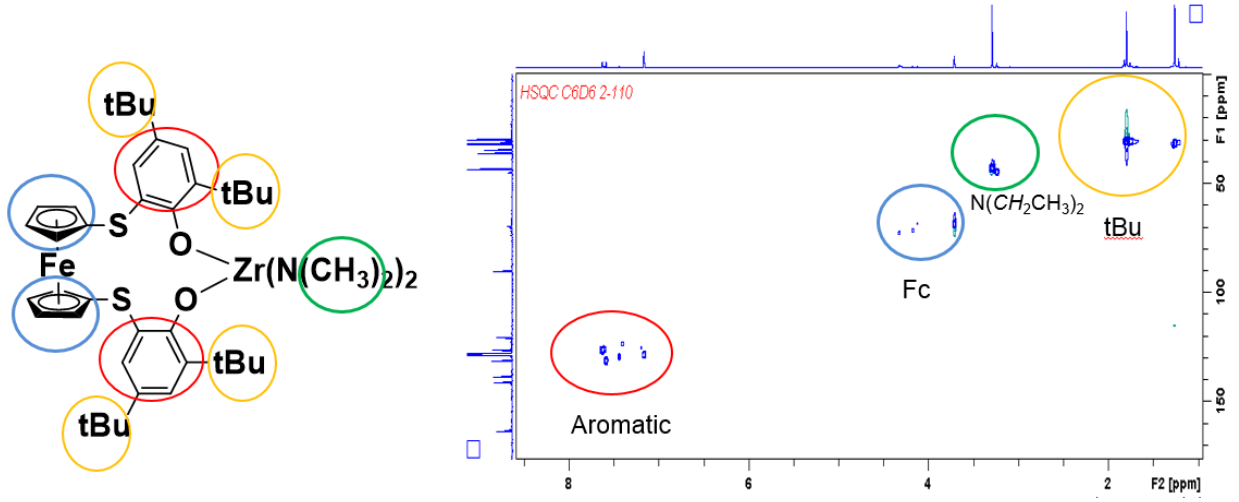

Figure 1.8: HSQC spectrum of (thiolfan*)Zr(NMe_2)$_2$

1.2.3 Electrochemical and chemical oxidation of (thiolfan*)Zr(NEt_2)$_2$ and (thiolfan*)Zr(NMe_2)$_2$

To investigate the redox properties of the newly synthesized zirconium compounds, cyclic voltammetry experiments were performed. For both compounds, 4 mL of *o*-$F_2C_6H_4$ was used as a solvent, 100 mM of $TPABAr^F$ was added as an electrolyte, and 10 mM of zirconium compound was added after recording the signal for a background. For (thiolfan*)Zr(NEt_2)$_2$, the most flat region in background scan was chosen from -1.6 to 1.6 V. Two oxidation peaks were observed but neither one was reversible. A narrower region was chosen for the second scan from 0 to 1.3 V to isolate the first oxidation peak, but it still did not result in a reversible event. The first oxidation peak was observed at 0.12 V versus the Fc/Fc^+ couple (Figure 1.9). A possible explanation for this observation is that once the zirconium compound is oxidized electrochemically, it undergoes a chemical reaction with the electrolyte or some impurities in the cell, and no reduction was observed.

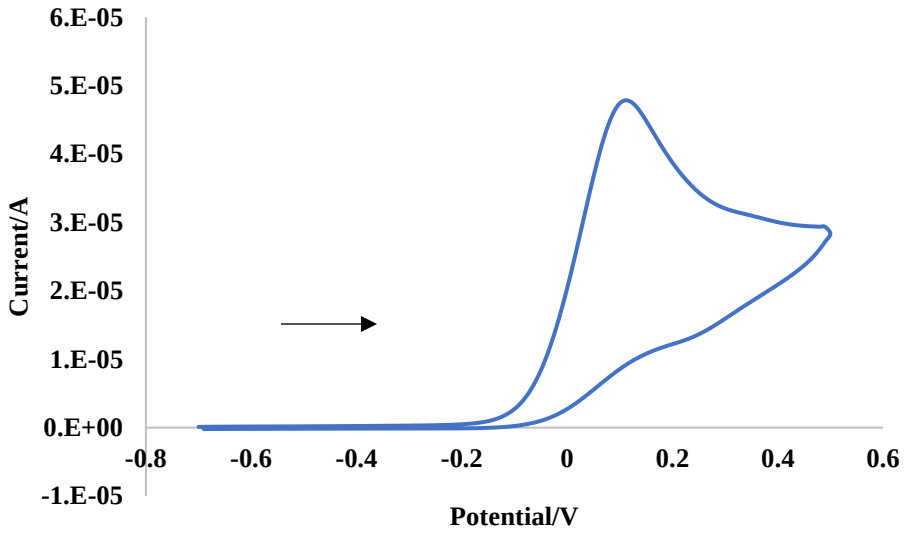

Figure 1.9: Cyclic voltammetry diagram of (thiolfan*)Zr(NEt_2)$_2$

Similar results were observed for (thiolfan*)Zr(NMe_2)$_2$. From -1.0-1.5 V two oxidation peaks were observed but neither was reversible. From 0 to 1.5 V one oxidation peak at 0.15 V versus the Fc/Fc^+ couple could be isolated but was not reversible (Figure 1.10). According to the cyclic voltammetry results, both oxidized zirconium compounds are reactive and unstable, and chemical events occur right after the electrochemical oxidation and the corresponding reduction event was not observed.

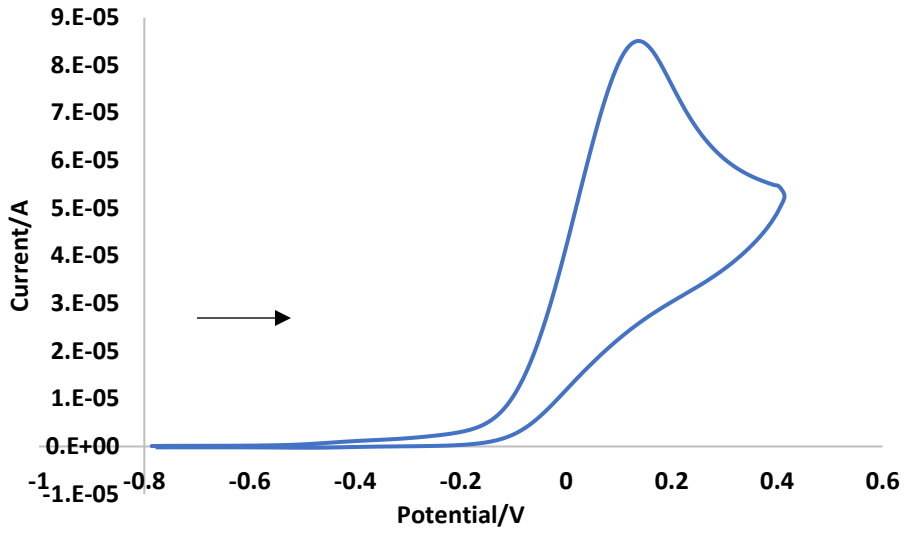

Figure 1.10: Cyclic voltammetry diagram of (thiolfan*)Zr(NMe_2)$_2$

Besides studying the electrochemical oxidation of the zirconium compounds, chemical oxidation studies were also carried out. $AcFcBAr^F$, AgOTf, $AgBF_4$, $AgBPh_4$, and $NOBF_4$ were used to oxidize (thiolfan*)Zr(NEt_2)$_2$, while the addition of $CoCp_2$ was employed to reduce the chemically oxidized species. However, no reversible oxidation/reduction was observed according to ^{1}H NMR spectra. Attempts to isolate an oxidized zirconium compound were carried out. After the reaction with $AcFcBAr^F$ in *o*-$F_2C_6H_4$, the volatiles were removed under a reduced pressure. The residual solid was washed with Hex and recrystallized from diethyl ether layered with Hex. However, because of the high reactivity of the oxidized compound and its observed decomposition, no clean product could be isolated.

1.3 Experimental

General: All reactions were performed in the glovebox or using standard Schlenk techniques unless noted otherwise. All glassware was stored in an oven at 200 °C before being brought into the

glovebox. Solvents were purified using a two-column solid-state purification system by the method of Grubbs and transferred to the glovebox without exposure to air. NMR solvents were obtained from Cambridge Isotope Laboratories, degassed, and stored over activated molecular sieves prior to use. NMR spectra were recorded at ambient temperature on Bruker AV-300, DRX-500, and AV-500. Proton chemical shifts are given relative to residual solvent peaks. All reagents were acquired from commercial sources and used as received unless otherwise noted.

1.3.1 Synthetic procedure of H_2(thiolfan)*

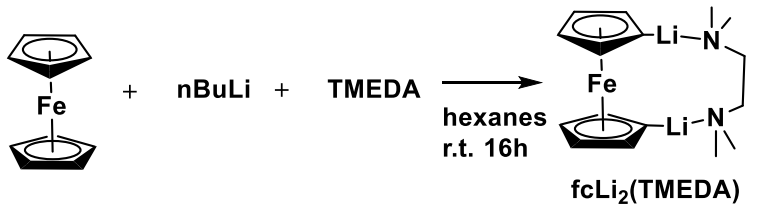

Ferrocene (5.58 g, 30 mmol) was dissolved in 100 mL hexanes in a 500 mL round bottom flask inside the glovebox. TMEDA (4.84 g, 36 mmol) was added to the flask secondly. An addition funnel was charged with ^{n}BuLi (2.2 M, 30 mL, 66 mmol) which was added dropwise over 30 min. The reaction solution was stirred for 16 hours at room temperature. The reaction mixture was filtered through a frit and the resulting orange solid was collected after washing with hexanes and dried under a reduced pressure (7.589 g, 80.6%).

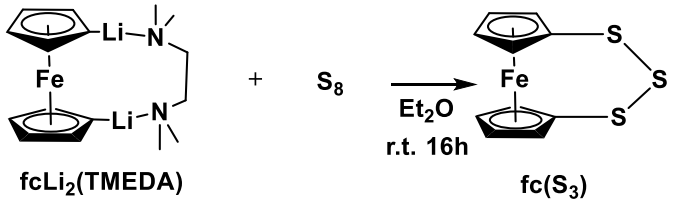

fcLi_2TMEDA (3.0667 g, 9.76 mmol) was dissolved in diethyl ether in a 500 mL round bottom flask, and S_8 (1.8807 g, 58.6 mmol) was added slowly to the flask inside the glovebox. The solution

turned green then black upon addition. Bubbles formed. The reaction solution was stirred overnight for 16 hours. After that, the flask was taken out of the box about 7 mL of a 3 M NaOH aqueous solution was added to quench the reaction. The resulting solution was extracted three times with diethyl ether, dried with $MgSO_4$. The volatiles were removed under a reduced pressure yielding dark orange solid 2.267 g (82.9%). ^{1}H NMR ($CDCl_3$, 300 MHz, 25 °C): δ 3.82 (s, 2H, Cp-*H*), 4.00 (s, 2H, Cp-*H*), 4.35 (s, 2H, Cp-*H*), 4.42 (s, 2H, Cp-*H*).

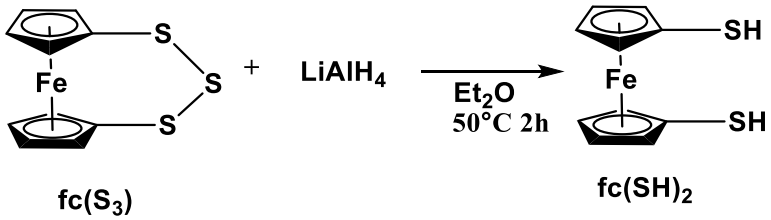

0.368 g of $LiAlH_4$ was dissolved in diethyl ether in a 250 mL Schlenk flask inside the glovebox. 0.907 g fcS_3 was added slowly to the slurry of LAH. Bubbles formed. The reaction solution was then heated outside of the box at 50 °C for 2 hours. After the reaction was completed, the solution was poured over 150 mL of deion water. Excess KOH was added. The product was extracted into diethyl ether, and concentrated HCl was added afterwards until the solution was acidic. The product was again extracted into diethyl ether. The volatiles were removed under a reduced pressure after dried with $MgSO_4$ yielding a red solid 0.617 g (77%). ^{1}H NMR ($CDCl_3$, 300 MHz, 25 °C): δ 4.00 (d, 2H, Cp-*H*), 3.82 (d, 2H, Cp-*H*), 4.35 (d, 2H, Cp-*H*), 4.42 (d, 2H, Cp-*H*),4.52 (m, 2H, Cp-*H*).

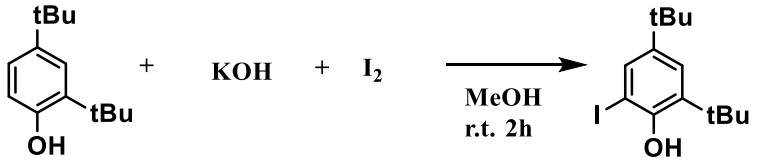

2,4-di-*tert*-Butylphenol (3.089 g, 14.9 mmol) and KOH (3.321 g, 59.9 mmol) were dissolved in 50 mL of MeOH in a 500 mL round bottom flask. I_2 (3.783 g, 14.9 mmol) was dissolved in 70 mL of MeOH and added dropwise through an addition funnel over 1 hour. The reaction solution was stirred for 1.5 hours. A saturated (2 M, 40 mL) Na_2SO_3 solution was added to quench the reaction. After quenching, HCl was added until the solution was acidic. The product was extracted into DCM and dried with $MgSO_4$. After the removal of volatiles, a yellowish-white solid was collected (5.616 g 112%). ^{1}H NMR ($CDCl_3$, 300 MHz, 25 °C): δ 1.13 (s, 9H, ^{t}Bu), 1.46 (s, 9H, ^{t}Bu), 3.01 (s, 1H, O*H*), 7.26 (d, 1H, Ar*H*), 7.55 (d, 1H, Ar*H*).

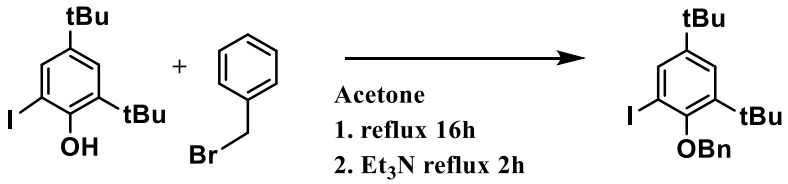

5.746 g (17.8 mmol) of 2-iodo-4,6-di–*tert*-butylphenol, 6.19 g (35.6 mmol) of benzyl bromide, and 7.372 g (53.4 mmol) of K_2CO_3 were dissolved in acetone in a 500 mL round bottom flask and refluxed for 24 hours. 1.801 g (5.746 mmol) of Et_3N was added to the reaction solution after cooling down then refluxed for two hours and stirred overnight. Acetone was removed after the reaction was done. The product was extracted with hexane/water, dried with $MgSO_4$ and filtered. After the removal of solvent, 6.931 g of yellowish-white solid (88%) was yielded. ^{1}H NMR ($CDCl_3$, 300 MHz, 25 °C): δ 1.33 (s, 9H, ^{t}Bu), 1.43 (s, 9H, ^{t}Bu), 5.10 (s, 2H, CH_2 in Bn group), 7.34-7.45 (m, 4H, Ar*H*), 7.61-7.63 (m, 2H, Ar*H*), 7.72 (d, 1H, Ar*H*).

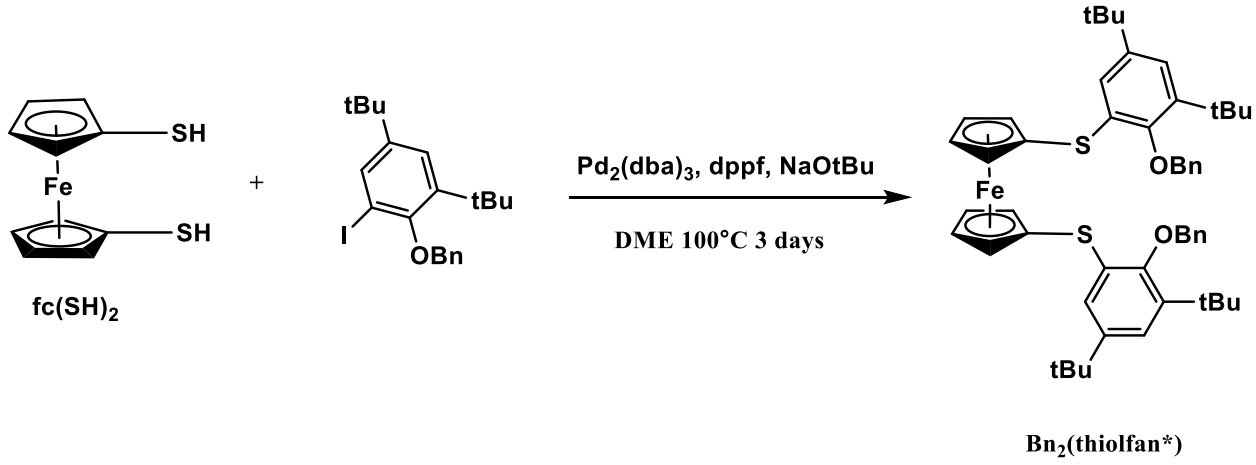

$fc(SH)_2$ 0.272 g (1.087 mmol), 2-iodo-4,6-di–*tert*-butylbenzylphenol 0.961g (2.174 mmol), $Pd_2(dba)_3$ 0.056 g (0.054 mmol), NaO^tBu 0.365 g (3.80 mmol), and dppf 0.06 g (0.1087 mmol) were dissolved in DME in a 100 mL Schlenk flask inside the glovebox and heated at 100 °C for three days. The reaction was worked up by quenching with water and extraction into diethyl ether, dried with $MgSO_4$, and the volatiles were removed under a reduced pressure. The crude product was purified by a silica column eluted with Hex:DCM in a 10:1 ratio yielding a yellow beige solid 1.52 g (>90%). ^1H NMR ($CDCl_3$, 300 MHz, 25 °C): δ 1.16 (s, 18H, ^{t}Bu), 1.40 (s, 18H, ^{t}Bu), 4.38 (t, 4H, Cp-*H*), 4.43 (t, 4H, Cp-*H*), 5.17 (s, 4H, C*H*$_2$Ph), 6.75 (d, 2H, Ar*H*), 7.12 (d, 2H, Ar*H*), 7.39 (m, 7H, Ar*H*), 7.61 (d, 4H, Ar*H*).

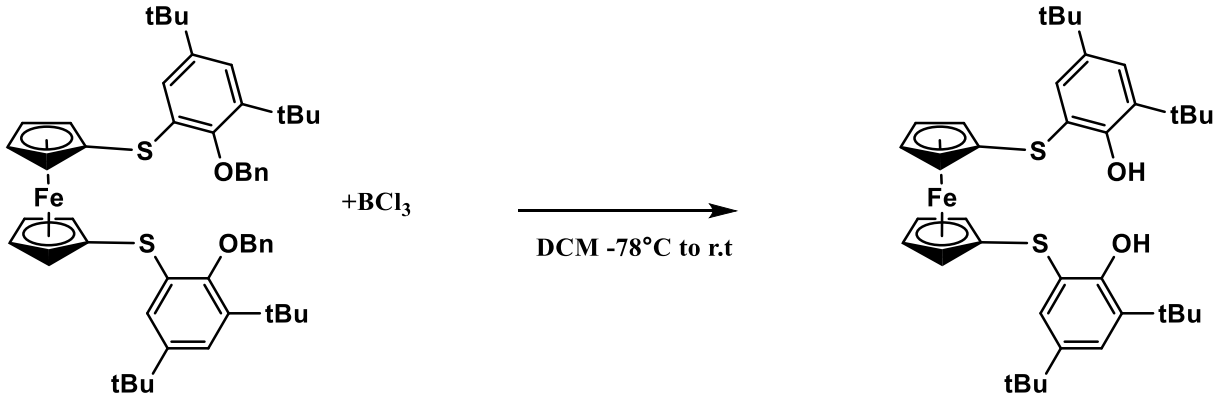

Bn_2(thiolfan*) **H_2(thiolfan*)**

1.80 g (2.1 mmol) of Bn_2(thiolfan*) was dissolved in DCM in a 250 mL round bottom flask and cooled to -78 °C for an hour. 10.7 mL (1 M, 10.72 mmol) of BCl_3 was added slowly to the flask while cooling. The reaction was stirred overnight at room temperature for 16 hours and worked up outside the glovebox by quenching with water and extraction into diethyl ether. The crude product was purified by a silica column with Hex: DCM in a 10:1 ratio yielding an orange solid which was recrystallized from Hex giving pure H_2(thiolfan*) 0.60 g (42%). ^{1}H NMR (C_6D_6, 300 MHz, 25 °C): δ 1.20 (s, 18H, ^{t}Bu), 1.59 (s, 18H, ^{t}Bu), 3.82 (t, 4H, Cp-*H*), 4.19 (t, 4H, Cp-*H*),7.48 (d, 2H, Ar*H*), 7.62 (d, 2H, Ar*H*).

1.3.2 Synthetic procedure for (thiolfan*)Zr(NEt_2)$_2$ and (thiolfan*)Zr(NMe_2)$_2$

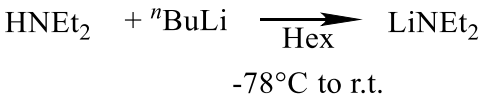

1.8642 g (25.48 mmol) of $HNEt_2$ was stirred in hexanes and cooled to -78 °C inside the glovebox. 11 mL (2.2 M) of ^{n}BuLi was added one hour later and stirred at room temperature overnight. The solid was filtered and washed with hexanes yielding 1.89 g (94%).

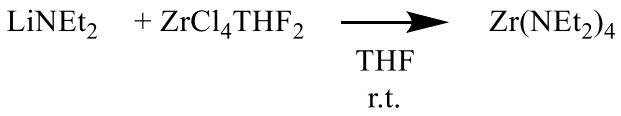

0.0822 g (1.04 mmol) of $LiNEt_2$ was dissolved in THF, 0.098 g (0.26 mmol) of $ZrCl_4THF_2$ was added slowly to the solution inside the glovebox. The reaction was stirred overnight at room temperature. THF was removed under a reduced pressure and product was extracted into hexanes and filtered through Celite. Hexanes was removed under a reduced pressure yielding yellow liquid. ^{1}H NMR (C_6D_6, 300 MHz, 25 °C): δ 3.66 (q, 16H, C*H*$_2$CH$_3$), 1.59 (t, 2H, CH$_2$C*H*$_3$).

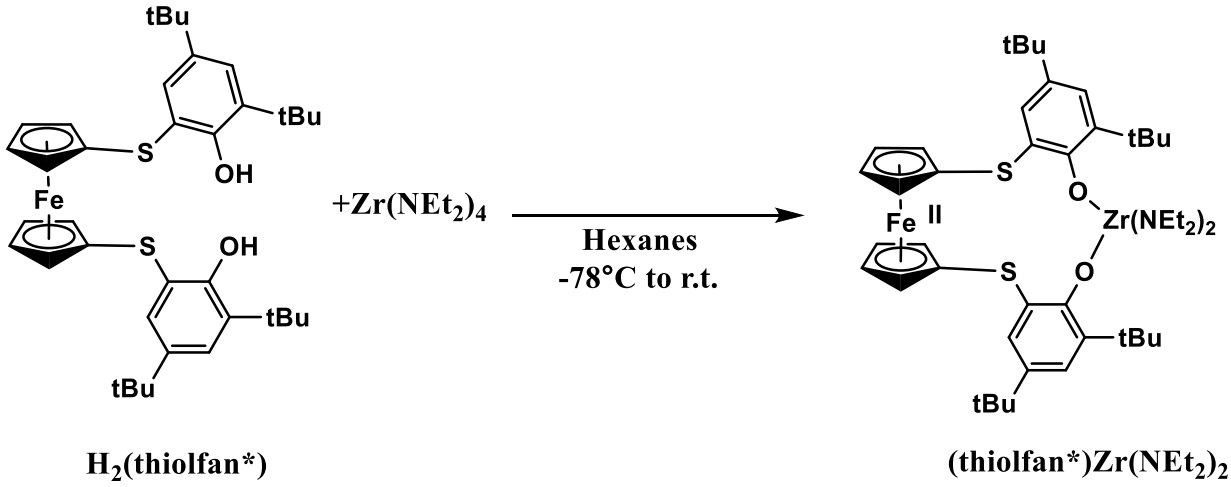

H_2(thiolfan*) **(thiolfan*)Zr(NEt$_2$)$_2$**

0.201 g (0.306 mol) of H_2(thiolfan*) was dissolved in 10mL of hexanes and cooled to -78 °C in a 25 mL vial. 0.101 g (0.306 mol) of $Zr(NEt_2)_4$ was dissolved in 2 mL of hexanes in a separate vial and cooled to -78°C. H_2(thiolfan*) solution was added dropwise to $Zr(NEt_2)_4$ and the reaction solution was stirred at room temperature for 30 min. The volatiles were removed under a reduced pressure. The crude yellow solid was recrystallized from pentanes giving 0.2 g (77%) of clean (thiolfan*)Zr(NEt$_2$)$_2$. ^{1}H NMR (C_6D_6, 300 MHz, 25 °C): δ 1.07 (t, 12H, NCH$_2$C*H*$_3$), 1.24 (s, 18H, C(*CH*$_3$)$_3$), 1.76(s, 18H, C(*CH*$_3$)$_3$), 3.68 (s, 6H, NC*H*$_2$CH$_3$), 3.90 (br, 10H, NC*H*$_2$CH$_3$ and Cp-

H),7.57 (d, 2H, Ar*H*), 7.60 (d, 2H, Ar*H*). ^{13}C NMR (C_6D_6, 500 MHz, 25°C): δ 14.79 ($NCH_2\mathit{CH}_3$), 29.6 ($C(\mathit{C}H_3)_3$), 31.3 ($C(\mathit{C}H_3)_3$), 34.0 ($\mathit{C}(CH_3)_3$), 35.4($\mathit{C}(CH_3)_3$), 42.5 ($N\mathit{C}H_2CH_3$), 65.1, 68.8,.70.5, 89.97 (Cp), 120.2 (Ar*C*), 125.6 (Ar*C*H), 130.6 (Ar*C*H), 137.6, (Ar*C*), 140.3 (Ar*C*), 163.0 (Ar*C*).

$$LiNMe_2 + ZrCl_4 \xrightarrow[\text{r.t.}]{\text{THF}} Zr(NMe_2)_4$$

Inside the glovebox, 0.438 g (17.1 mmol) of $LiNMe_2$ was dissolved in THF. 0.5 g (4.29 mmol) of $ZrCl_4$ was added slowly to the slurry. The reaction solution was stirred at room temperature overnight. The precipitate was filtered. THF was dried down under a reduced pressure and the residue was extracted into hexanes three times. After the removal of the volatiles, the resulting yellow-whitish solid was sublimed under a reduced pressure (763mg, 66%). ^{1}H NMR (C_6D_6, 300 MHz, 25 °C): δ 2.97 (s, 24H).

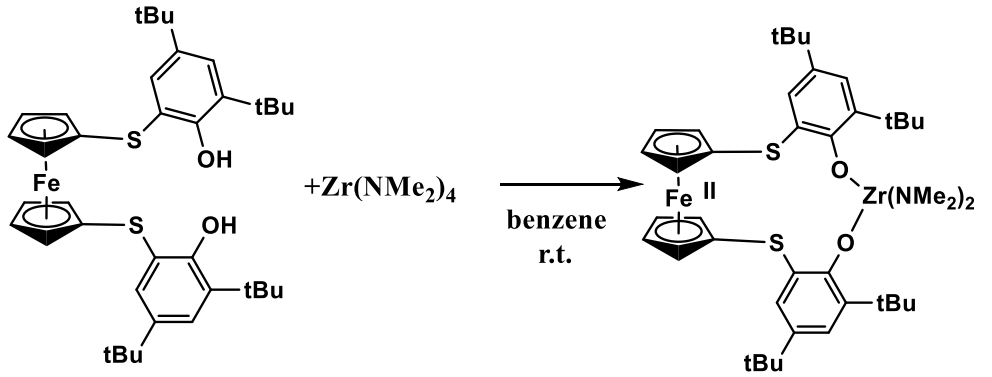

H_2(thiolfan*) **(thiolfan*)$Zr(NMe_2)_2$**

391 mg (0.594 mmol) of H_2(thiolfan*) was dissolved in 10 mL benzene at room temperature inside the glovebox and added to the benzene solution of $Zr(NMe_2)_4$. The reaction solution was stirred at room temperature for 5 min and the volatiles were remove under a reduced pressure. The crude

product was washed with cold pentanes and recrystallized from pentanes yielding yellow pure solid. ^{1}H NMR (C_6D_6, 300 MHz, 25 °C): δ 1.25 (s, 18H, C(*CH*$_3$)$_3$), 1.70(s, 18H, C(*CH*$_3$)$_3$), 3.20 (s, 12H, N*Me*), 3.69 (t, 4H Cp*H*), 4.30 (s, 4H Cp*H*), 7.57 (d, 2H Ar*H*), 7.61(d, 2H Ar*H*). ^{13}C NMR (C_6D_6, 500 MHz, 25°C): δ 21.9 (C(*C*H$_3$)$_3$), 31.7 (C(*C*H$_3$)$_3$), 34.3 (*C*(CH$_3$)$_3$), 35.9(*C*(CH$_3$)$_3$), 43.3 (N*Me*), 69.3, 90.1 (Cp), 120.1 (Ar*C*), 126.1 (Ar*C*H), 131.0 (Ar*C*H), 138.2, (Ar*C*), 140.8 (Ar*C*), 163.2 (Ar*C*).

1.3.3 Synthetic procedure for AcFcBAr^{F}

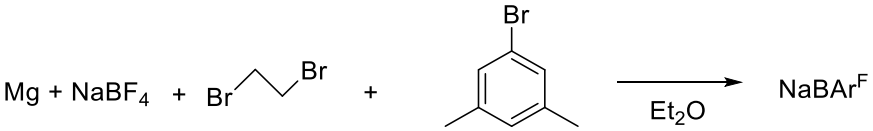

Synthetic procedure for NaBAr^{F}: A 500 mL three-necked flask fitted with a reflux condenser and an addition funnel was charged with Mg (1.01 g, 41.7 mmol), $NaBF_4$ (0.7 g, 6.4 mmol) and 150 ml of diethyl ether. 1,2-Dibromoethane (0.49 mL, 5.7 mmol) was added, and the flask was heated from several minutes with a heat gun to initiate the reaction. The mixture got cloudy and turned slightly brown upon heating. The heat was removed when bubbles can be seen from Mg. 3,5-bis(trifluoromethyl)bromobenzene (6.2 ml, 36 mmol), diluted with 50 mL diethyl ether was added dropwise over 30 min. The addition causes the solution to gently reflux and once all 3,5-bis(trifluoromethyl)bromobenzene added, the mixture was heated with a heat gun for 30 min to reflux. The heat was removed, and the mixture was stirred overnight. The reaction mixture was then poured into a solution of Na_2CO_3 (44 g), and $NaHCO_3$ (20 g) in 600 mL water (this amount is for 0.024 mmol $NaBF_4$, but this procedure can be scaled down). The mixture was stirred for 1 h, extracted with diethyl ether and washed with brine. After filtration and removal of the volatiles, the product was dried under a reduced pressure at 100 °C. [25]

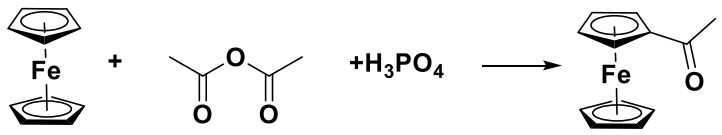

Synthetic procedure for AcFc: 5 g of ferrocene was dissolved in 17.5 mL of acetic anhydride. 3.5 mL of phosphoric acid was added dropwise while stirring. The reaction mixture was heated for 20 min at 80 to 85 °C with refluxing condenser attached. After that it was poured into a 150 mL of a 1M CH_3COONa solution at 0 °C. $NaHCO_3$ was added until the pH was 5. The solution was extracted with ethyl acetate and washed with water and dried with $MgSO_4$. The crude product was purified through a silica column with petroleum ether: ethyl acetate in an 8:2 ratio. ^{1}H NMR ($CDCl_3$, 400MHz, 25 °C): δ 2.39 (s, 3H COC*H*$_3$), 4.19 (s, 5H, Cp*H*), 4.49 (t, 2H, Cp*H*), 4.76 (t, 2H, Cp*H*). [26]

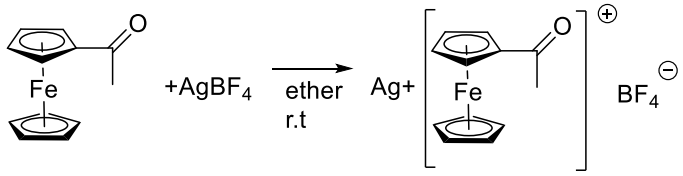

Synthetic procedure for AcFcBF$_4$: 340 mg (1.49 mmol) of AcFc was dissolved in diethyl ether. 377.2 mg (1.94 mmol) of $AgBF_4$ was weighed in the dark and added to the AcFc solution. The reaction was stirred for 15min at room temperature and a blue precipitate started to form. The liquid was decanted and the solid was dried under a reduced pressure. The crude product was extracted into DCM and filtered through Celite. The solution was concentrated and $AcFcBF_4$ was crystallized at -33 °C from DCM with a layer of diethyl ether yielding 214 mg of dark blue crystals.

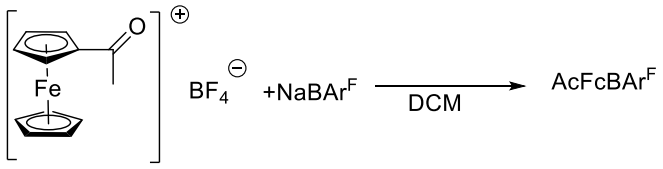

Synthetic procedure for AcFcBAr^F: 209.3 mg (0.665 mmol) of $AcFcBF_4$ was dissolved in DCM and added to 590.7 mg (0.665 mmol) of $NaBAr^F$ in DCM. The reaction mixture was stirred for 2 hours at room temperature and the volatiles were removed under a reduced pressure. The solid was extracted with diethyl ether and filtered through Celite. $AcFcBAr^F$ was crystallized from concentrated diethyl ether layered with hexanes at -33 °C yielding dark blue crystals; 611 mg (84%).

1.4 References

(1) Wilkinson, G.; Rosenblum, M.; Whiting, M. C.; Woodward, R. B. *J. Am. Chem. Soc.* **1952**, 74, 8, 2125.

(2) Gagne, R. R.; Koval, C. A.; Lisensky, G. C. *Inorg. Chem.* **1980**, 19, 2854.

(3) Conroy, D.; Moisala, A; Cardoso, S.; Windle, A.; Davidson, J. *Chem. Eng. Sci.* **2010**, 65, 10, 2965.

(4) Stepnicka, P. *Ferrocenes: Ligands, Materials and Biomolecules,* John Wiley & Sons Ltd: Chichester, **2008**.

(5) Fihri, A.; Meunier, P.; Hierso, J. C.; *Coordination Chemistry Reviews* 251, **2007**, 2017.

(6) Atkinson, R. C. J.; Gibson, V. C.; Long, N. J. *Chem. Soc. Rev*. **2004**, 33, 313.

(7) Huang, W.; Diaconescu, P. L. *Inorg. Chem*. **2016**, 55, 10013.

(8) Blanco, V.; Leigh, D. A.; Marcos, V. *Chem. Soc. Rev.* **2015**, 44, 5341.

(9) Broderick, E. M.; Guo, N.; Vogel, C. S.; Xu, C.; Sutter, J.; Miller, J. T.; Meyer, K.; Mehrkhodavandi, P.; Diaconescu, P. L. *J. Am. Chem. Soc.* **2011**, 133, 9278.

(10) Neumann, P.; Dib, H.; Caminade, A.M.; Hey-Hawkins, E. *Angew. Chem. Int. Ed*. **2015**, 54, 311.

(11) A. M. Allgeier, C. A. Mirkin, *Angew. Chem. Int. Ed.* **1998**, 37, 894; Angew. Chem. 1998, 110, 936.

(12) Lorkovic, I. M.; Duff, R. R.; Wrighton, M. S. *J. Am. Chem. Soc*. **1995**, 117, 3617.

(13) Gregson, C. K. A.; Gibson, V. C.; Long, N. J.; Marshall, E. L.; Oxford, P. J.; White, A. J. P. *J. Am. Chem. Soc.* **2006**, 128, 7410.

(14) Quan, S. M.; Wang, X.; Zhang, R.; Diaconescu, P. L. *Macromolecules* **2016**, 49, 6768.

(15) Shepard. S.M.; Diaconescu, P. L. *Organometallics* **2016**, 35, 2446.

(16) Beller, M.; Seayad, J.; Tillack, A.; Jiao, H. Angew. *Chem., Int. Ed*. **2004**, 43, 3368.

(17) Musacchio, A. J.; Nguyen, L. Q.; Beard, G. H.; Knowles, R. R. *J. Am. Chem. Soc.* **2014**, 136, 12217.

(18) Shigehisa, H.; Nishi, E.; Fujisawa, M.; Hiroya, K. *Org. Lett*. **2013**, 15, 5158.

(19) Shigehisa, H.; Koseki, N.; Shimizu, N.; Fujisawa, M.; Niitsu, M.; Hiroya, K. *J. Am. Chem. Soc*. **2014**, 136, 13534.

(20) Broderick, E. M.; Diaconescu, P. L. Inorg. Chem. **2009**, 48, 4701.

(21) Quan, S. M.; Diaconescu, P. L. Chem. Commun. **2015**, 51, 9643.

(22) Wei, J.; Riffel, M. N.; Diaconescu, P. L. *Macromolecules*, **2017**, *50*, 5, 1847.

(23) Storozhenkoa, P. A.; Shcherbakovaa, G. I.; Tsirlina, A. M.; Florinaa, E. K.; Izmailovaa, E. A.; Savitskiia, A. A.; Kuznetsovaa, M. G.; Kuznetsovaa, T. M.; Stolyarovaa, I. V.; Yurkovb, G. Y.; Gubinb, S. P.; *Inorganic Materials* **2006**, 42, 10,1159.

(24) Kim, H.; Lee, P. H.; Livinghouse, T.; *Chem. Commun.*, **2005**, 5205.

(25) Yakelis. N. A.; Bergman. R. G.; *Organometallics* **2005**, 24, 3579.

(26) He, P.; Du, Y.; Wang, S.; Cao, C.; Wang, X.; Pang, G.; Shi, Y.; *Z. Anorg. Allg. Chem*. **2013**, 639, 6, 1004.

Chapter 2. Hydroamination Reactions Catalyzed by (thiolfan*)Zr(NEt_2)$_2$ and (thiolfan*)Zr(NMe_2)$_2$

2.1 Introduction

2.1.1 Hydroamination reactions

Hydroamination, defined as the formal addition of an N-H bond across a unit of C-C unsaturation,[1, 2] is an atom-economical route to afford organonitrogen scaffolds. Metals involved in hydroamination span the entire periodic table including alkali metals, early and late transition metals, lanthanides, and actinides.[3] The intramolecular hydroamination/cyclization of aminoalkene/alkyne/allene/dienes can afford many useful scaffolds such as pyrrolidine, pyrrole, dihydropyrrole, and piperidine which are important building blocks in total synthesis and the pharmaceutical fields (Figure 2.1).[4]

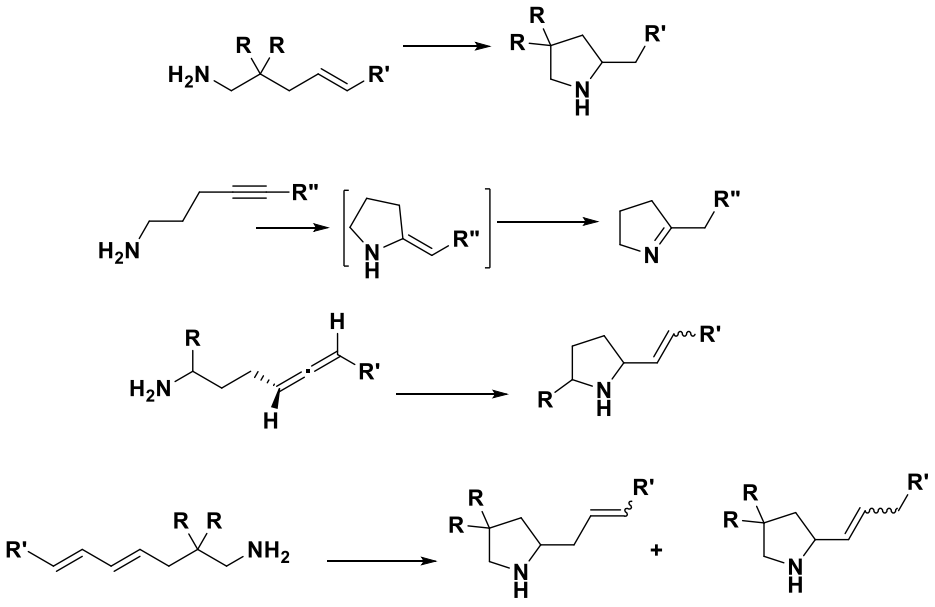

Figure 2.1. Scope of intramolecular hydroamination/cyclization.[1]

It is well-known that although hydroamination reactions are thermodynamically favored, catalysts are still required to overcome the high activation barrier.[5] It is commonly proposed that the intermolecular hydroamination is more difficult to achieve than intramolecular hydroamination due to the huge decrease in entropy,[3] and the hydroamination of alkenes is more difficult to achieve than that of alkynes.

The use of group 4 metals as catalysts for intramolecular hydroamination has been extensively studied since the late 1990s.[3] Zirconium catalysts have been proven to show great activity and selectivity in these reactions. For example, with few exceptions, neutral zirconium catalysts catalyze exclusively the formation of primary aminoalkenes,[6-10] while cationic zirconium catalysts can catalyze the formation of both primary and secondary aminoalkenes, [11,12] or catalyze selectively only the formation of secondary aminoalkenes. [13, 14]

More complicated *N*-heterocycles such as indolizidine, pyrrolizidine, and pyrazine are important building blocks in total synthesis and the pharmaceutical fields.[4] Bicyclization can make the synthesis of these scaffolds much simpler.[15,16] For example, in 1998, T. J. Marks reported that the organolanthanide complex can catalyze the bicyclization of aminodialkenes to generate pyrrolizidine skeletons.[15] Other synthetic pathways required four or five more steps comparing to the bicyclization of aminodialkenes (Figure 2.2).[16]

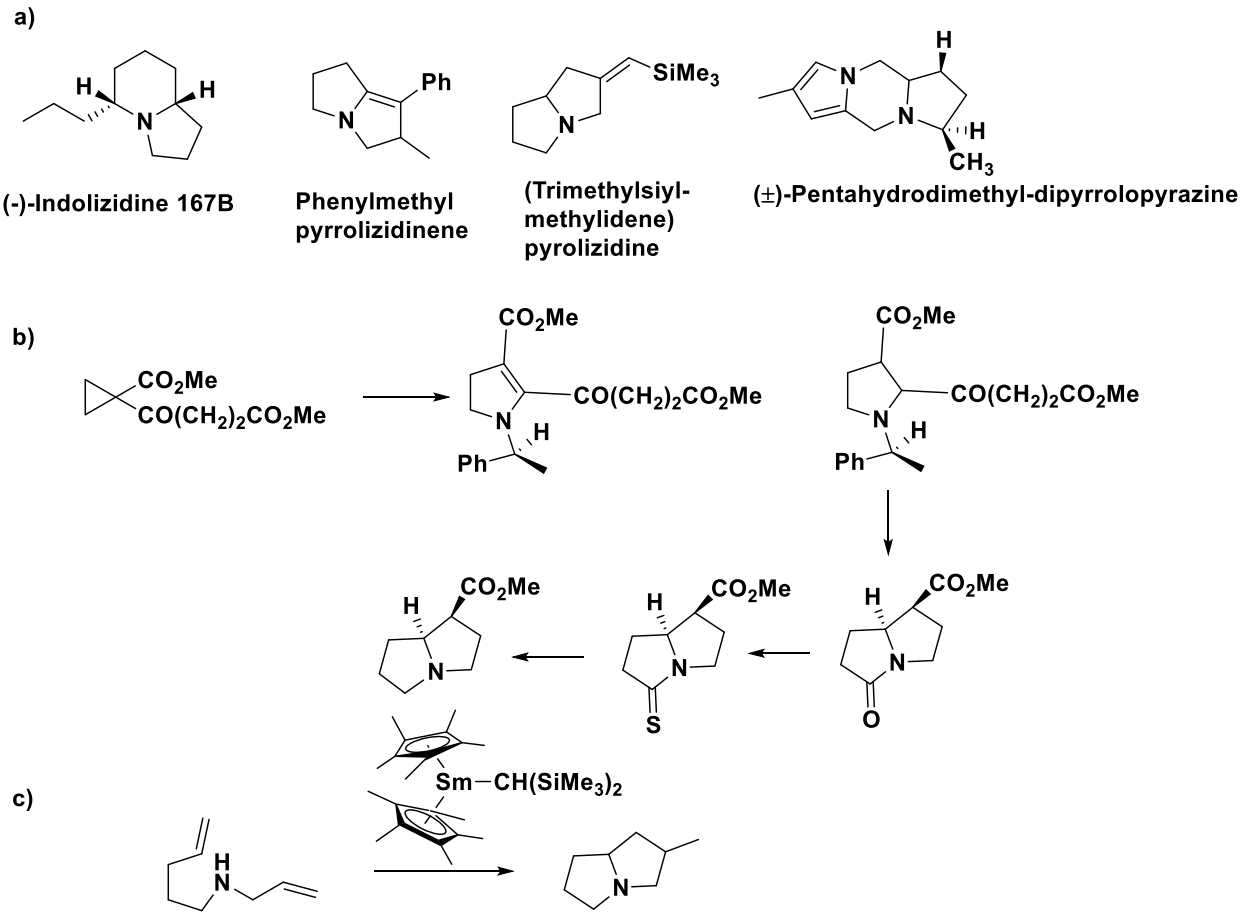

Figure 2.2 a) Indolizidine, pyrrolizidinene, pyrrolizidine and dipyroolopyrazine[4] b) Synthesis of pyrrolizidine alkaloids[16] c) pyrrolizidine formed by bicyclization[15]

Interestingly, in 2004, Wagner's group first proposed a bicyclization of an aminodialkene. In the presence of a catalyst, the aminodialkene was forced to undergo one cyclization at 25 °C and another cyclization at 60 °C. However, in their control experiments, the precursor $Y\{N(SiMe_3)_2\}_3$, used to synthesize the yttrium precatalyst can also catalyze the two-step bicyclization under the same condition.[17] In 2007, T.J. Marks and coworkers proposed that "constrained geometry" organoactinide complexes, $(CGC)An(NMe)_2$ (An =Th / U) can catalyze the bicyclization of one substrate, which has two unsaturated carbon--carbon bonds; this reaction has the potential to form two rings by changing temperature.[1] In 2016, the Shen group monitored

the formation of a two-step hydroamination catalyzed by cationic zirconium complexes stabilized by piperazidine and imidazolidine-bridged bis(phenolato) [ONNO]-type ligands (Figure 2.3).[18, 19] Recently, Sadow's group discovered that Y{N(SiHMe$_2$)^{t}Bu}$_3$(THF), at room temperature, can catalyze the bicyclization of an aminodialkene, or under the same conditions, catalyze the second cyclization from the intermediate monocyclized product.[22]

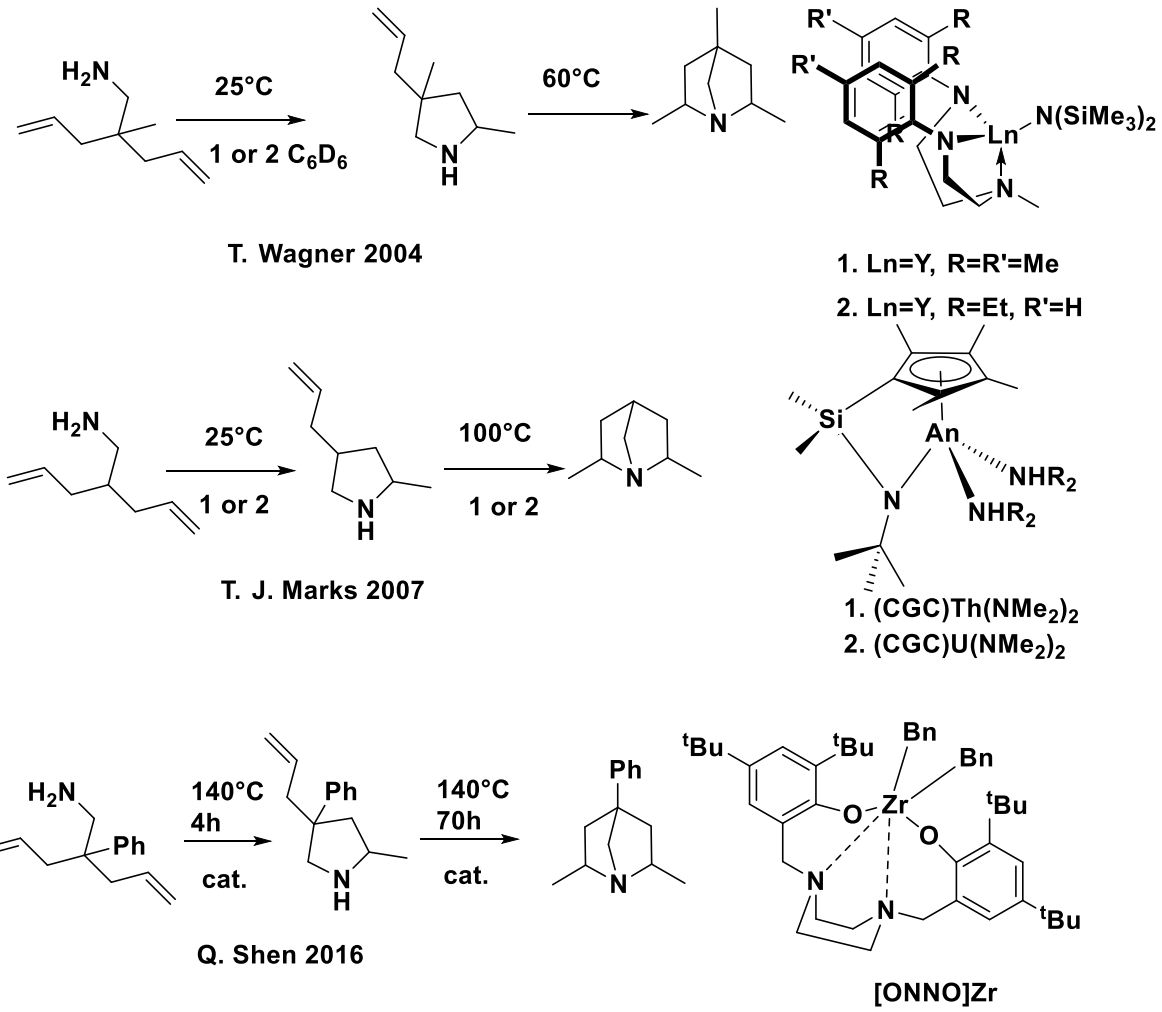

Figure 2.3. Examples of two-step hydroaminations.[1,18, 19, 21]

So far, several groups have successfully achieved a two-step bicyclization of aminodialkenes by using an increase of the reaction temperature. The second hydroamination of

the monocyclized product is more difficult to achieve so harsher conditions are required than for the first step.[22] However, there are other possible ways of achieving bicyclization which will be discussed in the next sections.

2.1.2 Mechanism

Two general mechanisms are commonly accepted as possible pathways for hydroamination reactions catalyzed by early transition metal complexes: the insertion mechanism and the imido mechanism.[21] The insertion mechanism shown in Figure 2.4 involves the formation of metal amido species upon protonolysis of a metal amido or alkyl bond. The first step of the catalytic cycle is the insertion of the alkene into the metal amido bond to form a seven-membered chair-like transition state. This step is generally considered to be the rate determining step.[21] The product is released upon the addition of another amine substrate. This mechanism has no limitation on the type of amine substrate (primary or secondary).

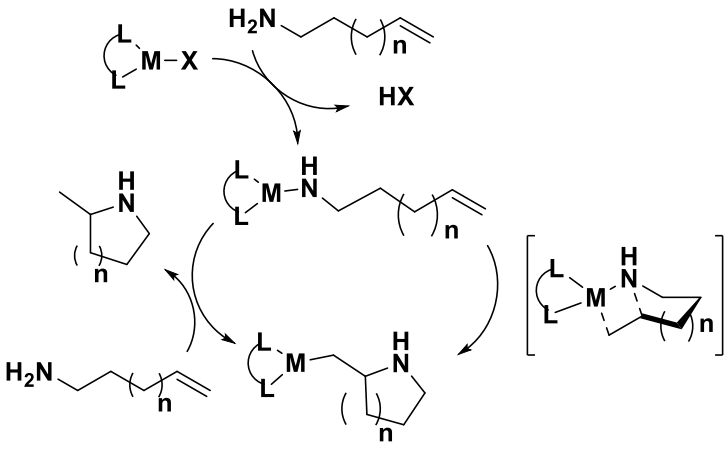

Figure 2.4: Insertion mechanism for hydroamination

The imido mechanism shown in Figure 2.5, on the contrary, is limited to primary aminoalkenes due to the formation of intermediate metal imido complex that is considered to be the catalytically active species. Figure 2.4 shows the proposed pathway for the intermolecular hydroamination of secondary amino alkenes and alkynes. The metal imido complex then undergoes a [2+2] cycloaddition to give an azametallacyclobutene species. This step is considered to be the rate limiting step. The product is released after a subsequent protonolysis.[21] However, for intramolecular hydroamination, only primary aminoalkenes/alkynes can form the catalytically active metal imido complex and undergo the [2+2] cyclization. Secondary aminoalkene/alkyne substrates cannot undergo this pathway for intramolecular hydroamination. The limitation on the type of substrate in the imido mechanism provides a possible way to react primary and secondary aminoalkenes in a selective manner.

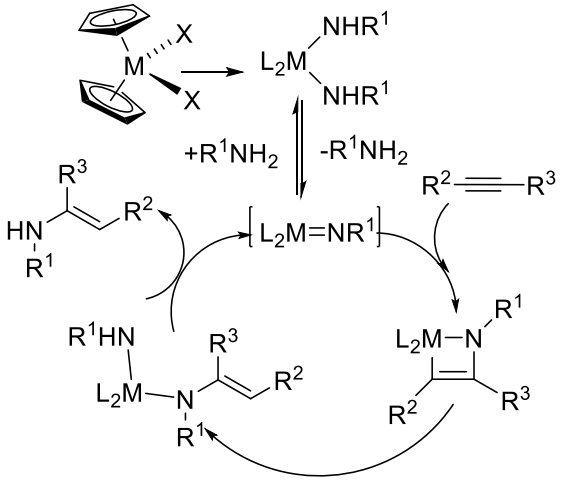

Figure 2.5: Imido mechanism for hydroamination reactions

In the example shown in Figure 2.6, the starting materials are primary aminoalkenes that can follow either pathway, but the product of monocyclization is a secondary aminoalkene that

can only follow the insertion pathway. It has been shown experimentally and computationally that neutral zirconium complexes catalyze exclusively the cyclization of primary amines following the imido pathway.[23, 24] On the contrary, cationic zirconium complexes have been shown to follow the insertion pathway.[12, 25] Based on these results, changing a zirconium catalyst from neutral to cationic should switch the mechanism that reaction is following and enable the monocyclized product to undergo a second hydroamination reaction. As shown in Figure 2.5, a two-step bicyclization can be switched on/off by changing the electronic properties of a zirconium catalyst.

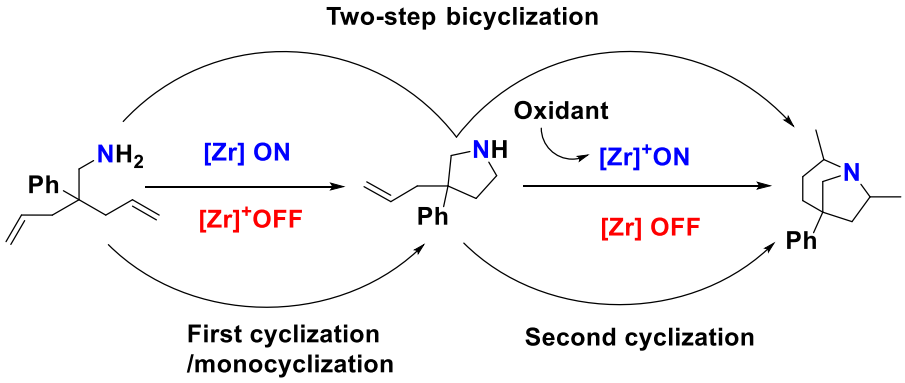

Figure 2.6: Proposed two-step bicyclization

2.1.3 Redox-active catalysts for monocyclization and bicyclization of aminodialkenes

We developed the [OSSO]-type ligated zirconium complexes (thiolfan*)$Zr(NEt_2)_2$ and (thiolfan*)$Zr(NMe_2)_2$ that can form neutral and oxidized zirconium compounds *in situ* when triggered by the oxidation/reduction of the redox-active ferrocene backbone. As discussed in the previous sections, the neutral zirconium compounds exclusively catalyze primary aminoalkenes following the imido pathway, whereas cationic zirconium compounds can catalyze both primary and secondary, or selectively catalyze only secondary aminoalkenes. [6-14, 26]

One can fuse the selectivity of primary and secondary amino substrate by designing a neutral zirconium catalyst that only catalyzes the hydroamination of primary amines following the imido pathway. After that, the cationic catalyst can be generated *in situ*, follows the insertion pathway and exclusively catalyzes secondary amino substrates. Thus, a selective hydroamination of primary or secondary aminoalkenes *in situ* with one catalyst by changing the oxidation state of the central metal is provided (Figure 2.7). We propose that the oxidation of the ferrocene backbone in our zirconium complexes can induce a positive charge to form a cationic/oxidized zirconium complex, whereas, in the previous studies, the zirconium cation was usually generated by adding $[Ph_3C][B(C_6F_5)_4]$.[11]

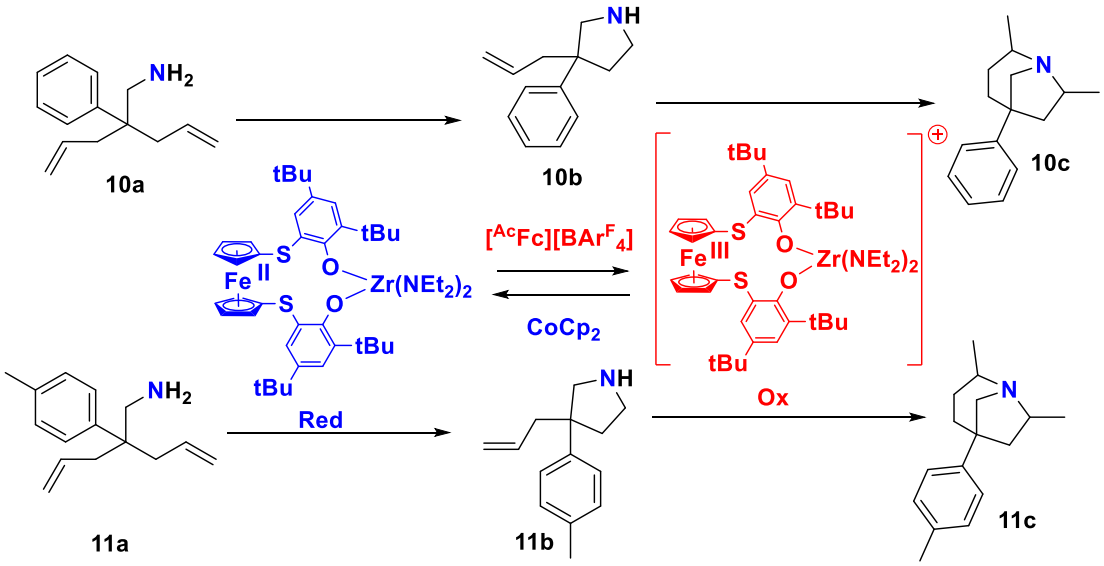

Figure 2.7: Proposed two-step-cyclization catalyzed by neutral (Red) and oxidized (Ox) (thiolfan*)$Zr(NEt_2)_2$

2.1.4 Bronsted acid catalysts for hydroamination reactions

The choice of oxidant was made based on the oxidation peak observed in the CV diagrams (Figures 1.9 and 1.10). The Fc/Fc^+ couple has been widely applied in redox reactions. However,

the choice of counter anion was tricky. Studies have shown that an increased catalytic activity of late transition metal complexes was observed with bulkier and less coordinating anions.[3] Although not many studies focused on the counter anion effect on early transition metal catalyzed hydroamination reactions, Bronsted acids have been shown to act as co-catalysts in late transition metal catalyzed hydroamination reactions.[3] For cationic zirconium catalyzed hydroamination reactions, $B(C_6F_5)_4^-$ has often been used as the counter ion.[11, 17] $[BAr^F]^-$ is similar to $B(C_6F_5)_4^-$, and, under most circumstances, can perform as a bulky and less coordinating counter anion.

However, recent studies have shown that the anions in common oxidants such as AgOTf, $AgBF_4$ and $AcFcBAr^F$ may act as co-catalysts that might get involved by forming the corresponding ammonium salt.[27] Studies have shown that ammonium salts such as $[PhMe_2NH][B(C_6F_5)_4]$ can effectively catalyze hydroamination reactions.[28]

2.2 Results and Discussion

2.2.1 Hydroamination reactions catalyzed by the reduced state of (thiolfan*)Zr(NEt$_2$)$_2$

To investigate the ability of neutral (thiolfan*)$Zr(NEt_2)_2$ to catalyze intramolecular hydroamination reactions, a catalytic amount (10 mol%) of (thiolfan*)$Zr(NEt_2)_2$ was added to a J-Young tube with the aminoalkene/alkyne of interest and an internal standard, HMB, and the reaction mixture was heated to 100 °C in C_6D_6. The conversion was calculated based on the increase of a product peak or the decrease of a reactant peak versus the peak at 2.13 ppm in ^{1}H NMR spectrum for the internal standard. A summary of experiments is presented in Figure 2.7. The results show that neutral (thiolfan*)$Zr(NEt_2)_2$ can catalyze cyclization of the primary aminoalkene **1a** in 48 h, while the oxidized (thiolfan*)$Zr(NEt_2)_2$ species showed no conversion after 20 h. In contrast, neutral (thiolfan*)$Zr(NEt_2)_2$ showed no reactivity toward the secondary

aminoalkene **2a**, but oxidized (thiolfan*)Zr(NEt_2)$_2$ can catalyze the cyclization of **2a** in 20h. Unfortunately, (thiolfan*)Zr(NEt_2)$_2$ was not active towards other substrates: no conversion was observed for substrates **3a-6a** with either state of the catalyst, likely due to steric or electronic reasons. However, the results obtained with **1a** and **2a** indicate that there is selectivity between primary and secondary aminoalkenes triggered by the oxidation state of the zirconium catalyst.

Unfortunately, the selectivity was lost with primary aminoalkynes: **7a** was observed to cyclize in the presence of both neutral and oxidized (thiolfan*)Zr(NEt_2)$_2$. Interestingly, the hydroamination of the secondary aminoalkyne **8a** can only be catalyzed by the oxidized catalyst.

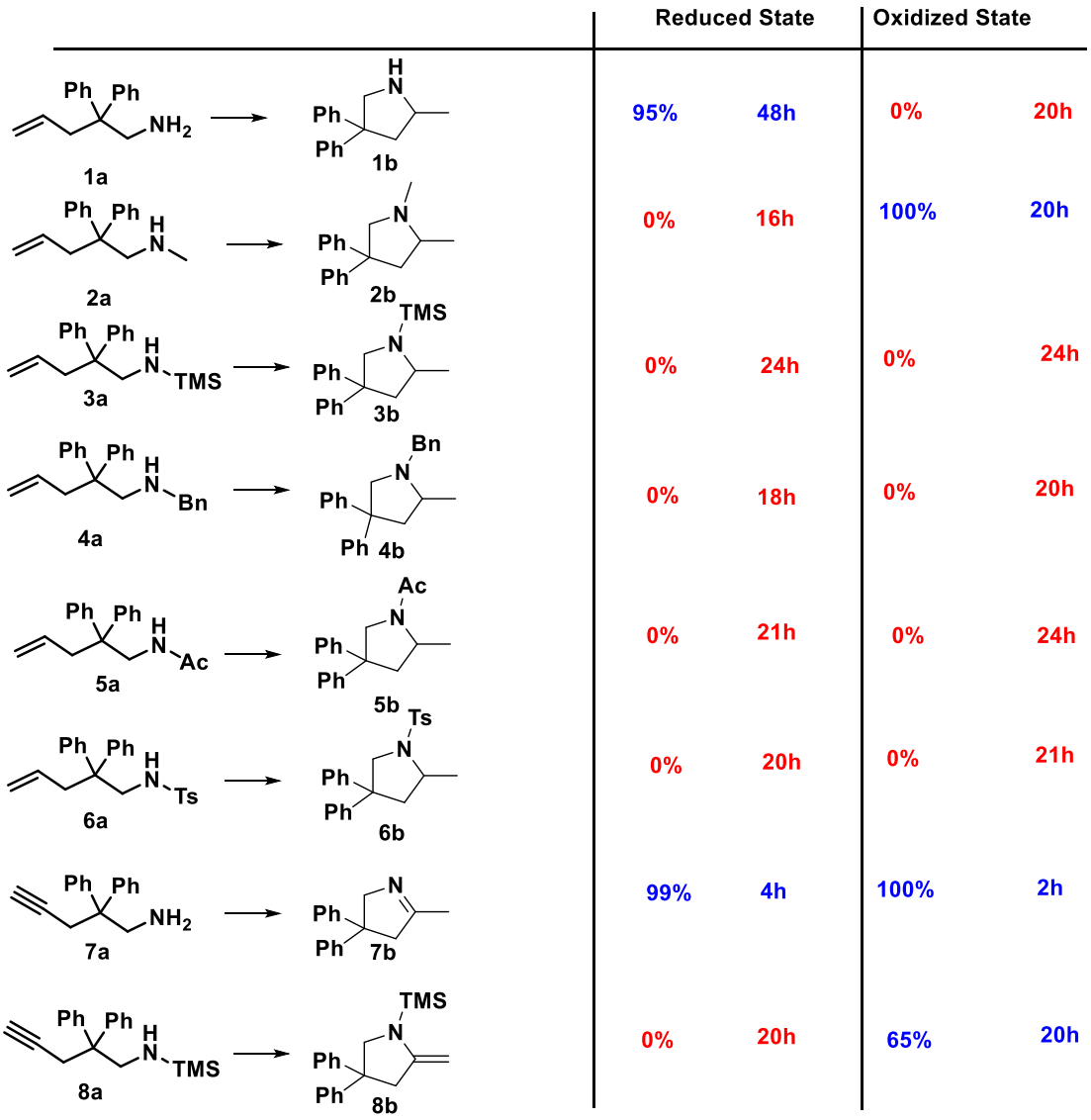

Table 2.1 Intramolecular hydroamination catalyzed by (thiolfan*)$Zr(NEt_2)_2$; conditions: 10 mmol% (thiolfan*)$Zr(NEt_2)_2$, 0.5 mL C_6D_6, 100 °C

Based on the results obtained with **1a** and **2a**, we decided to test the selectivity between primary and secondary aminoalkenes within one substrate. Aminodialkene substrates **9a**, **10a**, and **11a** were synthesized and tested for the two-step bicyclization reaction discussed in Section 2.1.3. Due to a lower Thorpe-Ingold effect, [27] no conversion of **9a** to **9b** was observed. Fortunately, **10a**

was successfully converted to **10b** in the presence of neutral (thiolfan*)$Zr(NEt_2)_2$ in *o*-$C_6F_2H_4$ at 110 °C. As described in Figure 2.7, the primary aminodialkene should undergo one cyclization to form the five-membered heterocycle **10b**. The monocyclized product **10b** is a secondary aminoalkene and should undergo the second cyclization to form the bicyclic product **10c**. Same principle applies to **11a** and the formation of the monocyclized product **11b** was observed. However, the second hydroamination reaction was not successfully achieved. One possible explanation is that the zirconium catalyst decomposed after the reaction was completed. To verify that, the reaction mixture from **10b** was divided into two portions equally. Additional 0.5 eq of (thiolfan*)$Zr(NEt_2)_2$ and 0.5 eq of the oxidant $AcFcBAr^F$ were added to one portion. No extra zirconium but only 0.5 eq of the oxidant was added to the other portion. Neither reaction showed conversion to the final product **10c** after heating. Interestingly, when only the oxidant was added at room temperature to the solution of **10b**, the two doublets at 1.2 ppm in ^1H NMR spectrum from **10b** started merging together and forming a triplet which indicates the formation of a new species. However, the triplet started splitting upon heating the reaction mixture and only **10b** was isolated after the work-up. Unfortunately, no other peaks for **10c** was not observed. The changes in the ^1H NMR spectrum of this reaction are possible due to the decomposition of the oxidized zirconium complex. The triplet may indicate an intermediate formed during the decomposition. Purified **10b** was employed to react with the oxidized (thiolfan*)$Zr(NEt_2)_2$ in *o*-$F_2C_6H_4$ and heated to 110 °C. No product was observed after 46 hours.

Another possible explanation for the inability to obtain **10c** is that the oxidized (thiolfan*)$Zr(NEt_2)_2$ compound was unstable at high temperature so it decomposed and reacted with some impurities in the reaction mixture before it had a chance to react with **10b**. In addition, the second cyclization requires harsher reaction condition as shown in the examples in Figure 2.3.

Therefore, several factors likely contribute to the failure to achieve the bicyclization reaction when employing a redox switch.

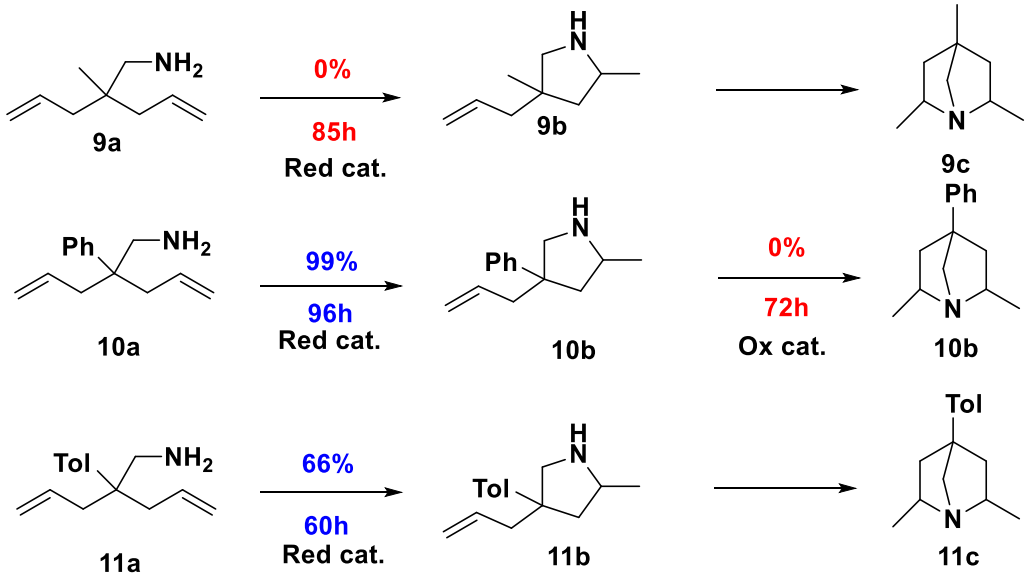

Figure 2.8 Bicyclization catalyzed by neutral ("Red cat.") and oxidized ("Ox cat.") (thiolfan*)$Zr(NEt_2)_2$; conditions: 10 mmol% (thiolfan*)$Zr(NEt_2)_2$, 2 ml *o*-$F_2C_6H_4$, 110 °C

2.2.2 Intermolecular hydroamination reactions

Intermolecular hydroamination reactions were also tested and the results are summarized in Figure 2.9. Unfortunately, no reactivity was observed using (thiolfan*)$Zr(NEt_2)_2$. Since intermolecular hydroamination is more difficult to achieve than intramolecular hydroamination, harsher conditions are necessary. Our zirconium compound, unfortunately, is not active enough to catalyze intermolecular hydroamination reactions at 100 °C in C_6D_6.

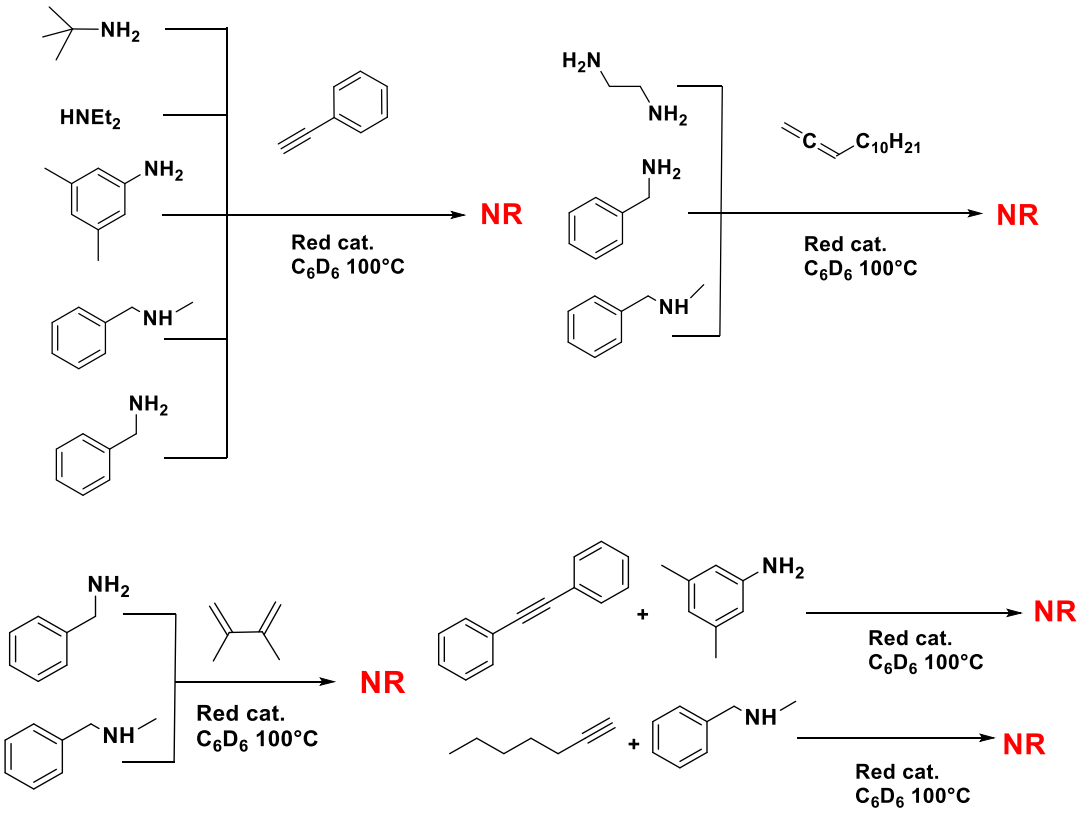

Figure 2.9 Intermolecular hydroamination catalyzed by (thiolfan*)Zr(NEt_2)$_2$

2.2.3 Control reactions

Control experiments were performed to minimize the effect of $AcFcBAr^F$ in the cyclization reactions. Full conversion of **2a** to **2b** was observed when a catalytic amount of $AcFcBAr^F$ was added and the reaction was heated to 100 °C. To further understand the reasons behind this observation, several experiments using a catalytic amount of AcFc, $FcPF_6$, $NaBAr^F$, and $FcBAr^F$ were performed with **2a**. After 2 hours, no conversion was observed for AcFc and $FcPF_6$, partial conversion was observed for $NaBAr^F$, and full conversion was observed for $FcBAr^F$. AcFc was shown in ^{1}H NMR spectra of $AcFcBAr^F$, $NaBAr^F$, and $FcBAr^F$.

One possible explanation is that the aminoalkene reduced $AcFcBAr^F$ to AcFc and the reaction was catalyzed by a Bronsted acid.[17] Michon and coworkers reported that HBF_4, generated *in situ* from $AgBF_4$ was able to catalyze the hydroamination of secondary aminoalkynes.[30] Similarly, when $AcFcBAr^F$ was served as a precatalyst in the hydroamination reactions, $HBAr^F$ was generated *in situ* and combined with the amine substrate to generate an ammonium $[BAr^F]^-$ salt as the active catalyst (Figure 2.10). The difference in reaction rate was resulted from the difference in solubility of the $[BAr^F]^-$ precatalysts. However, it remained puzzled that the $[BAr^F]^-$ precatalysts only promoted the cyclization of the secondary aminoalkenes but not the primary aminoalkenes.

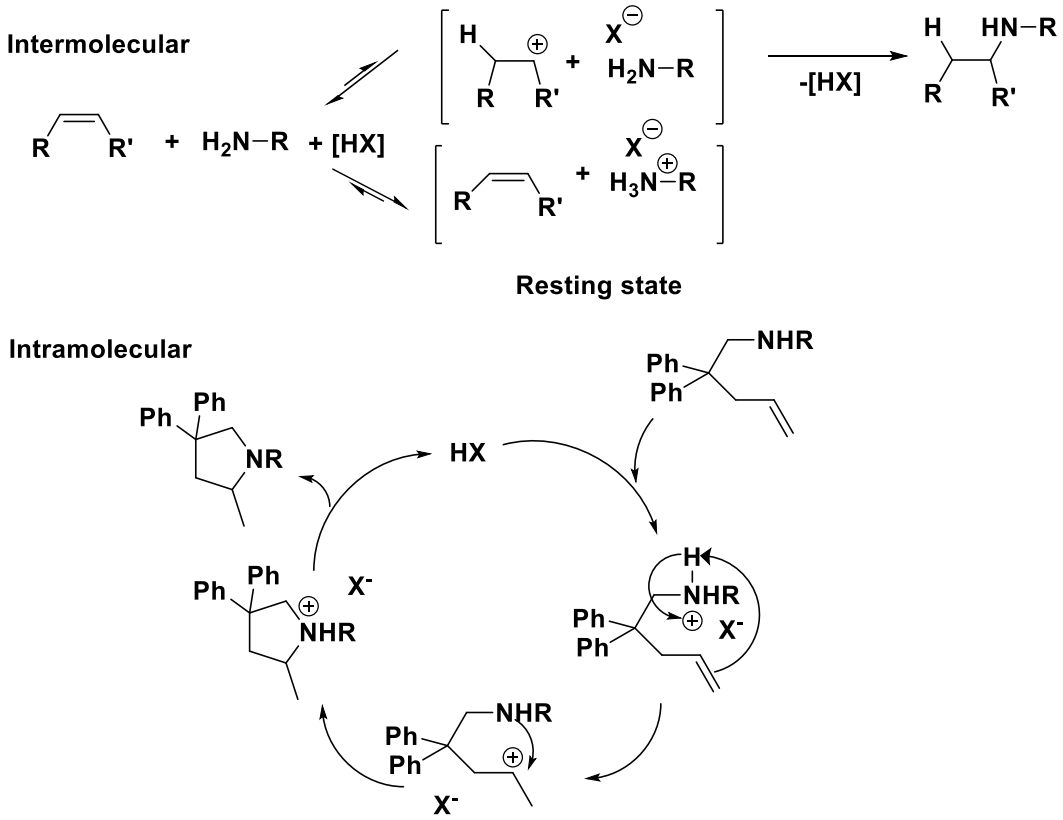

Figure 2.10: Bronsted acid catalyzed hydroamination

Fortunately, the neutral (thiolfan*)$Zr(NEt_2)_2$ cannot catalyze hydroamination of the secondary aminoalkene, so we decided to make the ratio of zirconium compound to the oxidant 10:9. Excess neutral zirconium compound should not affect the results of hydroamination of the secondary aminoalkene. By premixing the oxidant (9 mol%) with (thiolfan*)$Zr(NEt_2)_2$ (10 mol%) before the addition of substrate, we ensured that all $AcFcBAr^F$ was used up to oxidized (thiolfan*)$Zr(NEt_2)_2$, so that Bronsted acid-catalyzed hydroamination should be avoided.

2.3 Experimental

2.3.1 Synthesis and characterization of amine substrates

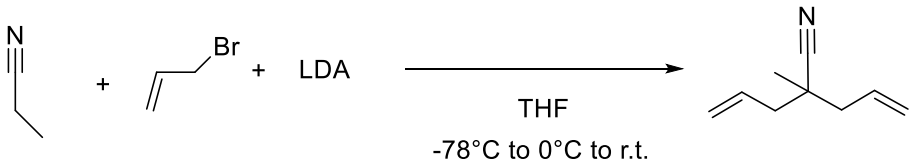

2-allyl-2-methylpent-4-enenitrile was synthesized according to a published procedure.[31] A solution of ^{n}BuLi (38.5 mL, 100 mmol, 2.5 M in hexanes) was added dropwise to a solution of di-*iso*-propylamine (10.38 g, 102.6 mmol) in THF (45 mL) at -78 °C. The resulting light-yellow solution was stirred for 90 min at 0 °C. 49 mL of lithium di-*iso*-propylamine (LDA) solution was transferred to an addition funnel and added dropwise to a solution of propionitrile (2.89 g, 52.5 mmol) in THF at -78 °C. The solution was stirred for 90 min at this temperature and then treated with allyl bromide (5.99 g, 49.5 mmol). The solution was stirred for another 30 min at -78 °C and allowed to warm up to room temperature. After one hour, the solution was cooled back to -78 °C, and the second portion of LDA was added over 30 min. The solution was allowed to warm to 0 °C and stirred for 30 min. After cooling back to -78 °C, the solution was treated with allyl bromide (7.30 g, 60.3 mmol). The reaction mixture was allowed to warm up to the room temperature and

stirred overnight. The reaction was quenched by the addition of water. Then the volatiles were removed under a reduced pressure. The product was extracted into diethyl ether (200 mL), washed with brine (2×30 mL), and then water (10 mL). After drying over $MgSO_4$, the volatiles were removed under a reduced pressure. A silica column eluted with 5% ethyl acetate in hexanes was used to purify the crude product, yielding 6 g of a yellow liquid (48%). ^{1}H NMR ($CDCl_3$, 300 MHz, 25 °C): δ 1.20 (s, 3H, CH_3), 2.20-2.30 (dq, 4H *C*H_2CCN), 5.19 (m, 4H, C*H*$_2$=CH), 5.84 (m, 2H CH_2=C*H*).

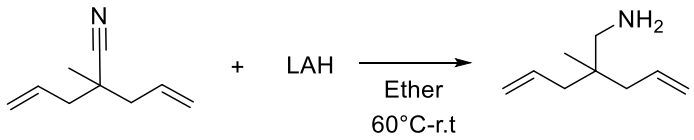

2-ally-2-(methyl)-pent-4-en-1-amine was synthesized according to a published procedure.[31] 1.162 g (30.6 mmol) of LAH was dissolved in 20 mL of diethyl ether. 3.765 g (27.8 mmol) of 2-allyl-2-methylpent-4-enenitrile was dissolved in 10 mL of diethyl ether and added to the slurry of LAH in a 100 mL Schlenk tube inside the glovebox. The reaction solution was refluxed at 60 °C for 2 h and stirred at room temperature overnight. The suspension was diluted with a double amount of diethyl ether and quenched with 10 mL of water. 4 mL of 15% NaOH followed by 10 mL of water was added. The diethyl ether phase was decanted from the white precipitate. The precipitate was extracted into diethyl ether 3 times, 60 mL total. The organic layers were combined and dried over $MgSO_4$. The volatiles were removed under a reduced pressure yielding 1.9 g (50%) of a light yellow liquid. ^{1}H NMR ($CDCl_3$, 300 MHz, 25 °C): δ 0.83 (s, 3H, CH_3), 2.00(d, 4H, *C*H_2CCN), 2.46 (s, 2H, C*H*$_2$$NH_2$) 5.0 (m, 4H, C*H*$_2$=CH), 5.84 (m, 2H CH_2=C*H*).

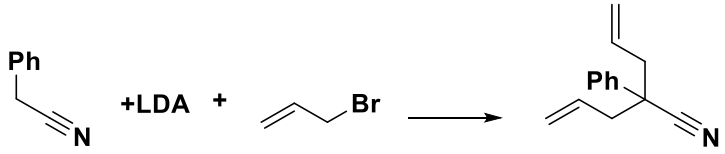

2-allyl-2-phenylpent-4-enenitrile was synthesized according to a published procedure.[31] 4.2 g (2.3 eq) of LDA was dissolved in THF and cooled to -78 °C inside the glovebox. 2 g (17 mmol, 1 eq) of benzyl cyanide was dissolved in 5 mL THF and added dropwise to LDA solution and stirred at -78 °C for 30 min. Allyl bromide (5.14 g, 42.5 mmol, 2.5 eq) was added neat and the mixture was stirred at -78 °C to room temperature for 1 h. The reaction solution was taken out of the box and saturated ammonium chloride (10 mL) was added. The mixture was extracted with diethyl ether. The combined organic layer was washed with brine and dried over Na_2SO_4. The crude product was passed through a silica column eluted with pure hexanes.^{1}H NMR ($CDCl_3$, 300 MHz, 25 °C): δ 2.89 (m, 4H, C*H*$_2$CCN), 5.15 (m, 4H C*H*$_2$=CH), 5.66 (m, 2H, CH_2=C*H*).

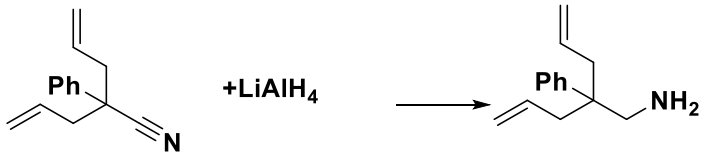

2-allyl-2-(phenyl)-pent-4-en-1-amine was synthesized according to published procedure.[31] 2.4 g (12.2 mmol) of 2-allyl-2-phenylpent-4-enenitrile was dissolved in 5 mL of THF and added slowly to a suspension of LAH (1.39 g, 36.5 mmol) cooled at -78 °C. The mixture was stirred at room temperature overnight. The mixture was quenched by a 1 M NaOH solution and the solids were filtered off, rinsed with diethyl ether and concentrated under a reduced pressure. The crude solution mixture was stirred with CaH_2 for an hour in dry diethyl ether and the volatiles were removed under a reduced pressure. ^{1}H NMR ($CDCl_3$, 300 MHz, 25 °C): δ 0.42 (br, 2H, N*H*$_2$), 2.40 (d, 4H, C*H*$_2$CCN), 2.76 (s, 2H, C*H*$_2$NH$_2$) 4.97 (m, 4H, C*H*$_2$=CH), 5.60 (m, 2H, CH_2=C*H*).

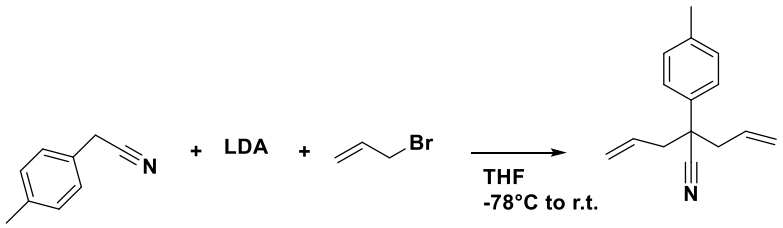

2-allyl-2-(*p*-tolyl)-pent-4-enenitrile was synthesized according to a published procedure.[31] Inside the glovebox, 12.07 mL (2.2 M, 26.3 mmol) of ^{n}BuLi was added to a di-*iso*-propylamine (3.177 g) solution in 30 mL of THF at -78 °C. The LDA solution was stirred for 1h at 0 °C. 21 mL of the LDA solution was added to a *p*-tolyacetonitrile (1.75 g, 13.3 mmol) solution in 35 mL THF solution resulting in an orange solution which was stirred at -78 °C for 90 min. 1.57 g (24.99 mmol) of allyl bromide was added dropwise at -78 °C and stirred for 15 min then slowly warmed up to room temperature. and stirred for 90 min. The resulting light orange solution was again cooled to -78 °C and 15 mL of LDA solution was added. The solution was stirred at 0 °C for 1 h then cooled to -78 °C and 1.94 g (30.6 mmol) of allyl bromide was added. The reaction was slowly warmed to room temperature and stirred overnight. The reaction was worked up by quenching it with 10 mL of water and removal of all solvent. The resulting crude product was extracted with diethyl ether, washed with water and brine, and dried over Na_2SO_4. The volatiles were removed under a reduced pressure and the crude product was purified by a silica column eluted with 10% ethyl acetate in Hex yielding a light yellow liquid 2.07 g (72%). ^{1}H NMR ($CDCl_3$, 300 MHz, 25 °C): δ 2.39 (s, 3H, C*H*$_3$), 2.79 (d, 4H, C*H*$_2$CCN), 5.20 (m, 4H, C*H*$_2$=CH), 5.88 (m, 2H, CH$_2$=*CH*), 7.21 (d, 2H Ar*H*), 7.34 (d, 2H Ar*H*).[20]

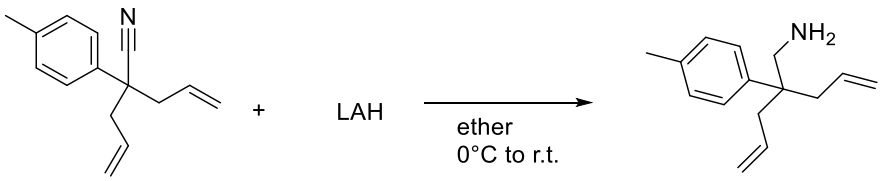

2-allyl-2-(*p*-tolyl)-pent-4-en-1-amine was synthesized according to a published procedure.[31] 0.92 g (4.35 mmol) of 2-allyl-2-(*p*-tolyl)-pent-4-enenitrile was added to 0.5 g (13.2 mmol) of a LAH solution in 100 mL diethyl ether at 0 °C. The reaction was warmed to room temperature and stirred overnight. The reaction was quenched by adding 10 mL of water at 0 °C and stirred at room temperature for an hour. The diethyl ether fraction was decanted, and the precipitate was extracted with diethyl ether 3 times and combined with the decanted fraction. The combined fraction was dried by Na_2SO_4 and the volatiles were removed under a reduced pressure yielding 0.89 g (96%) of a light yellow liquid. ^{1}H NMR ($CDCl_3$, 300 MHz, 25 °C): δ 0.84 (br, 2H N*H*$_2$), 2.32 (s, 3H, C*H*$_3$), 2.44 (d, 4H, C*H*$_2$CCN), 2.88 (s, 2H, *CH*$_2$NH$_2$), 5.00 (m, 4H, C*H*$_2$=CH), 5.61 (m, 2H, CH$_2$=*CH*), 7.16 (m, 4H Ar*H*).

2.3.2 Hydroamination reactions catalyzed by the reduced state of (thiolfan*)Zr(NEt$_2$)$_2$

General procedure: (thiolfan*)Zr(NEt$_2$)$_2$ (0.01 mmol, 10 mol%) was dissolved in C_6D_6 and added to a J-Young tube. The hydroamination substrate (0.1 mmol) was also dissolved in C_6D_6 and added to the J-Young tube. The tube was sealed and analyzed for a 0-hour ^{1}H NMR spectrum before being heated to 100 °C. Reactions were monitored by ^{1}H NMR spectroscopy.

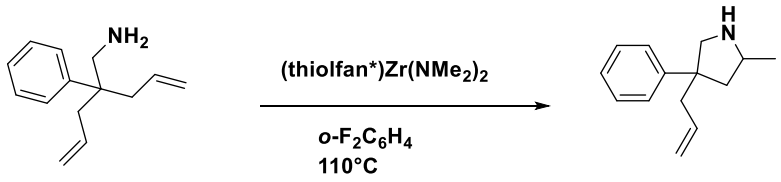

Inside the glovebox, 39 mg (0.048 mmol 10 mol%) of (thiolfan*)Zr(NEt$_2$)$_2$ was dissolved in 2mL *o*-$F_2C_6H_4$ in a 25 mL Schlenk tube, then 96.5 mg (0.48 mmol) of substrate was added. ^{1}H NMR spectrum was taken at t=0 by taking an aliquot of the reaction solution. The reaction was monitored

by ^{1}H NMR spectroscopy. 50% conversion was achieved at t=36 h after heating at 110 °C and full conversion was achieved after heating for 4 days.

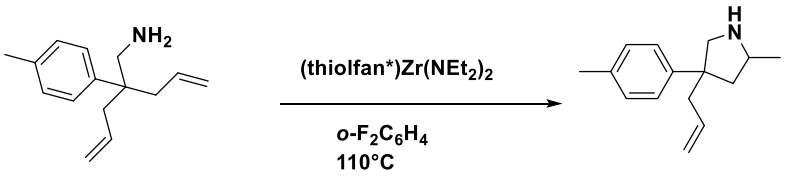

Inside the glovebox, 18.4 mg (0.021 mmol 10 mol%) of (thiolfan*)Zr(NEt_2)$_2$ was dissolved in 1 mL *o*-$F_2C_6H_4$ in a 25 mL Schlenk tube, then 46.96 mg (0.218 mmol) of substrate was added. ^{1}H NMR spectrum was taken at t=0 by taking an aliquot of the reaction solution. The reaction was monitored by ^{1}H NMR spectroscopy. 60% conversion was achieved after heating for 60 hours at 110 °C.

2.3.3 Hydroamination reactions catalyzed by the oxidized state of (thiolfan*)Zr(NEt_2)$_2$

General procedure: (thiolfan*)Zr(NEt_2)$_2$ (0.01 mmol, 10 mol%) was dissolved in C_6D_6 and added to a J-Young tube. $AcFcBAr^F$ (10.91 mg, 0.009 mmol, 9 mol%) was then added to the J-Young tube leading to a color change from yellow to brown. The tube was shaken until all solids dissolved. Then the hydroamination substrate (0.1 mmol) was dissolved in C_6D_6 and added to the J-Young tube. The tube was then sealed and analyzed for a 0-hour ^{1}H NMR spectrum before being heated to 100°C. Reactions were monitored by ^{1}H NMR spectroscopy.

2.3.4 Control experiments

General procedure: (1) $AcFcBAr^F$ (0.01 mmol, 10 mol%) was dissolved in C_6D_6 and added to a J-Young tube. The hydroamination substrate (0.1 mmol) was dissolved in C_6D_6 and added to the J-

Young tube. The tube was then sealed and analyzed for a 0-hour ^{1}H NMR spectrum before being heated to 100 °C. Reactions were monitored by ^{1}H NMR spectra. (2) (0.01 mmol 10 mol%) of AcFc/ $FcPF_6$/ $NaBAr^F$/ or $FcBAr^F$ was dissolved in 0.5 mL of C_6D_6: *o*-$F_2C_6H_4$ in a volume ratio of 4:1 with *N*-methyl-2,2-diphenylpent-4-en-1-amine in a J-Young tube. The tube was then sealed and analyzed for a 0-hour ^{1}H NMR spectrum before being heated to 100 °C.

2.4 References

(1) Stubbert, B. D; Marks, T. J. *J. Am. Chem. Soc***. 2007**, 129, 4253.

(2) Odom, A. L. *Dalton Trans.* **2005**, 225.

(3) Muller, T. E.; Kai C. Hultzsch, K. C.; Yus, M.; Foubelo, F.; Tada, M. *Chem. Rev.* **2008,** *108,* 3795.

(4) (a) Tian, S.; Arredondo, V. M.; Stern, C. L.; Marks, T. J. *Organometallics* **1999**, *18*, 2568.

(b) Li, Y.; Marks, T. J. *J. Am. Chem. Soc.* **1996**, *118*, 9295. (c) Li, Y.; Marks, T. J. *J. Am. Chem. Soc.* **1996**, *118*, 707.

(5) Seayad, J.; Tillack, A.; Hartung, C. G.; Beller, M. *Adv. Synth. Catal.* **2002**, 344, 795.

(6) Majumder, S.; Odom, A. L. *Organometallics*, **2008**, 27, 1174.

(7) Stubbert, B. D.; Marks, T. J. *J. Am. Chem. Soc.* **2007**,129, 6149.

(8) Meuller, C.; Saak, W.; Doye, S. *Eur. J. Org. Chem.* **2008**, 2731.

(9) Leitch, D. C.; Payne, P. R.; Dunbar, C. R.; Schafer, L. L. *J. Am.Chem. Soc*. **2009**, 131, 18246.

(10) Hu, Y.-C.; Liang, C.-F.; Tsai, J.-H.; Yap, G. P. A.; Chang, Y.-T.; Ong, T.-G. *Organometallics* **2010**, 29, 3357.

(11) Wang, X.; Chen, Z.; Sun, X.; Yong Tang, Y.; Xie, Z. *Org. Lett.* 13, 18, **2011** 13(18), 4758.

(12) Gribkov, D. V.; Hultzsch, K. C. *Angew. Chem. Int. Ed*. **2004**, 43, 5542.

(13) Knight, P. D.; Munslow, I.; O'Shaughnessy, P. N.; Scott, P. *Chem. Commun.* **2004**, 894.

(14)Tobisch, S. *Inorg. Chem*. **2012**, 51, 3786.

(15) Li, Y.; Marks, T. J. *J. Am. Chem. Soc*. **1998**, 120, 1757.

(16) Robins, D. J. *Nat. Prod. Rep.* **1994**, *11*, 613.

(17) Hultzsch, K. C.; Hampel, F.; Wagner, T. *Organometallics* **2004,** *23*, 2601.

(18) Zhang, Y.; Sun, Q.; Wang, Y.; Yuan, D.; Yao, Y.; Shen, Q. *RSC Adv*. **2016**, 6, 10541.

(19) Zhou, X.; Wei, B.; Sun, X. L.; Tang, Y.; Xie, Z. *Chem. Commun*. **2015**, 51, 5751.

(20) Eedugurala, N.; Wang, Z.; Yan, K.; Boteju, K. C.; Chaudhary, U.; Kobayashi, T.; Ellern, A.; Slowing, I. I.; Pruski, M.; Sadow, A. D. *Organometallics* **2017**, 36, 1142.

(21) Ananikov, W. P.; Tanaka, M. *Hydrofunctionalization* Springer: New York, **2013**.

(22) Hultzsch. K. C.; Gribkov, D. V.; Hampel, F. *Journal of Organometallic Chemistry* **2005**, 690, 4441.

(23) McGrane, P. L.; Jensen, M.; Livinghouse, T. *J. Am. Chem. Soc*. **1992**, 114, 5459.

(24) Watson, D. A.; Chiu, M.; Bergman, R. G. *Organometallics* **2006**, 25, 4731.

(25) Knight, P. D.; Munslow, I.; O'Shaughnessy, P. N.; Scott, P.; *Chem. Commun*. **2004**, 894.

(26) Tobisch, S. *Inorg. Chem.* **2012**, 51, 3786−3795.

(27) Chen, J.; Goforth, S. K.; McKeown, B. A.; Gunnoe, T. B.; *Dalton Trans*. **2017**, 46, 2884.

(28) Ackermann, L.; Kaspar, L. T.; Althammer, A. *Org. Biomol. Chem*. **2007**, 5, 1975.

(29) Jung, M. E.; Piizzi, G. *Chem. Rev*. **2005**, 105, 1735.

(30) Michon, C.; Medina, F.; Capet, F.; Roussel P.; Agbossou-Niedercorn, F. *Adv. Synth. Catal.* **2010**, 352, 3293.

(31) Manna, K.; Naresh Eedugurala, N.; Sadow, A. D. *J. Am. Chem. Soc*. **2015**, 137, 425.

Chapter 3: Conclusions

(thiolfan*)$Zr(NEt_2)_2$ and (thiolfan*)$Zr(NMe_2)_2$ were successfully synthesized and characterized by ^1H NMR spectroscopy, ^{13}C NMR spectroscopy, and elemental analysis. Cyclic voltammetry was used to understand the electrochemical properties of the zirconium compounds. The intramolecular hydroamination of aminoalkenes and alkynes was achieved with (thiolfan*)$Zr(NEt_2)_2$. We found that the reduced form of (thiolfan*)$Zr(NEt_2)_2$ can catalyze the hydroamination reactions of the primary aminoalkenes, whereas the oxidized form can catalyze the hydroamination reactions of the secondary aminoalkenes. Switching the metal complex *in situ* between its reduced and oxidized state with redox reagents resulted in selectivity towards the primary versus the secondary aminoalkenes. The selectivity was lost in cyclizing the primary aminoalkyne substrate. No catalytic activity was observed for the neutral (thiolfan*)$Zr(NEt_2)_2$ in intermolecular hydroamination reactions. A bicyclization reaction of aminodialkenes was performed with neutral and oxidized (thiolfan*)$Zr(NEt_2)_2$, but only monocyclization catalyzed by the neutral zirconium compound was observed.

Appendix:

Chapter 1:

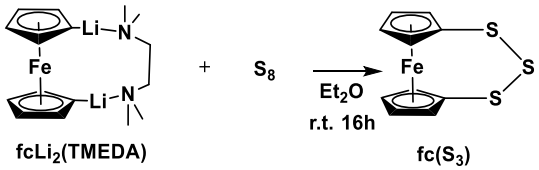

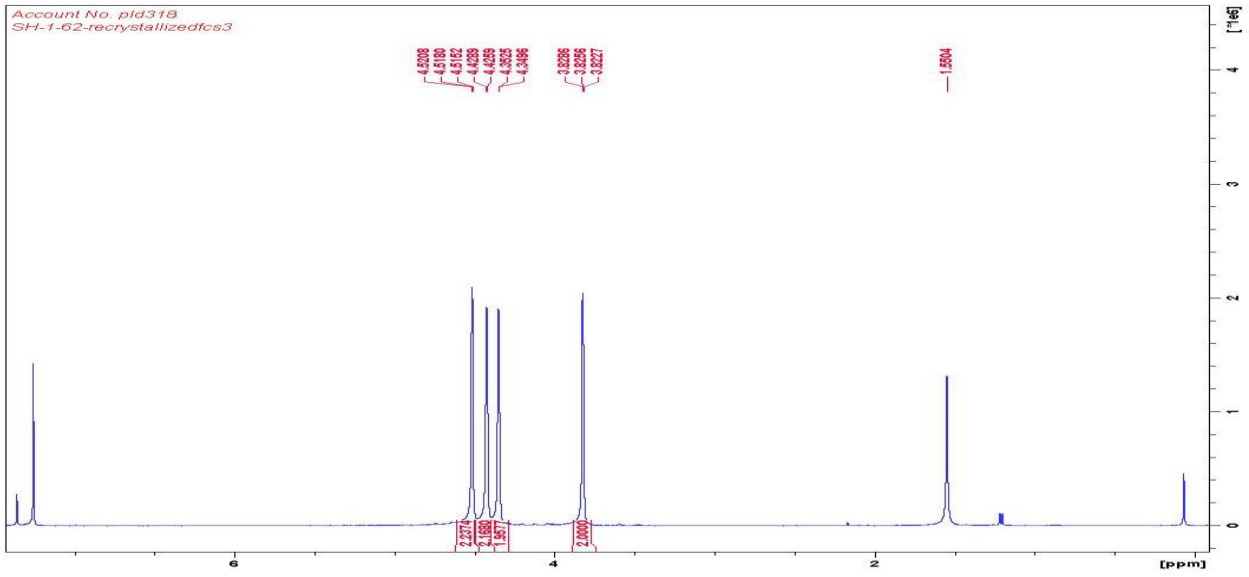

Figure A-1: ^{1}H NMR spectrum ($CDCl_3$, 400MHz, 298K) of 1,2,3-trithia-[3]-ferrocenophane

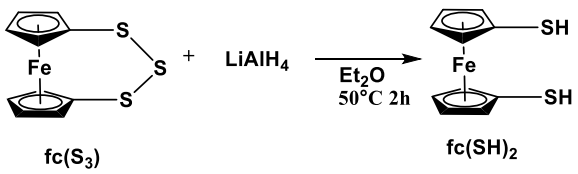

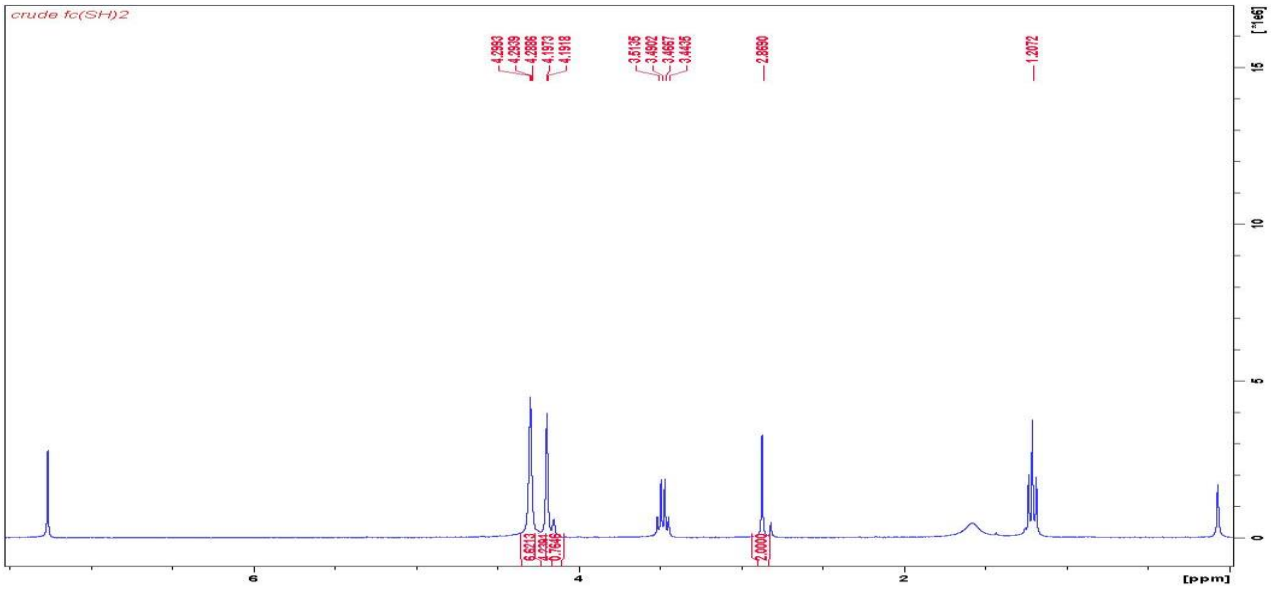

Figure A-2: ^{1}H NMR spectrum ($CDCl_3$, 400MHz, 298K) of 1,1'-dithiolferrocene

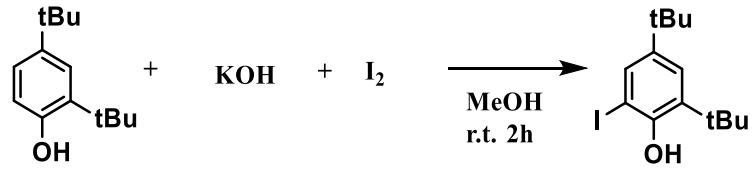

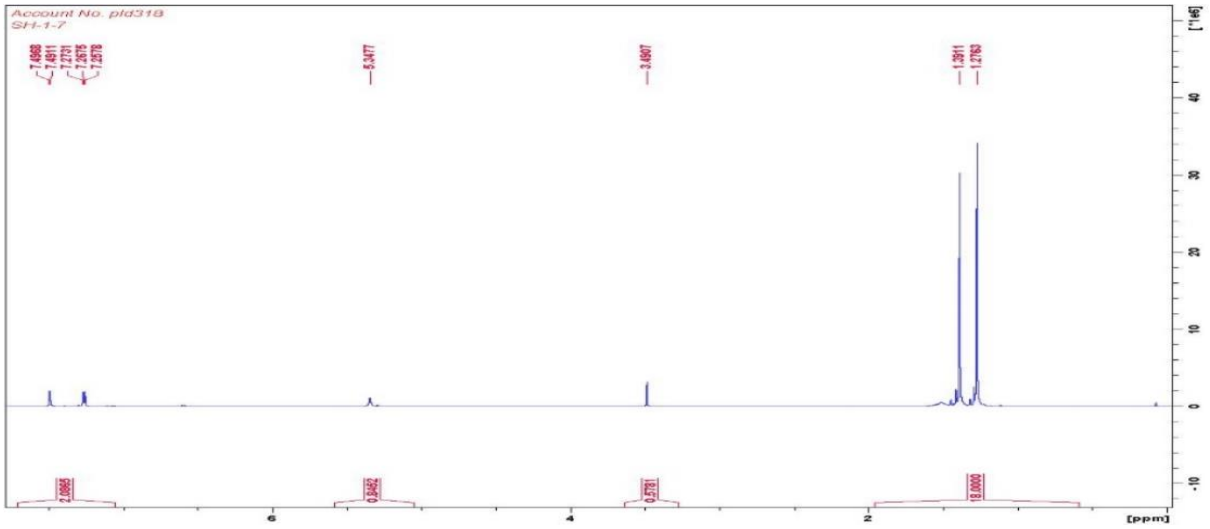

Figure A-3: ^{1}H NMR spectrum ($CDCl_3$, 400MHz, 298K) of 2,4-di-*tert*-butyl-6-(hydroxymethyl)phenol

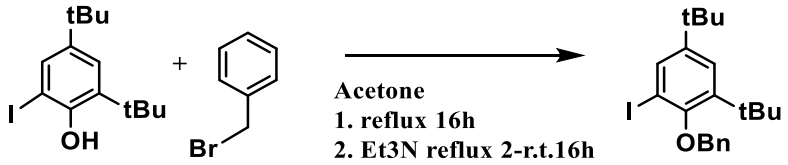

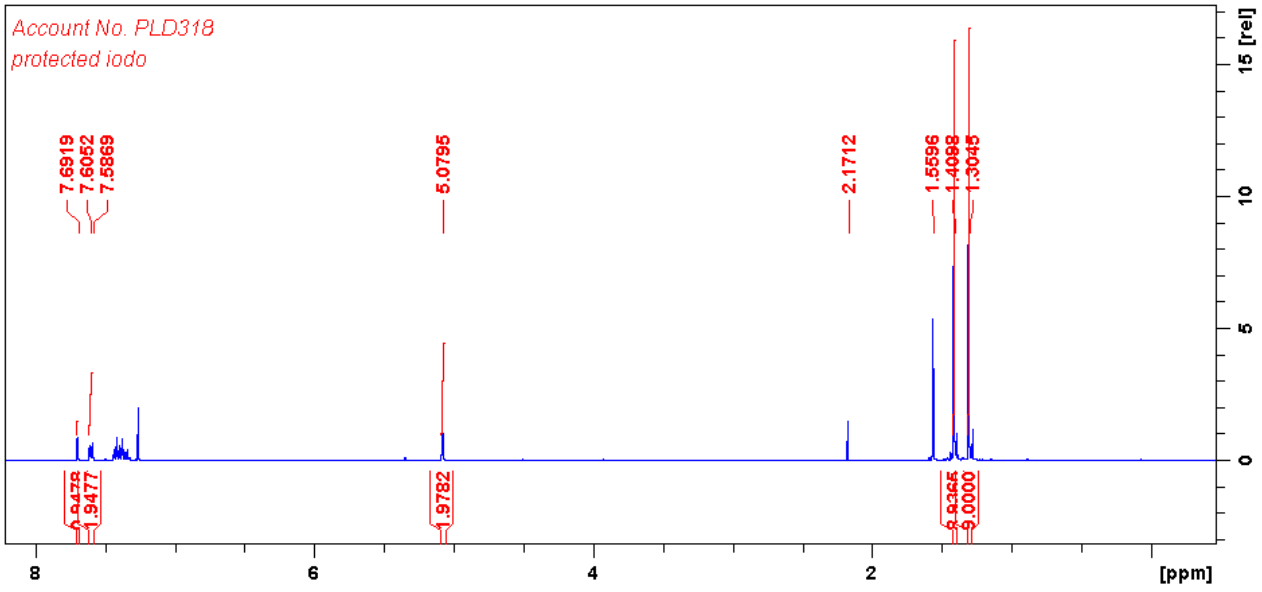

Figure A-4: ^{1}H NMR spectrum ($CDCl_3$, 300MHz, 298K) of 2-(bromomethyl)-4,6-di-*tert*-butylphenol

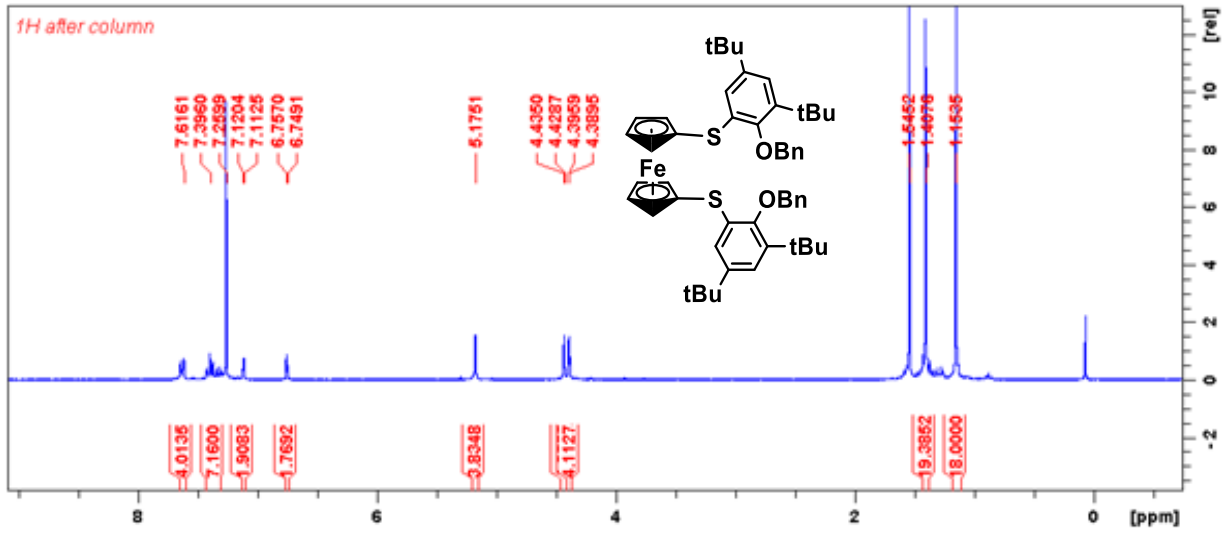

Figure A-5: ^{1}H NMR spectrum ($CDCl_3$, 300MHz, 298K) of 2-benzoxy-3,5-di-*tert*-butyl-phenyl-1,1'-ferrocenyl-dithiol, Bn_2(thiolfan*)

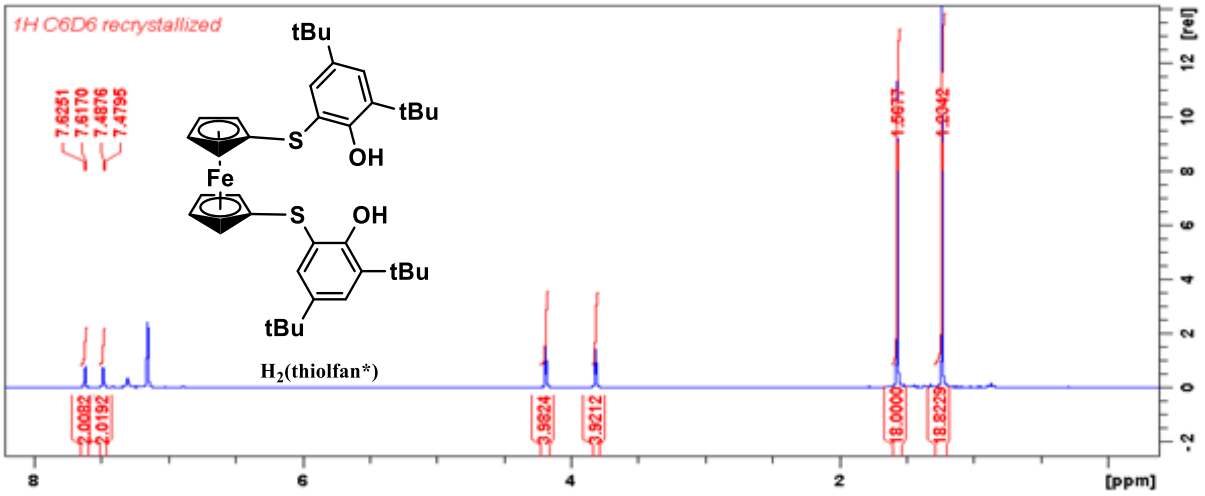

Figure A-6: ^{1}H NMR spectrum ($CDCl_3$, 300MHz, 298K) of 2-hydroxy-3,5-di-*tert*-butyl-phenyl-1,1'-ferrocenediyl-dithiol, H_2(thiolfan*)

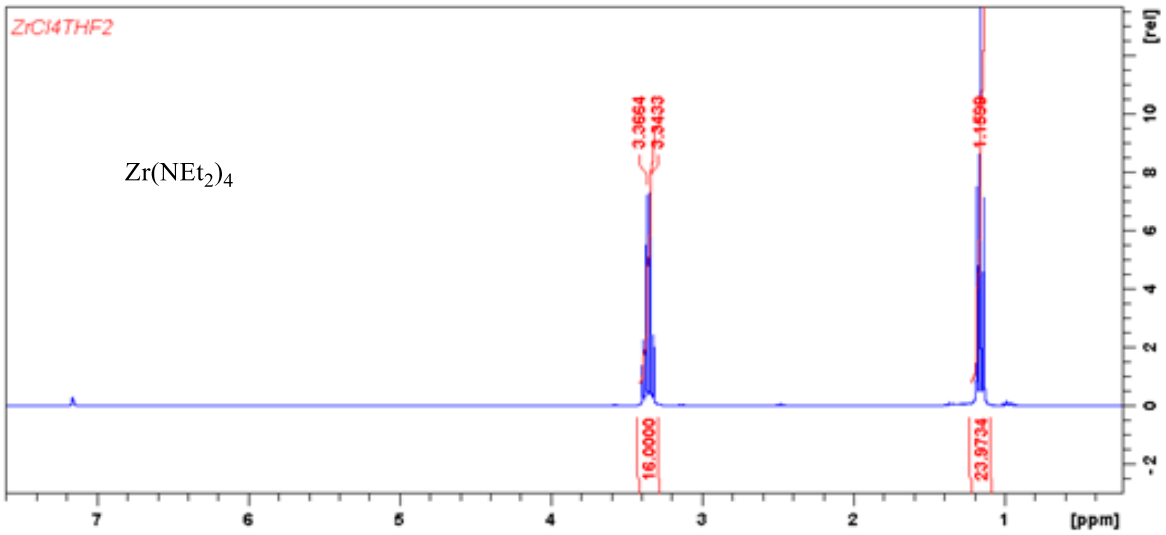

Figure A-7: ^{1}H NMR spectrum (C_6D_6, 300MHz, 298K) of tetrakis(diethylamido)zirconium(IV)

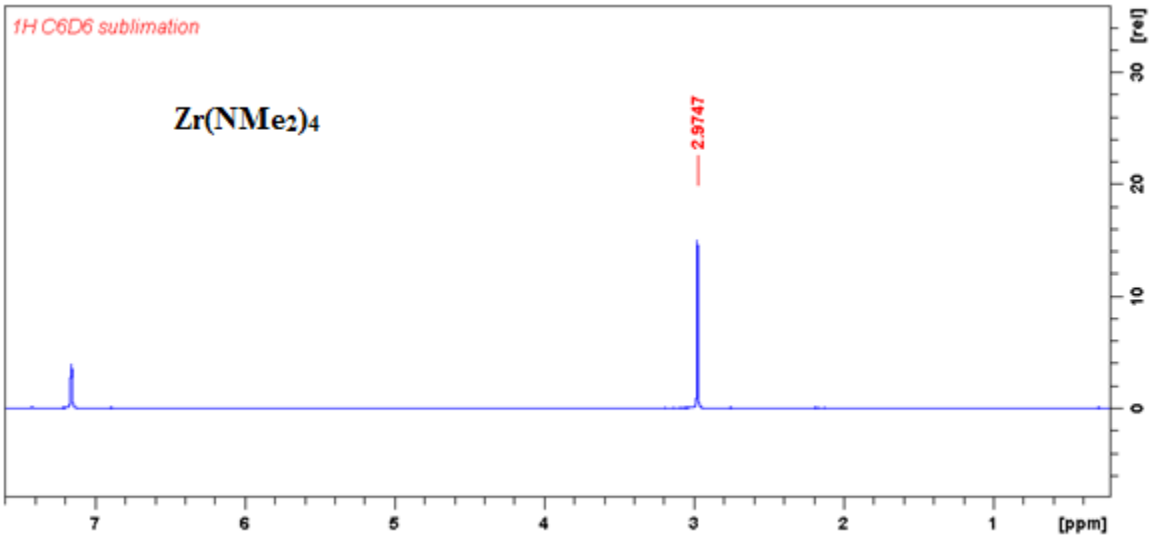

Figure A-8: ^{1}H NMR spectrum (C_6D_6, 300MHz, 298K) of tetrakis(dimethylamido)zirconium(IV)

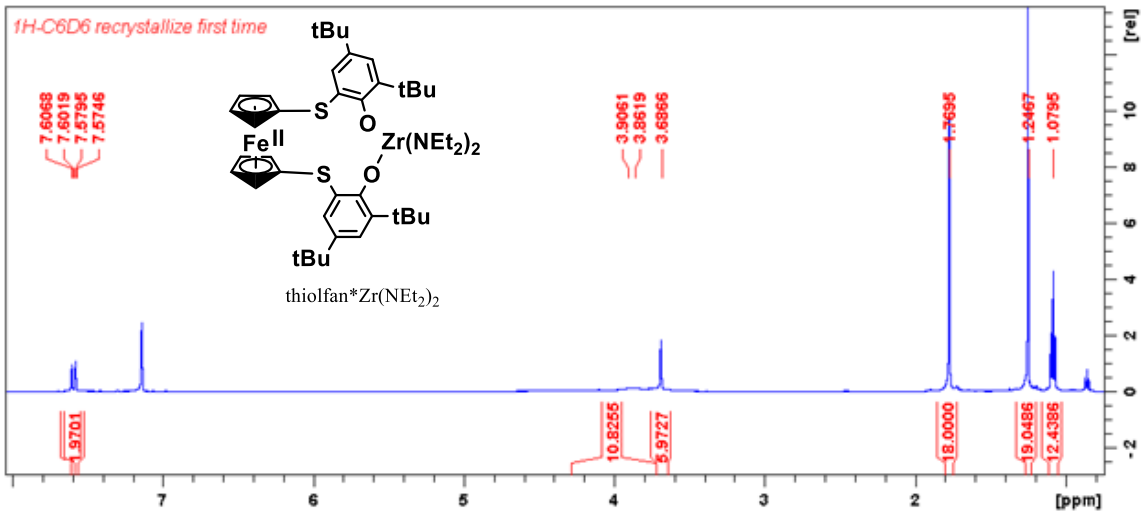

Figure A-9: ^{1}H NMR spectrum (C_6D_6, 500MHz, 298K) of (thiolfan*)$Zr(NEt_2)_2$

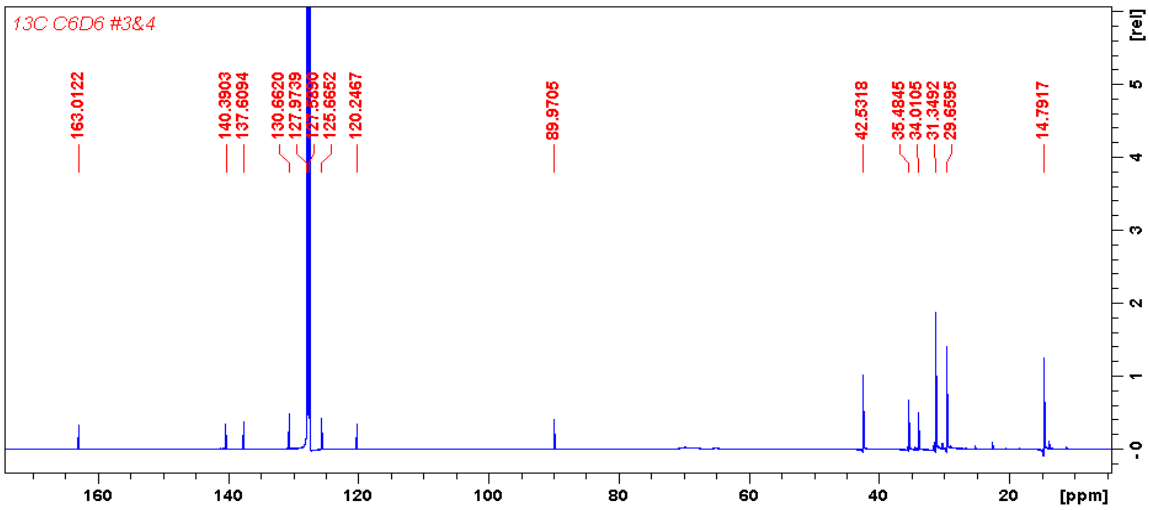

Figure A-10: ^{13}C NMR spectrum (C_6D_6, 500MHz, 298K) of (thiolfan*)$Zr(NEt_2)_2$

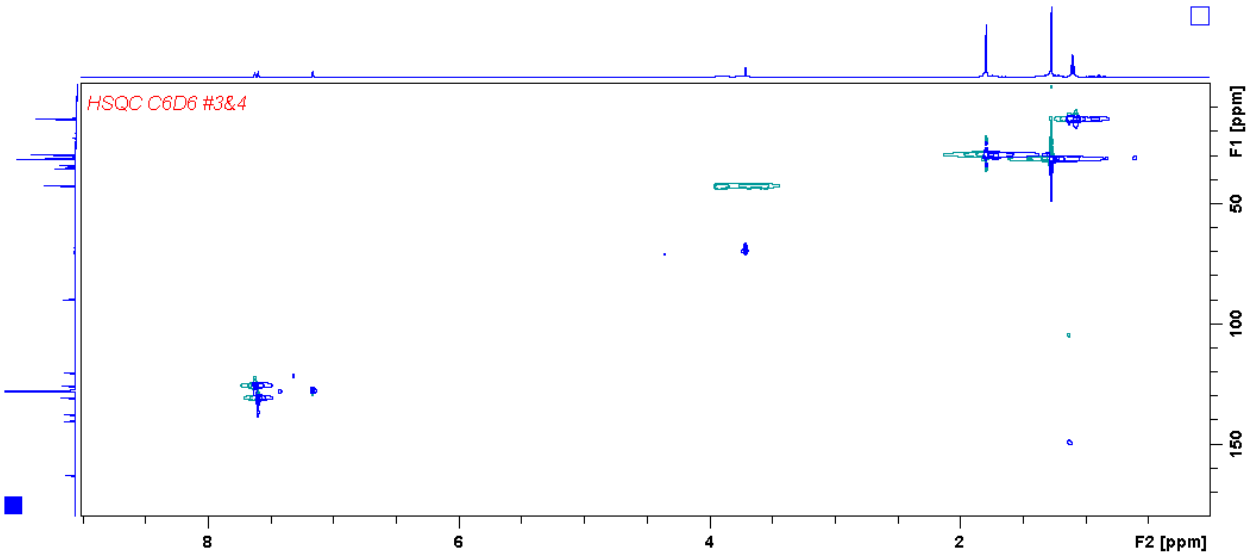

Figure A-11: HSQC spectrum (C_6D_6, 500MHz, 298K) of (thiolfan*)Zr(NEt_2)$_2$

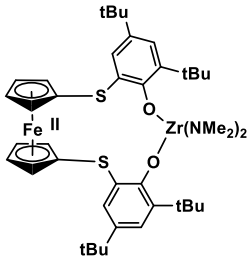

thiolfan*Zr(NMe_2)$_2$

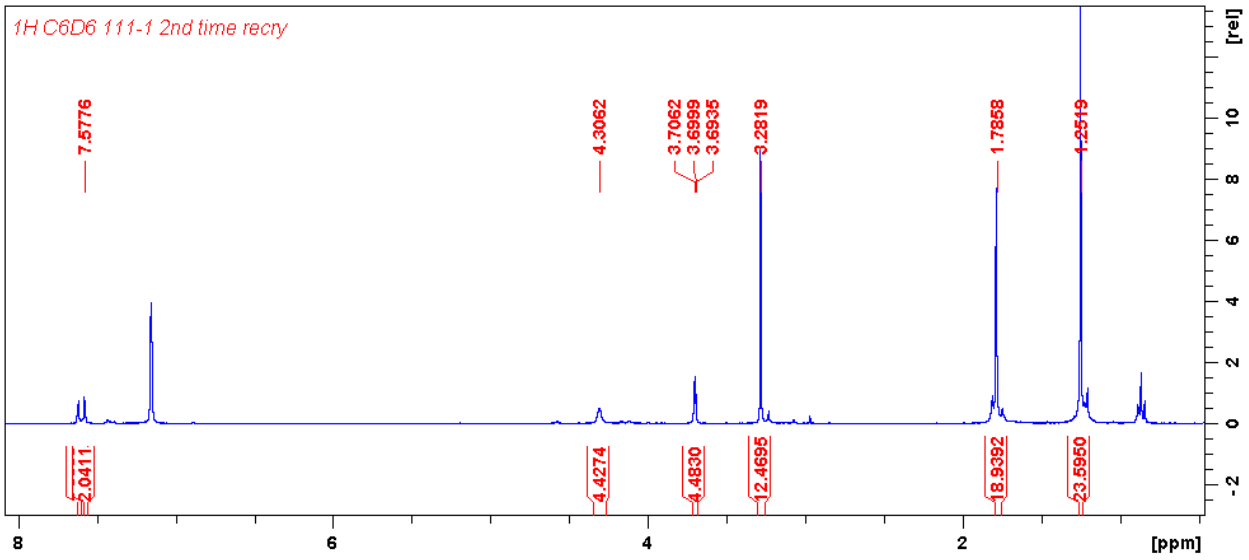

Figure A-12: ^{1}H NMR spectrum (C_6D_6, 300MHz, 298K) of (thiolfan*)Zr(NMe_2)$_2$

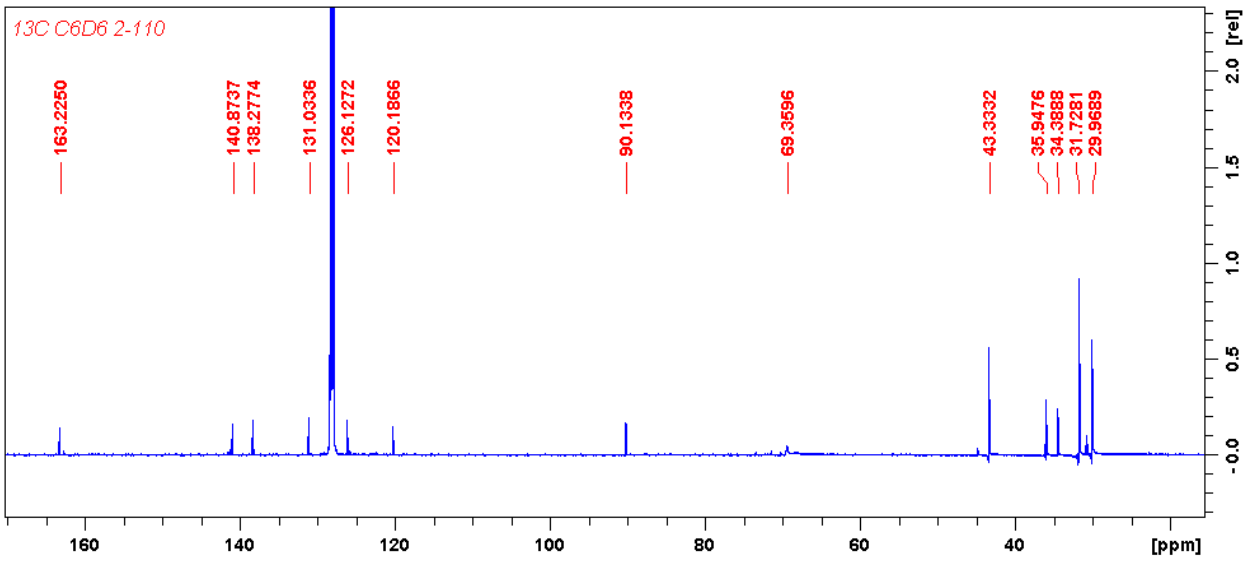

Figure A-13: ^{13}C NMR spectrum (C_6D_6, 500MHz, 298K) of (thiolfan*)$Zr(NEt_2)_2$

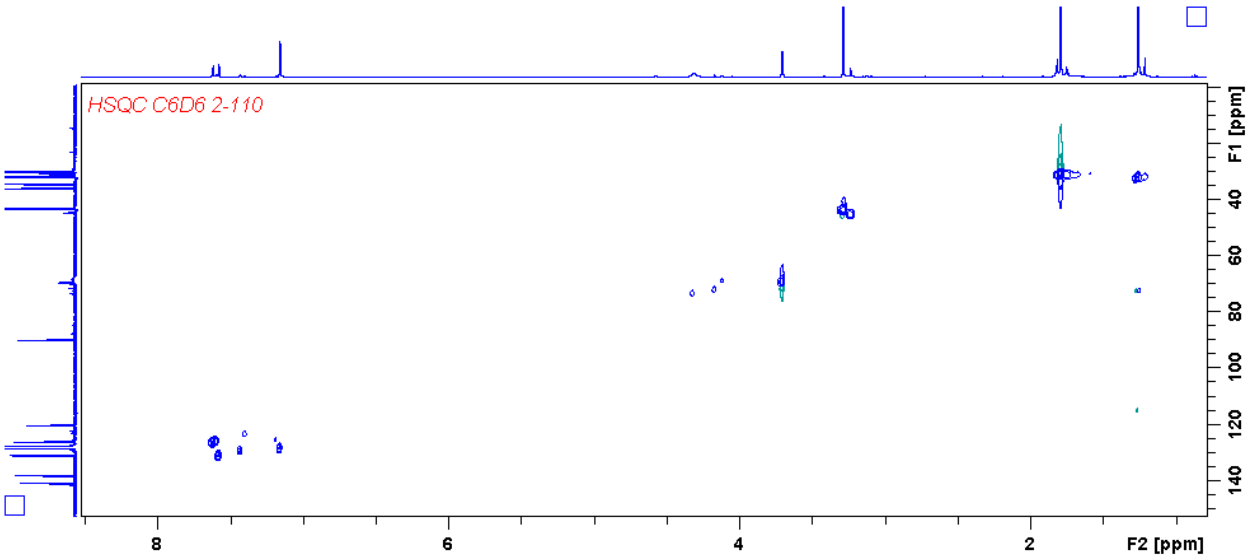

Figure A-14: HSQC spectrum (C_6D_6, 500MHz, 298K) of (thiolfan*)$Zr(NMe_2)_2$

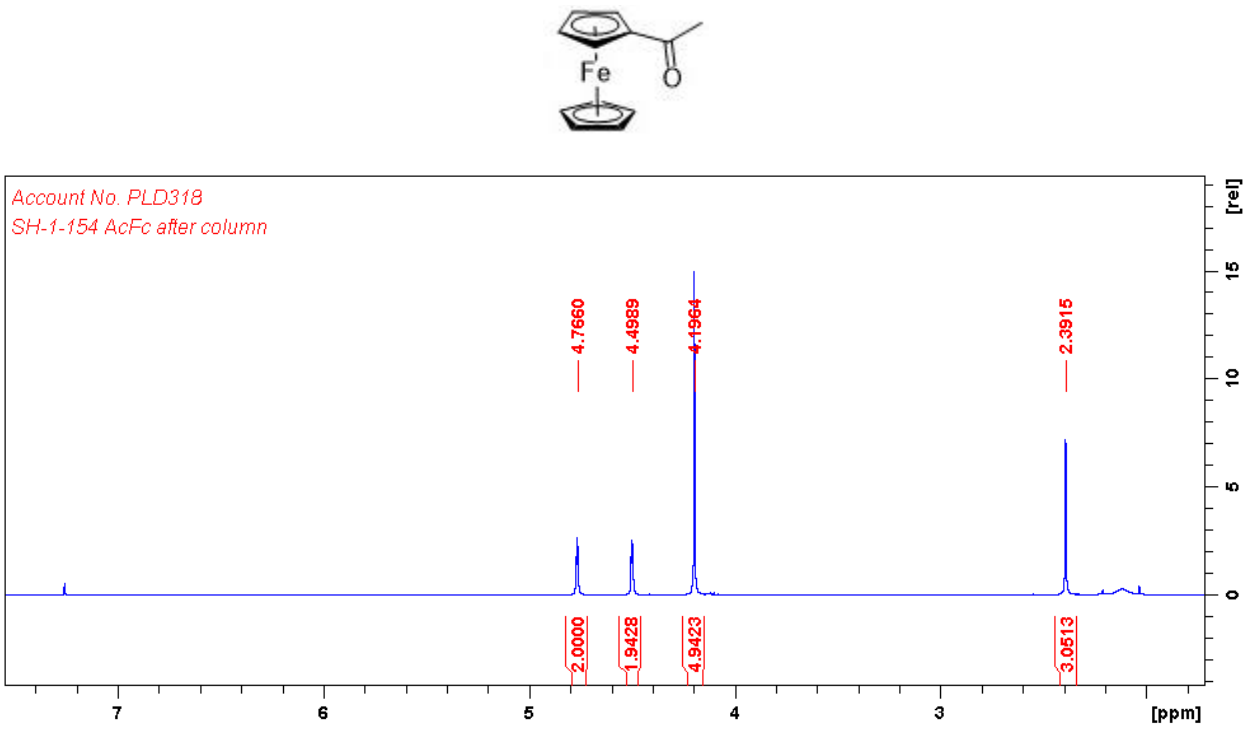

Figure A-15: ^{1}H NMR spectrum ($CDCl_3$, 300MHz, 298K) of acetylferrocene

Chapter 2:

Synthesis of amine substrates:

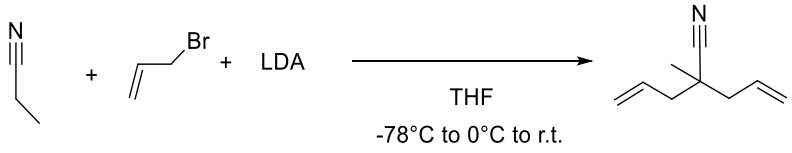

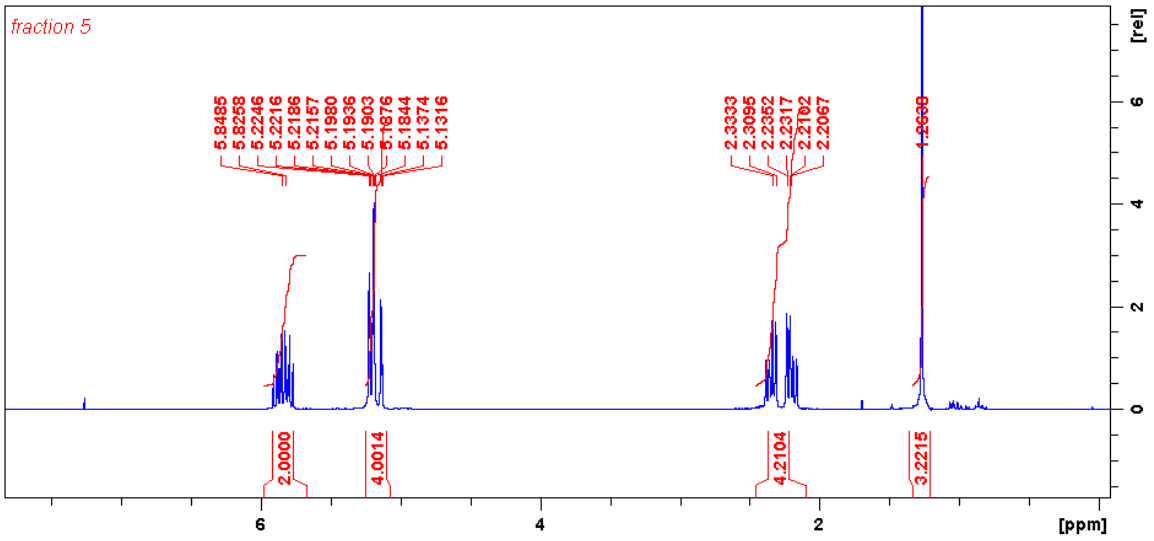

Figure A-16: ^{1}H NMR spectrum ($CDCl_3$, 300MHz, 298K) of 2-allyl-2-methylpent-4-enenitrile

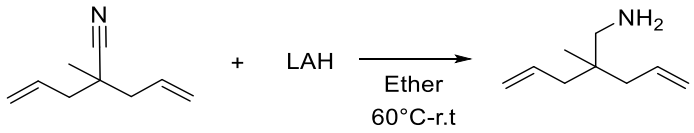

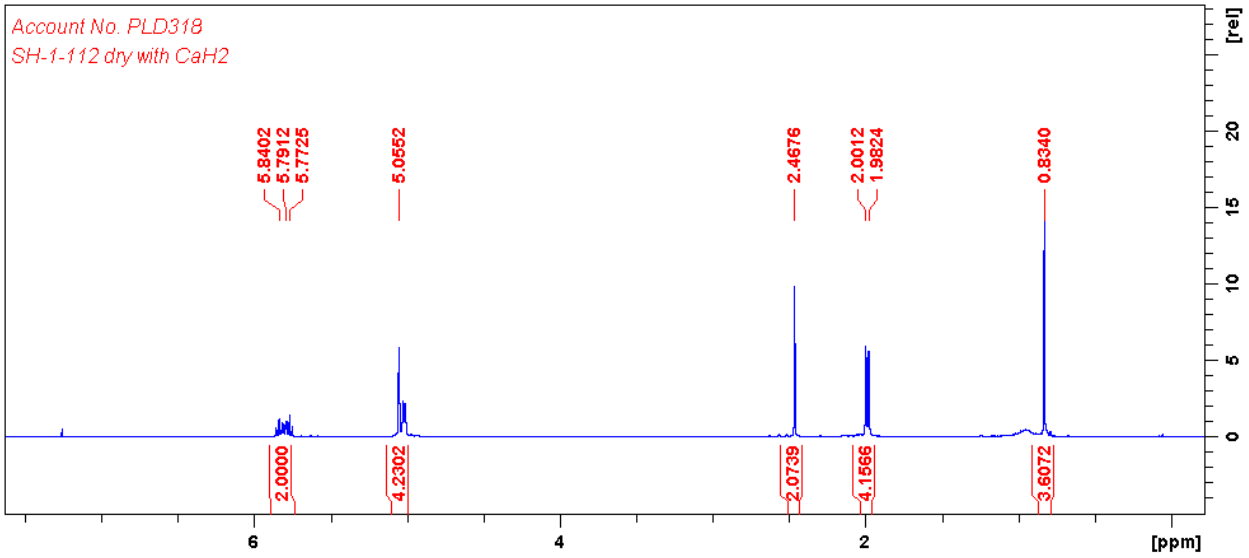

Figure A-17: ^{1}H NMR spectrum ($CDCl_3$, 300MHz, 298K) of 2-allyl-2-(methyl)-pent-4-en-1-amine

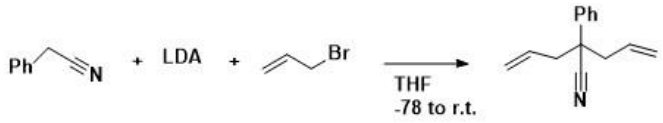

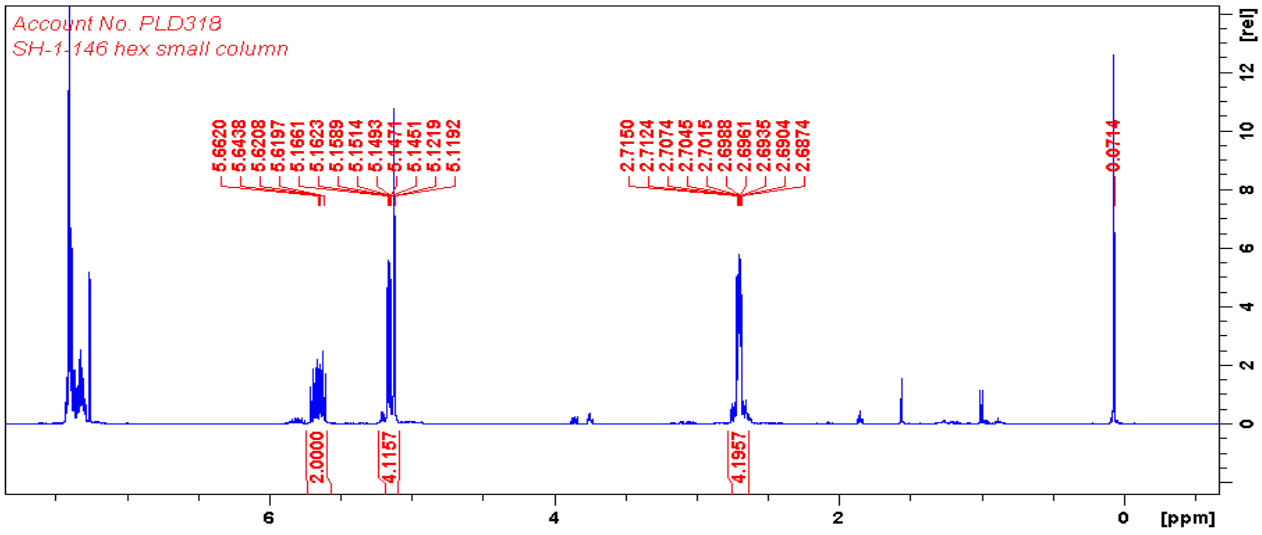

Figure A-18: ^{1}H NMR spectrum ($CDCl_3$, 300MHz, 298K) of 2-allyl-2-phenylpent-4-enenitrile

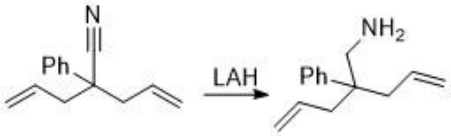

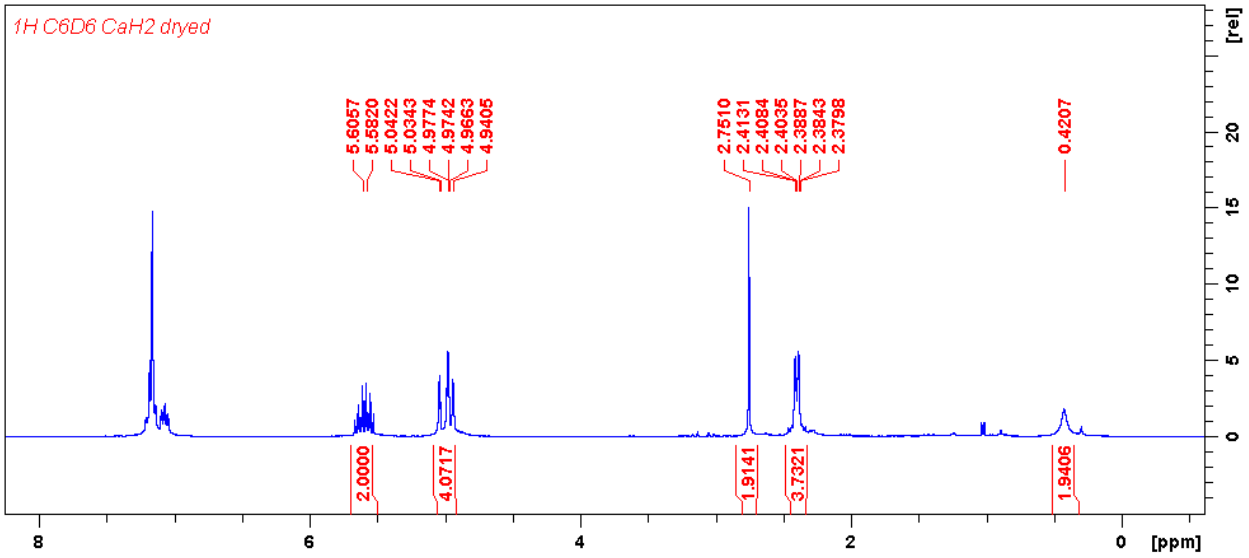

Figure A-19: ^{1}H NMR spectrum ($CDCl_3$, 300MHz, 298K) of 2-allyl-2-(phenyl)-pent-4-en-1-amine

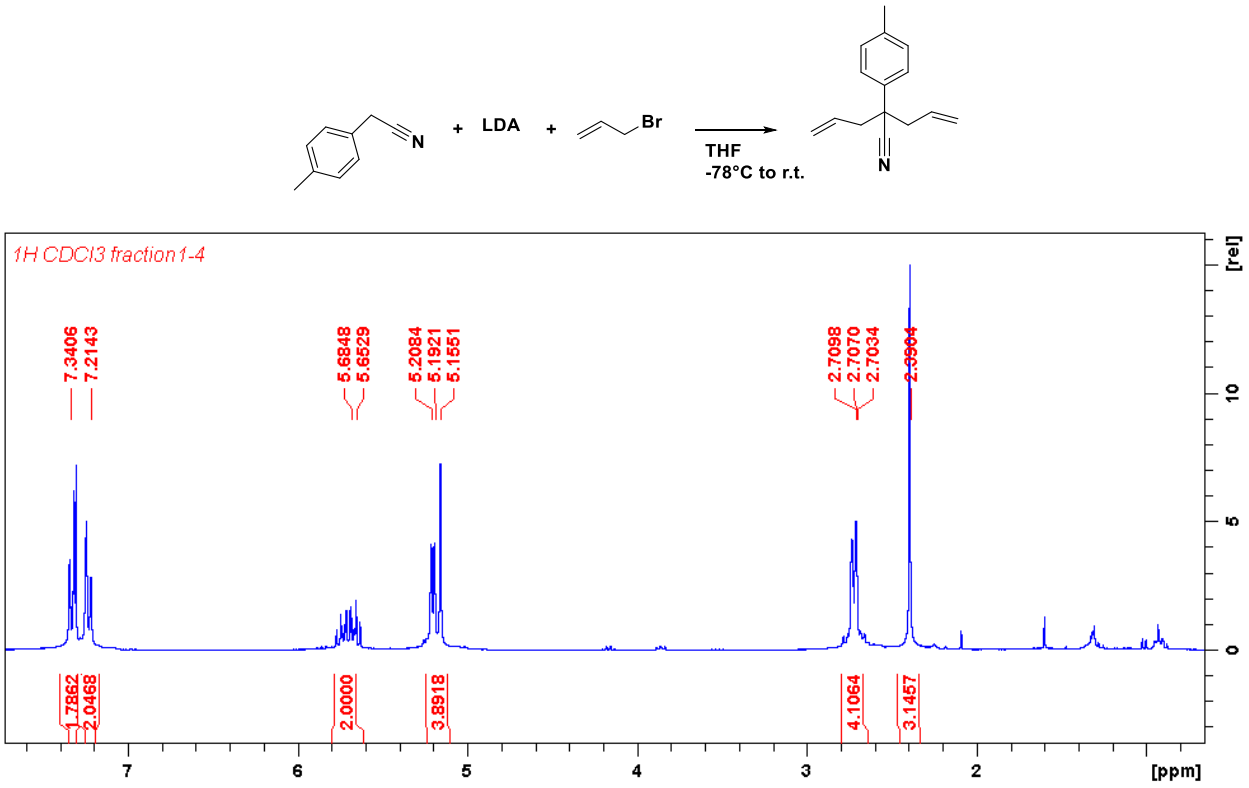

Figure A-20: ^{1}H NMR spectrum ($CDCl_3$, 300MHz, 298K) of 2-allyl-2-(*p*-tolyl)-pent-4-enenitrile

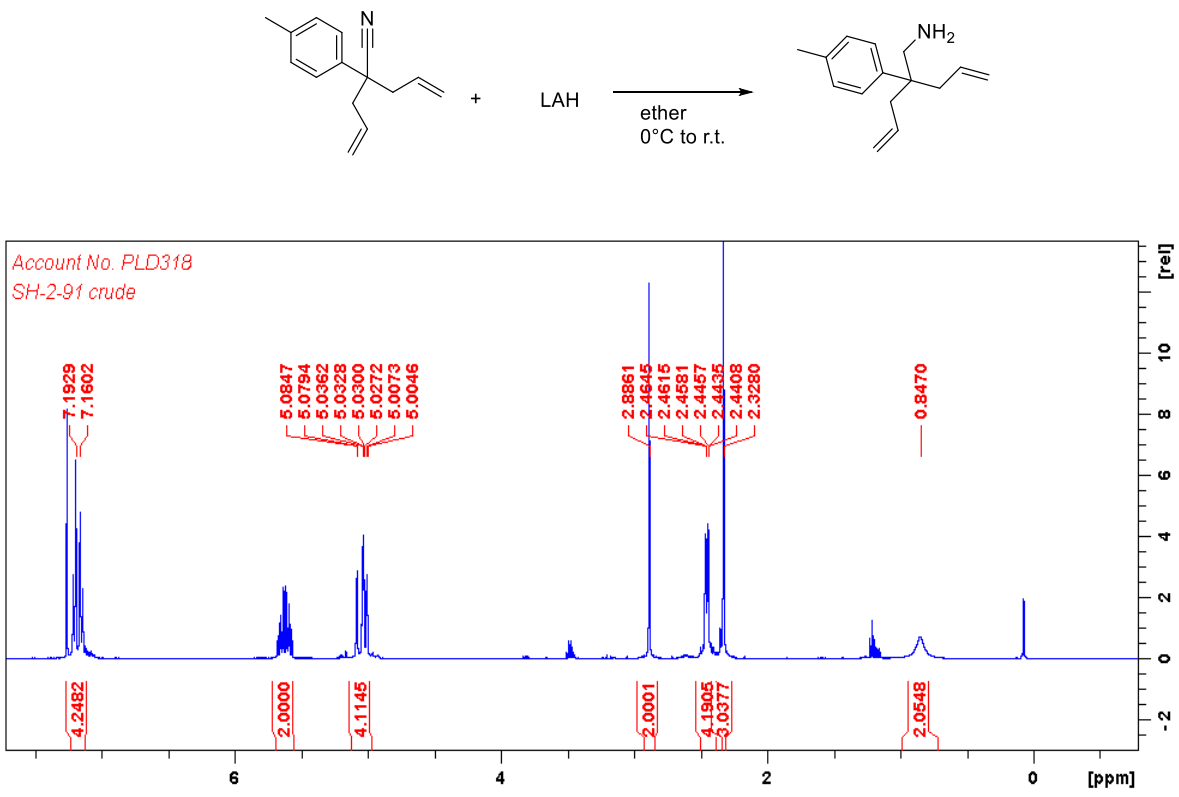

Figure A-21: ^{1}H NMR spectrum ($CDCl_3$, 300MHz, 298K) of 2-allyl-2-(*p*-tolyl)-pent-4-en-1-amine

Hydroamination reactions:

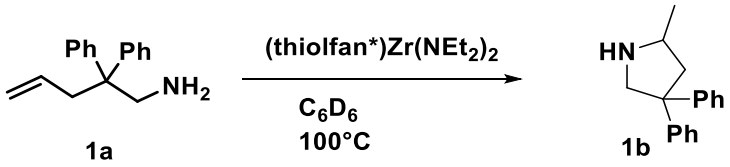

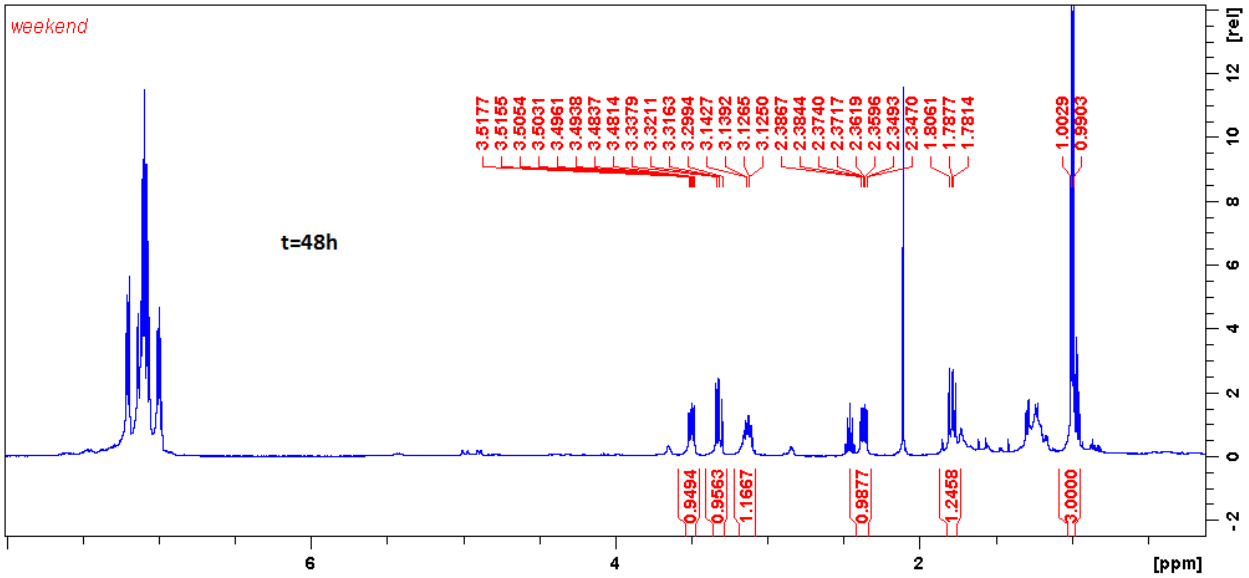

Figure A-22: ^{1}H NMR spectrum (C_6D_6, 300MHz, 298K) of **1a**.

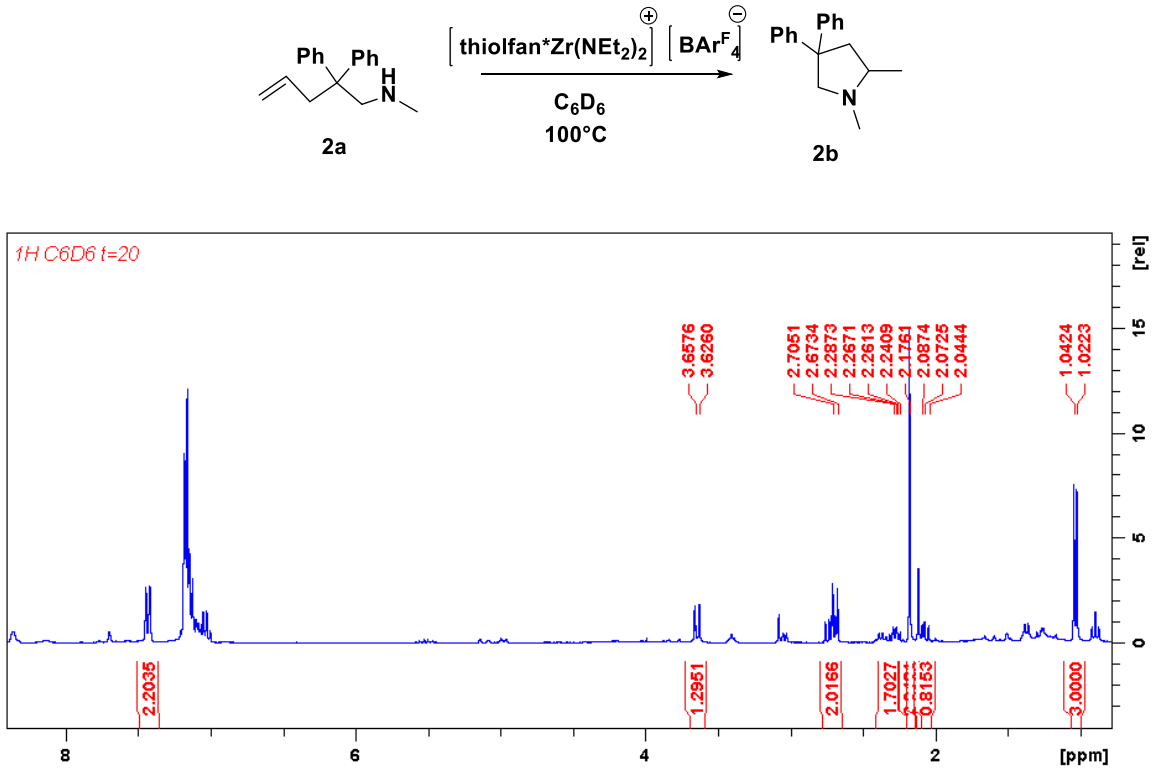

Figure A-23: ^{1}H NMR spectrum (C_6D_6, 500MHz, 298K) of **2b**.

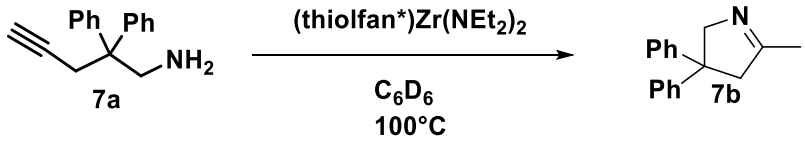

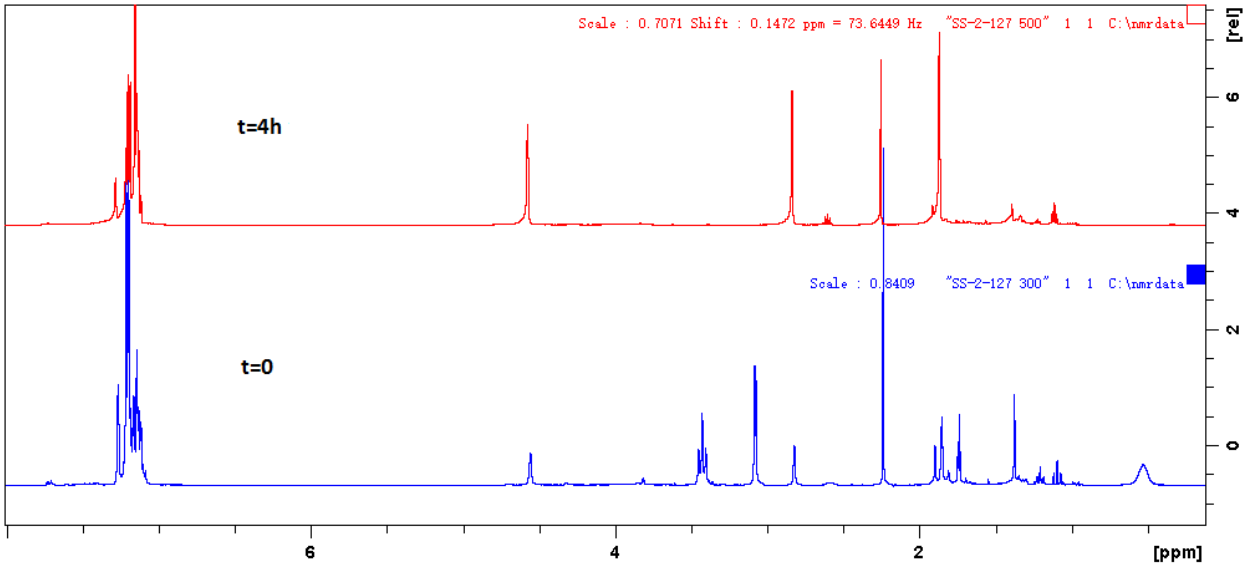

Figure A-24: ^{1}H NMR spectrum (C_6D_6, 500MHz, 298K) of time-monitored experiment: neutral (thiolfan*)$Zr(NEt_2)_2$ with **7a**.

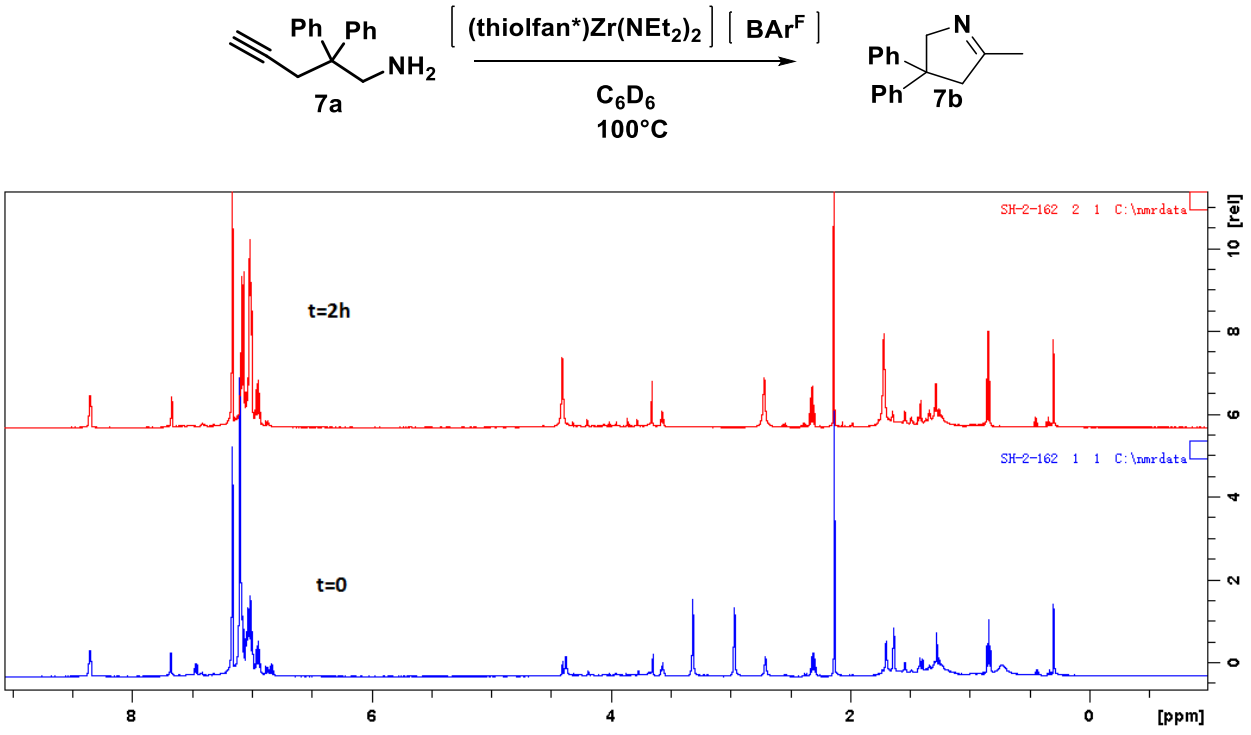

Figure A-25: ^{1}H NMR spectrum (C_6D_6, 500MHz, 298K) of time-monitored experiment: oxidized (thiolfan*)Zr(NEt_2)$_2$ with **7a**.

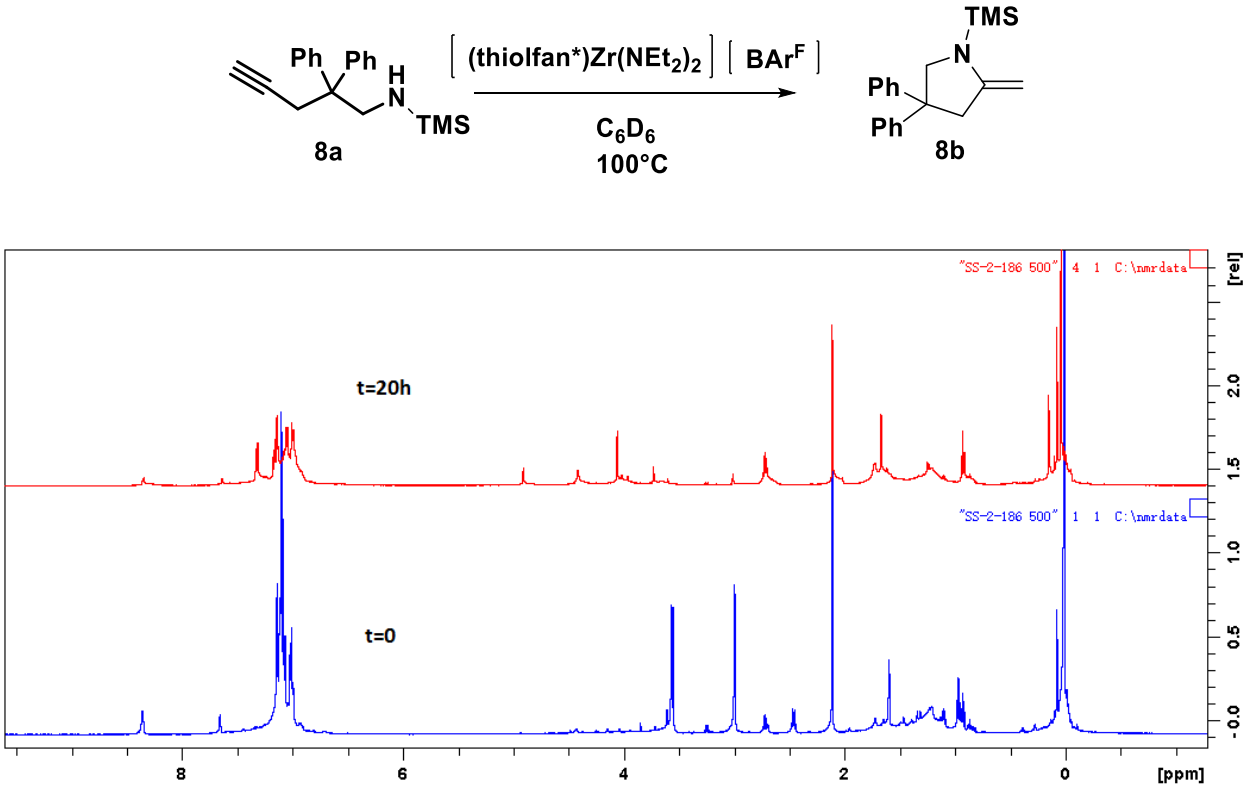

Figure A-26: ^{1}H NMR spectrum (C_6D_6, 500MHz, 298K) of time-monitored experiment: oxidized (thiolfan*)$Zr(NEt_2)_2$ with **8a**.

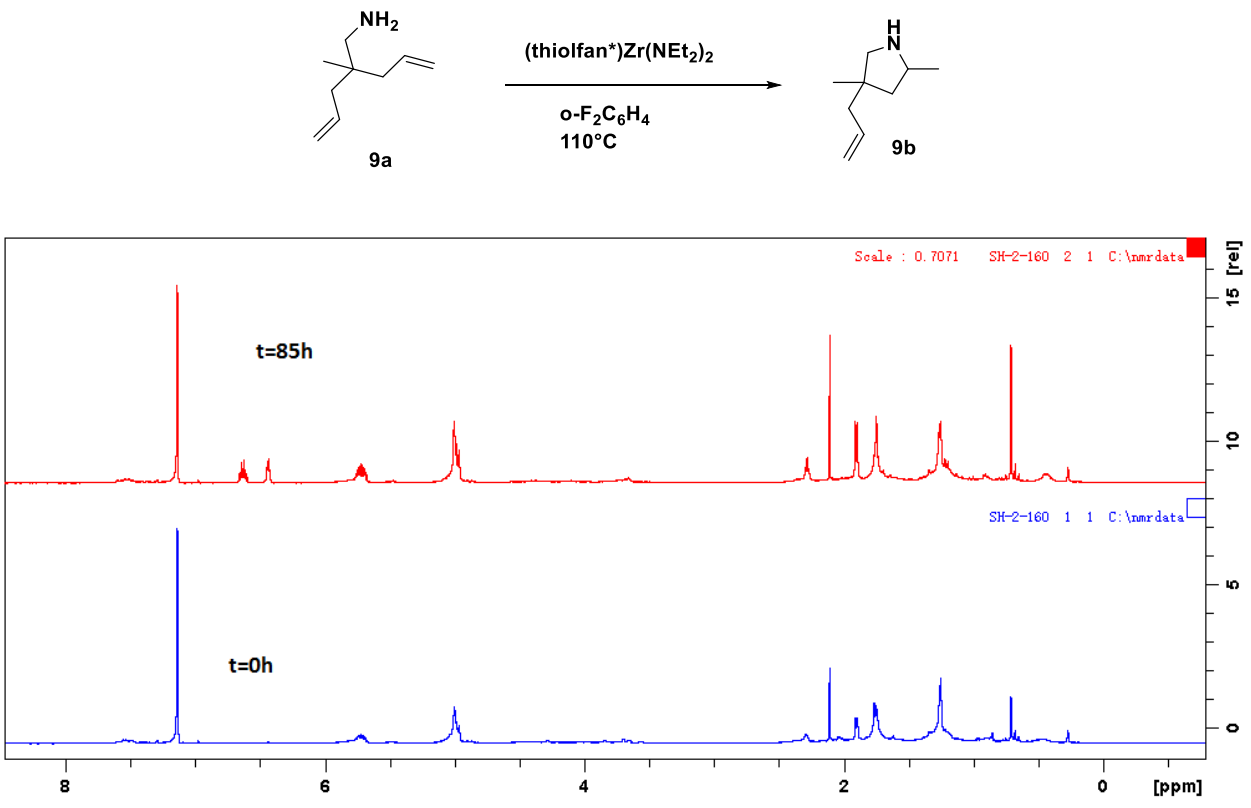

Figure A-27: ^{1}H NMR spectrum (C_6D_6, 500MHz, 298K) of time-monitored experiment: neutral (thiolfan*)$Zr(NEt_2)_2$ with **9a**.

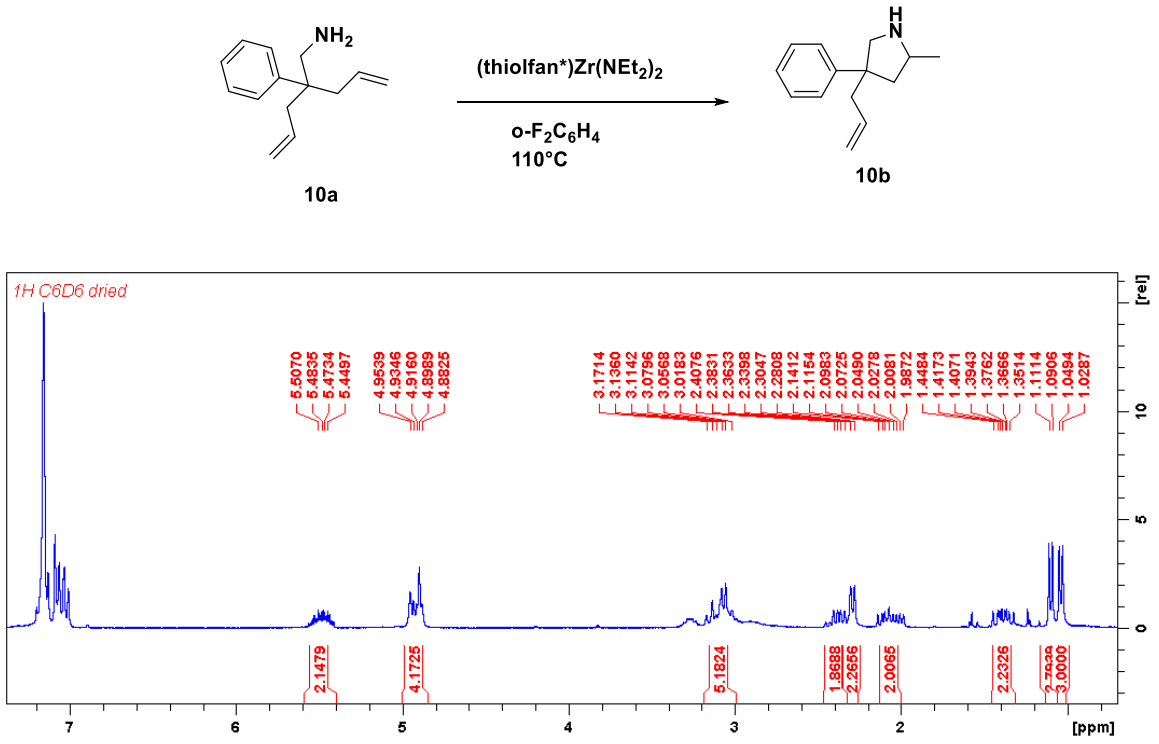

Figure A-28: ^{1}H NMR spectrum (C_6D_6, 500MHz, 298K) of time-monitored experiment: neutral (thiolfan*)Zr(NEt_2)$_2$ with **10a**.

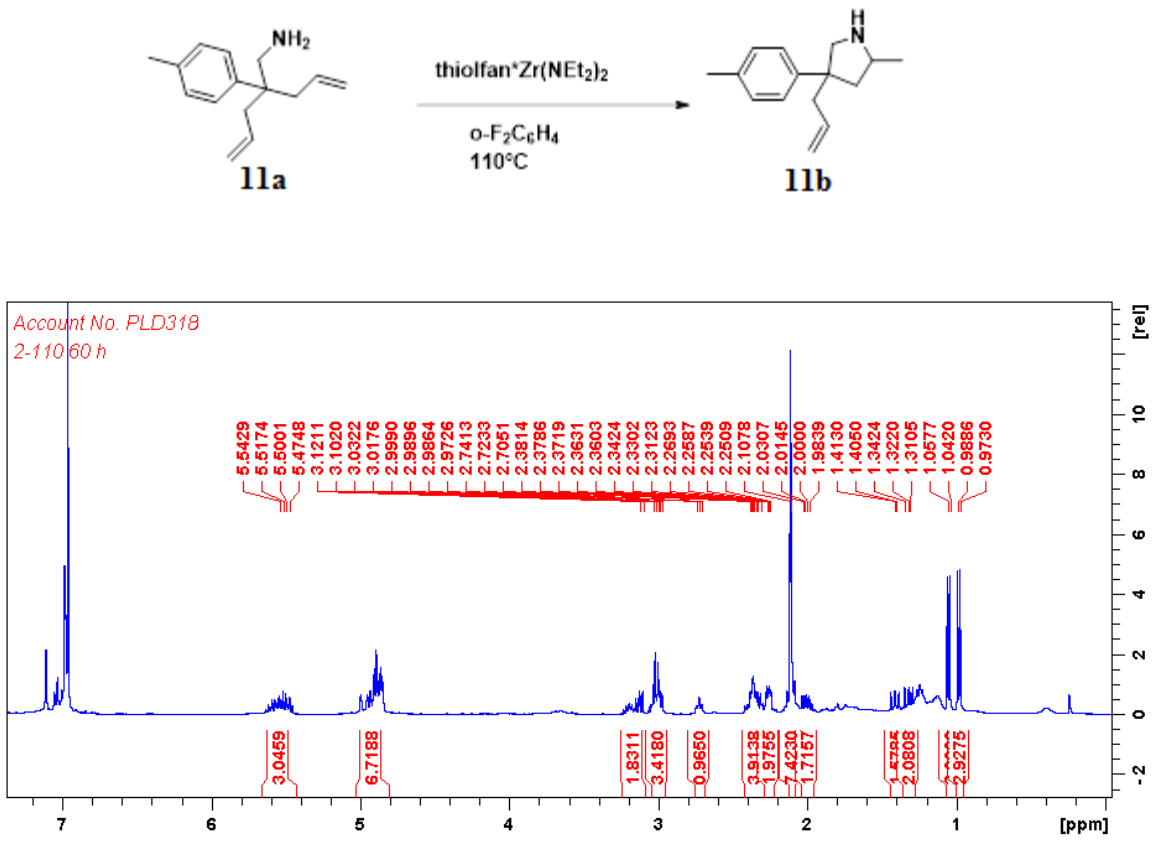

Figure A-29: ^{1}H NMR spectrum (C_6D_6, 500MHz, 298K) of time-monitored experiment: neutral (thiolfan*)$Zr(NEt_2)_2$ with **11a**.

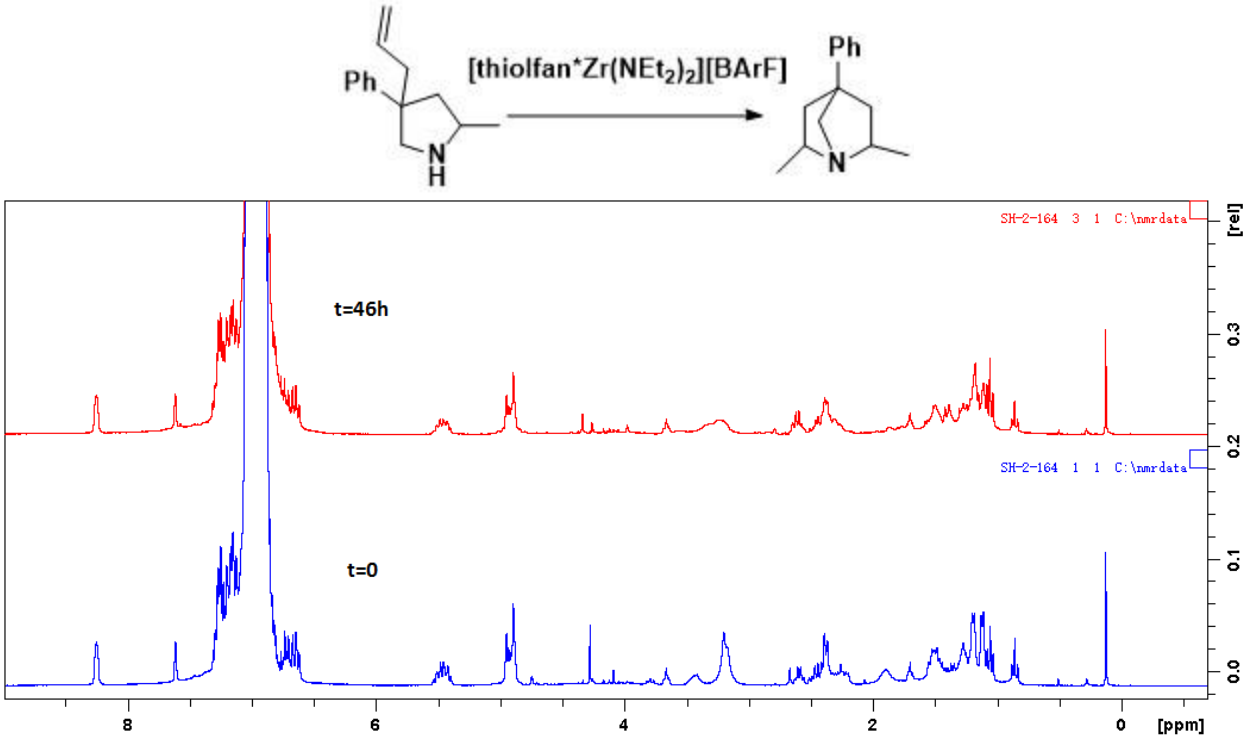

Figure A-30: ^{1}H NMR spectrum (C_6D_6, 300MHz, 298K) of time-monitored experiment: oxidized (thiolfan*)$Zr(NEt_2)_2$ with **10b**

Control Experiments:

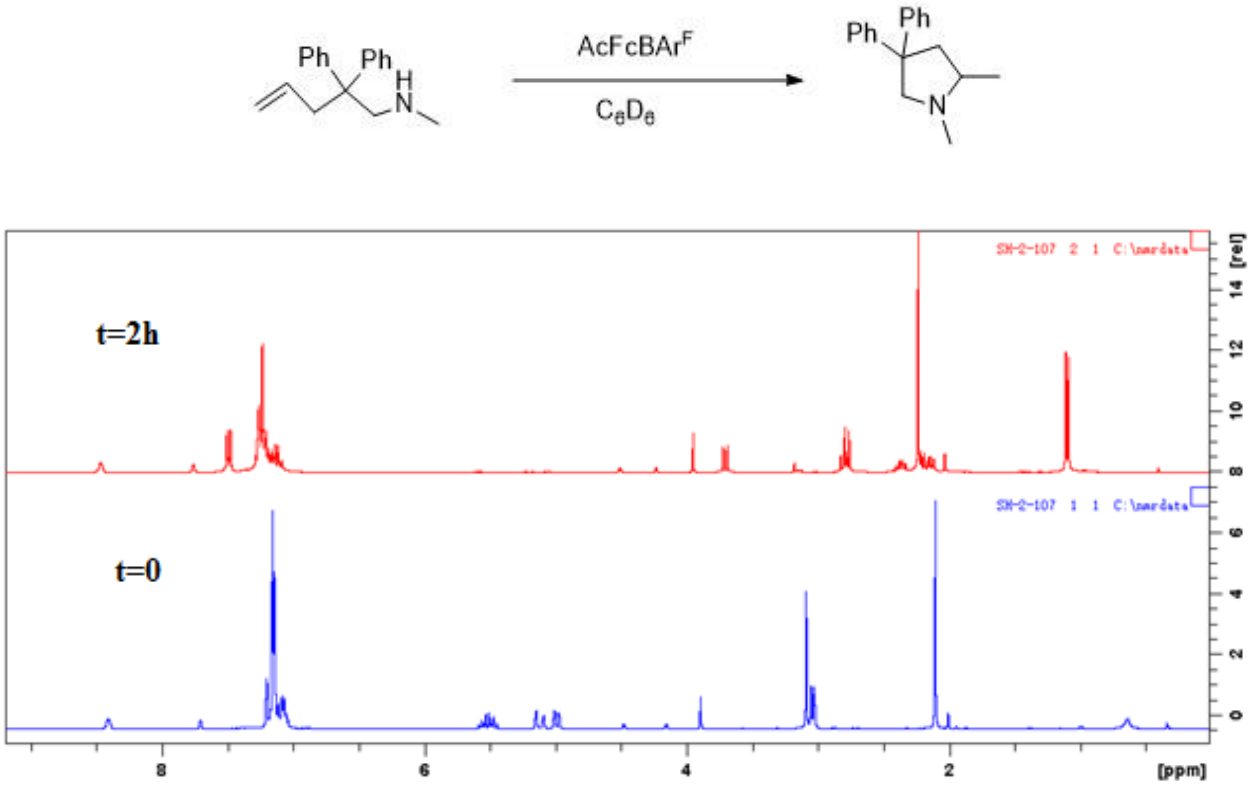

Figure A-31: ^{1}H NMR spectrum (C_6D_6, 500MHz, 298K) of time-monitored experiment: AcFcBAr^F with **2a**.

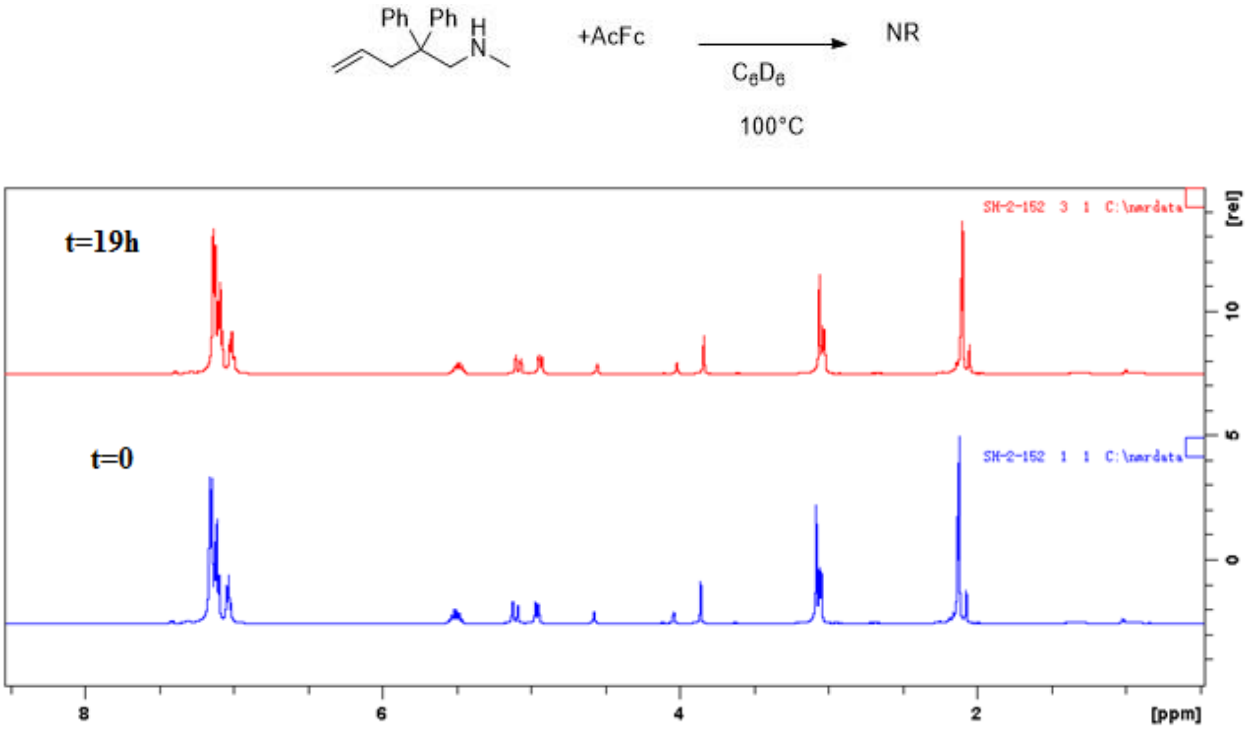

Figure A-32: ^{1}H NMR spectrum (C_6D_6, 500MHz, 298K) of time-monitored experiment: AcFc with **2a**.

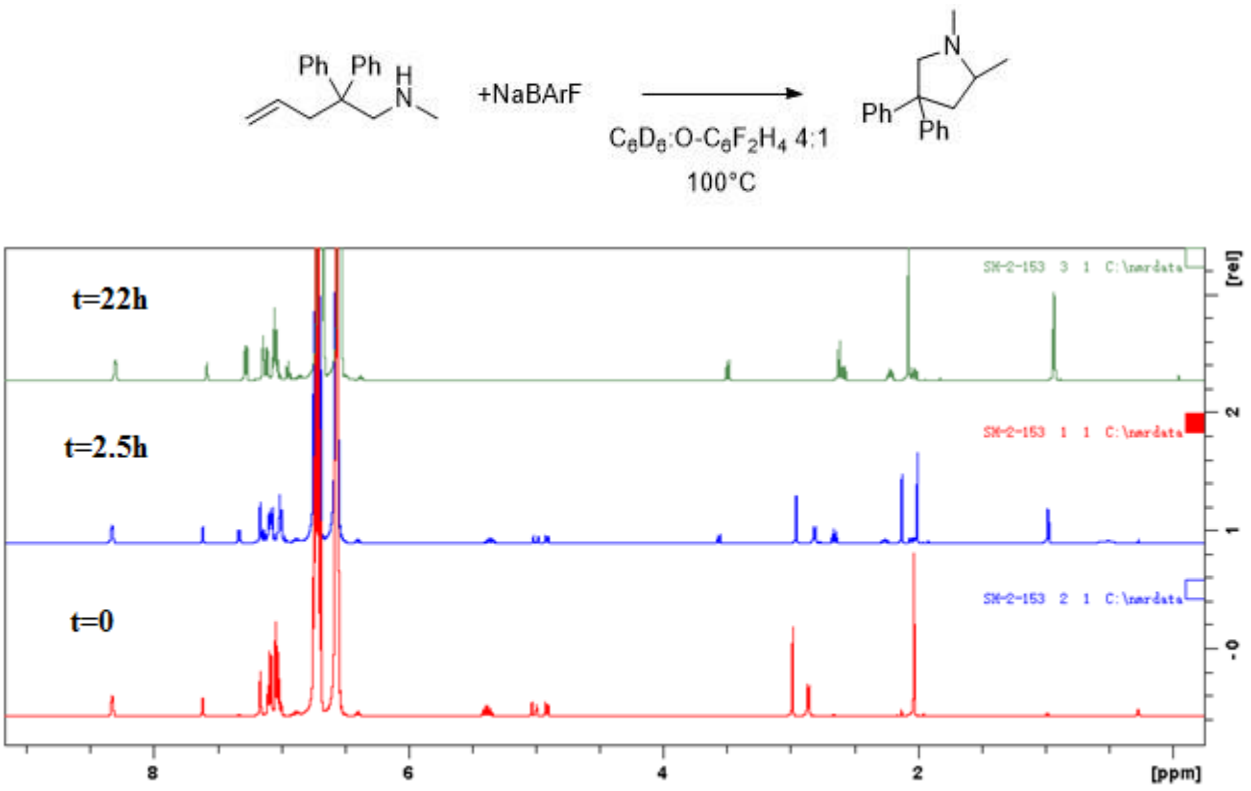

Figure A-33: ^{1}H NMR spectrum (C_6D_6, 500MHz, 298K) of time-monitored experiment: $NaBAr^F$ with **2a**.

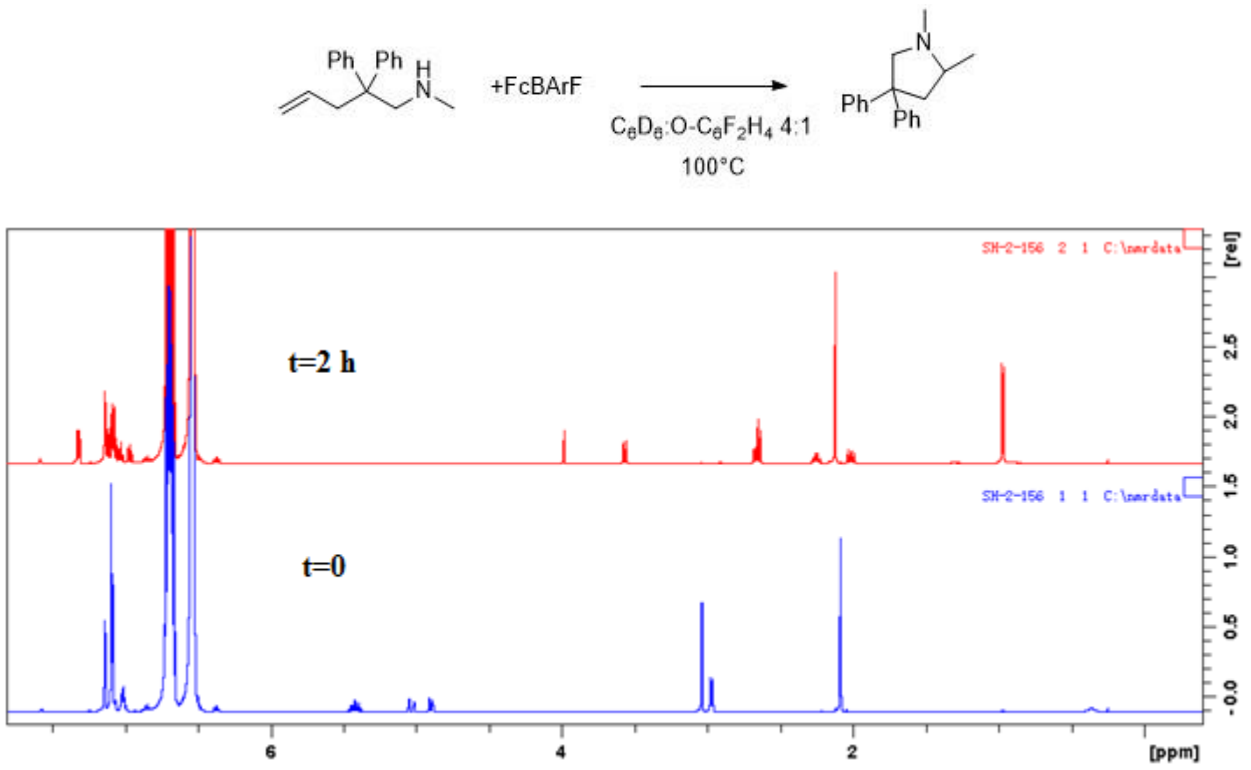

Figure A-34: ^{1}H NMR spectrum (C_6D_6, 500MHz, 298K) of time-monitored experiment: $FcBAr^F$ with **2a**.